NCAR/TN-461+STR
NCAR TECHNICAL NOTE

May 2004

Technical Description of the Community Land Model (CLM)

Keith W. Oleson

Yongjiu Dai

Gordon Bonan
Mike Bosilovich
Robert Dickinson
Paul Dirmeyer
Forrest Hoffman
Paul Houser
Samuel Levis
Guo-Yue Niu
Peter Thornton
Mariana Vertenstein
Zong-Liang Yang
Xubin Zeng

Terrestrial Sciences Section
Climate and Global Dynamics Division

NATIONAL CENTER FOR ATMOSPHERIC RESEARCH
BOULDER, COLORADO

NCAR TECHNICAL NOTES

The Technical Note series provides an outlet for a variety of NCAR Manuscripts that contribute in specialized ways to the body of scientific knowledge but that are not suitable for journal, monograph, or book publication. Reports in this series are issued by the NCAR scientific divisions. Designation symbols for the series include:

EDD – Engineering, Design or Development Reports
Equipment descriptions, test results, instrumentation, and operating and maintenance manuals.

IA – Instruction Aids
Instruction manuals, bibliographies, film supplements, and other research, or instructional aids.

PPR – Program Progress Reports
Field program reports, interim and working reports, survey reports, and plans for experiments.

PROC – Proceedings
Documentation or symposia, colloquia, conferences, workshops, and lectures. (Distribution may be limited to attendees.)

STR – Scientific and Technical Reports
Data compilations, theoretical and numerical investigations, and experimental results.

The National Center for Atmospheric Research (NCAR) is operated by the nonprofit University Corporation for Atmospheric Research (UCAR) under the sponsorship of the National Science Foundation. Any opinions, findings, conclusions, or recommendations expressed in this publication are those of the author(s) and do not necessarily reflect the views of the National Science Foundation.

NCAR/TN-461+STR
NCAR TECHNICAL NOTE

May 2004

Technical Description of the Community Land Model (CLM)

Keith W. Oleson

Yongjiu Dai

Gordon Bonan
Mike Bosilovich
Robert Dickinson
Paul Dirmeyer
Forrest Hoffman
Paul Houser
Samuel Levis
Guo-Yue Niu
Peter Thornton
Mariana Vertenstein
Zong-Liang Yang
Xubin Zeng

Terrestrial Sciences Section
Climate and Global Dynamics Division

NATIONAL CENTER FOR ATMOSPHERIC RESEARCH
BOULDER, COLORADO

TABLE OF CONTENTS

LIST OF FIGURES

LIST OF TABLES

ACKNOWLEDGEMENTS

The authors would like to acknowledge the following people for their contributions to the development of the Community Land Model: Ian Baker, Marcia Branstetter, Scott Denning, Jared Entin, Jay Famiglietti, Jon Foley, Jon Radakovich, Adam Schlosser, Guiling Wang. The work of Keith Oleson was supported by the NASA Land Cover Land Use Change program through a grant W-19,735.

Current affiliations for the authors are as follows:

- Keith Oleson, Gordon Bonan, Samuel Levis, Peter Thornton, Mariana Vertenstein (National Center for Atmospheric Research)
- Yongjiu Dai (Beijing Normal University)
- Mike Bosilovich (Global Modeling and Assimilation Office, NASA/GSFC)
- Robert Dickinson (Georgia Institute of Technology)
- Paul Dirmeyer (Center for Ocean-Land-Atmosphere Studies)
- Forrest Hoffman (Oak Ridge National Laboratory)
- Paul Houser (Hydrological Sciences Branch, NASA/GSFC)
- Guo-Yue Niu, Zong-Liang Yang (University of Texas at Austin)
- Xubin Zeng (University of Arizona)

1. Introduction

This technical note describes the physical parameterizations and numerical implementation of version 3.0 of the Community Land Model (CLM3.0) which is the land surface parameterization used with the Community Atmosphere Model (CAM3.0) and the Community Climate System Model (CCSM3.0). Chapters 1-11 constitute the description of CLM when coupled to CAM or CCSM, while Chapter 12 describes processes that pertain specifically to the operation of CLM in offline mode (uncoupled to an atmospheric model). This technical note, the CLM3.0 Developer's Guide (Hoffman et al. 2004), and the CLM3.0 User's Guide (Vertenstein et al. 2004) together provide the user with the scientific description, coding implementation, and operating instructions for CLM. The CLM Dynamic Global Vegetation Model (CLM-DGVM) is described in Levis et al. (2004).

1.1 Model History and Overview

1.1.1 History

The development of the Community Land Model can be described as the merging of a community-developed land model focusing on biogeophysics and a concurrent effort at NCAR to expand the NCAR Land Surface Model (NCAR LSM) to include the carbon cycle, vegetation dynamics, and river routing. The concept of a community-developed land component of the Community Climate System Model (CCSM) was initially proposed at the CCSM Land Model Working Group (LMWG) meeting in February 1996. Initial software specifications and development focused on evaluating the best features of three existing land models: the NCAR LSM (Bonan 1996, 1998) used with the Community Climate Model (CCM3) and in the initial version of CCSM; the Institute of

Atmospheric Physics, Chinese Academy of Sciences land model (IAP94) (Dai and Zeng 1997); and the Biosphere-Atmosphere Transfer Scheme (BATS) (Dickinson et al. 1993) used with CCM2. A scientific steering committee was formed to review the initial specifications of the design provided by Robert Dickinson, Gordon Bonan, Xubin Zeng, and Yongjiu Dai and to facilitate further development. Steering committee members were selected so as to provide guidance and expertise in disciplines not generally well-represented in land surface models (e.g., carbon cycling, ecological modeling, hydrology, and river routing) and included scientists from NCAR, the university community, and government laboratories (R. Dickinson, G. Bonan, X. Zeng, Paul Dirmeyer, Jay Famiglietti, Jon Foley, and Paul Houser).

The specifications for the new model, designated the Common Land Model, were discussed and agreed upon at the June 1998 CCSM Workshop LMWG meeting. An initial code was developed by Y. Dai and was examined in March 1999 by Mike Bosilovich, P. Dirmeyer, and P. Houser. At this point an extensive period of code testing was initiated. Keith Oleson, Y. Dai, Adam Schlosser, and P. Houser presented preliminary results of offline 1-dimensional testing at the June 1999 CCSM Workshop LMWG meeting. Results from more extensive offline testing at plot, catchment, and large scale (up to global) were presented by Y. Dai, A. Schlosser, K. Oleson, M. Bosilovich, Zong-Liang Yang, Ian Baker, P. Houser, and P. Dirmeyer at the LMWG meeting hosted by COLA (Center for Ocean-Land-Atmosphere Studies) in November 1999. Field data used for validation included sites adopted by the Project for Intercomparison of Land-surface Parameterization Schemes (Henderson-Sellers et al. 1993) (Cabauw, Valdai, Red-Arkansas river basin) and others [FIFE (Sellers et al. 1988), BOREAS (Sellers et al. 1995), HAPEX-MOBILHY (André et al. 1986), ABRACOS (Gash et al. 1996), Sonoran Desert (Unland et al. 1996), GSWP (Dirmeyer et al. 1999)]. Y. Dai also presented results from a preliminary coupling of the Common Land Model to CCM3, indicating that the land model could be successfully coupled to a climate model.

Results of coupled simulations using CCM3 and the Common Land Model were presented by X. Zeng at the June 2000 CCSM Workshop LMWG meeting. Comparisons with the NCAR LSM and observations indicated major improvements to the seasonality of runoff, substantial reduction of a summer cold bias, and snow depth. Some deficiencies related to runoff and albedos were noted, however, that were subsequently addressed. Z.-L. Yang and I. Baker demonstrated improvements in the simulation of snow and soil temperatures. Sam Levis reported on efforts to incorporate a river routing model to deliver runoff to the ocean model in CCSM. Soon after the workshop, the code was delivered to NCAR for implementation into the CCSM framework. Documentation for the Common Land Model is provided by Dai et al. (2001) while the coupling with CCM3 is described in Zeng et al. (2002). The model was introduced to the modeling community in Dai et al. (2003).

Concurrent with the development of the Common Land Model, the NCAR LSM was undergoing further development at NCAR in the areas of carbon cycling, vegetation dynamics, and river routing. The preservation of these advancements necessitated several modifications to the Common Land Model. The biome-type land cover classification scheme was replaced with a plant functional type (PFT) representation with the specification of PFTs and leaf area index from satellite data (Oleson and Bonan 2000, Bonan et al. 2002a,b). This also required modifications to parameterizations for vegetation albedo and vertical burying of vegetation by snow. Changes were made to canopy scaling, leaf physiology, and soil water limitations on photosynthesis to resolve deficiencies indicated by the coupling to a dynamic vegetation model. Vertical heterogeneity in soil texture was implemented to improve coupling with a dust emission model. A river routing model was incorporated to improve the fresh water balance over oceans. Numerous modest changes were made to the parameterizations to conform to the strict energy and water balance requirements of CCSM. Further substantial software development was also required to meet coding standards. The model that resulted was adopted in May 2002 as the Community Land Model (CLM2.0) for use with the Community Atmosphere Model (CAM2.0, the successor to CCM3) and version 2 of the Community Climate System Model (CCSM2.0).

K. Oleson reported on initial results from a coupling of CCM3 with CLM2 at the June 2001 CCSM Workshop LMWG meeting. Generally, the CLM2 preserved most of the improvements seen in the Common Land Model, particularly with respect to surface air temperature, runoff, and snow. These simulations are documented in Bonan et al. (2002a). Further small improvements to the biogeophysical parameterizations, ongoing software development, and extensive analysis and validation within CAM2.0 and CCSM2.0 culminated in the release of CLM2.0 to the community in May 2002.

Following this release, Peter Thornton implemented changes to the model structure required to represent carbon and nitrogen cycling in the model. This involved changing data structures from a single vector of spatially independent sub-grid patches to one that recognizes three hierarchical scales within a model grid cell: land unit, snow/soil column, and PFT. Furthermore, as an option, the model can be configured so that PFTs can share a single soil column and thus "compete" for water. This version of the model (CLM2.1) was released to the community in February 2003. CLM2.1, without the compete option turned on, produces only roundoff level changes when compared to CLM2.0.

CLM3.0 (denoted hereafter as CLM) contains further software improvements related to performance and model output, a re-writing of the code to support vector-based computational platforms, and improvements in biogeophysical parameterizations to correct deficiencies in the coupled model climate. Competition between PFTs for water, in which all PFTs share a single soil column, is the default mode of operation in this model version.

Active research is underway to mitigate known deficiencies and expand the capabilities of the model. Long term research areas related to biogeophysics include fractional vegetation cover, emissivity, leaf temperature and canopy storage, interception, infiltration and runoff, and temperature diagnostics. Biogeochemical research includes carbon and nitrogen cycles, dynamic vegetation, mineral aerosols, dry deposition, and water and carbon isotopes. Research related to land use and land cover change includes urbanization, soil degradation, and agricultural modeling.

The CLM is designed for coupling to atmospheric numerical models. It provides surface albedos (direct beam and diffuse for visible and near-infrared wavebands), upward longwave radiation, sensible heat flux, latent heat flux, water vapor flux, and zonal and meridional surface stresses required by atmospheric models. These are regulated in part by many ecological and hydrological processes, and the model simulates processes such as leaf phenology, stomatal physiology, and the hydrologic cycle. The model accounts for ecological differences among vegetation types, hydraulic and thermal differences among soil types, and allows for multiple land cover types within a grid cell. A river transport model routes runoff downstream to oceans. Future versions of the model will include the carbon cycle and biogeochemical cycles. Because the model is designed for coupling to climate and numerical weather prediction models, there is a compromise between computational efficiency and the complexity with which land surface processes are parameterized. The model is not meant to be a detailed description of hydrometeorology and terrestrial ecosystems, but rather a simplified treatment of surface processes that reproduces at minimal computational cost the essential characteristics of land-atmosphere interactions important for climate simulations and weather prediction.

1.1.2 Surface Heterogeneity and Data Structure

Spatial land surface heterogeneity in CLM is represented as a nested subgrid hierarchy in which grid cells are composed of multiple landunits, snow/soil columns, and PFTs (Figure 1.1). Each grid cell can have a different number of landunits, each landunit can have a different number of columns, and each column can have multiple PFTs. The first subgrid level, the landunit, is intended to capture the broadest spatial patterns of subgrid heterogeneity. The specific landunits are glacier, lake, wetland, urban, and vegetated. Physical soil properties such as texture, color, depth, and thermal conductivity are defined at the landunit subgrid level and hence landunits can vary in soil properties.

The second subgrid level, the column, is intended to capture potential variability in the soil and snow state variables within a single landunit. For example, the vegetated landunit may contain several columns with independently evolving vertical profiles of soil water and temperature. The snow/soil column is represented by 10 layers for soil and up to five layers for snow, depending on snow depth. The central characteristic of the column subgrid level is that this is where the state variables for water and energy in the soil and snow are defined, as well as the fluxes of these components within the soil and snow. Regardless of the number and type of PFTs occupying space on the column, the column physics operates with a single set of upper boundary fluxes, as well as a single set of transpiration fluxes from multiple soil levels. These boundary fluxes are weighted averages over all PFTs.

The third subgrid level is referred to as the PFT level, but it also includes the treatment for bare ground. It is intended to capture the biogeophysical and biogeochemical differences between broad categories of plants in terms of their functional characteristics. Up to 4 of 15 possible PFTs that differ in physiology and structure may coexist on a single column. All fluxes to and from the surface are defined at the PFT level, as are the vegetation state variables (e.g. vegetation temperature and canopy water storage).

In addition to state and flux variable data structures for conserved components at each subgrid level (e.g., energy, water, carbon), each subgrid level also has a physical state data structure for handling quantities that are not involved in conservation checks (diagnostic variables). For example, soil texture is defined through physical state variables at the landunit level, the number of snow layers and the roughness lengths are defined as physical state variables at the column level, and the leaf area index and the fraction of canopy that is wet are defined as physical state variables at the PFT level.

The current default configuration of the model subgrid hierarchy is illustrated in Figure 1.1. The vegetated landunit consists of a single column with up to four PFTs occupying space on the column.

Figure 1.1. Current default configuration of the CLM subgrid hierarchy.

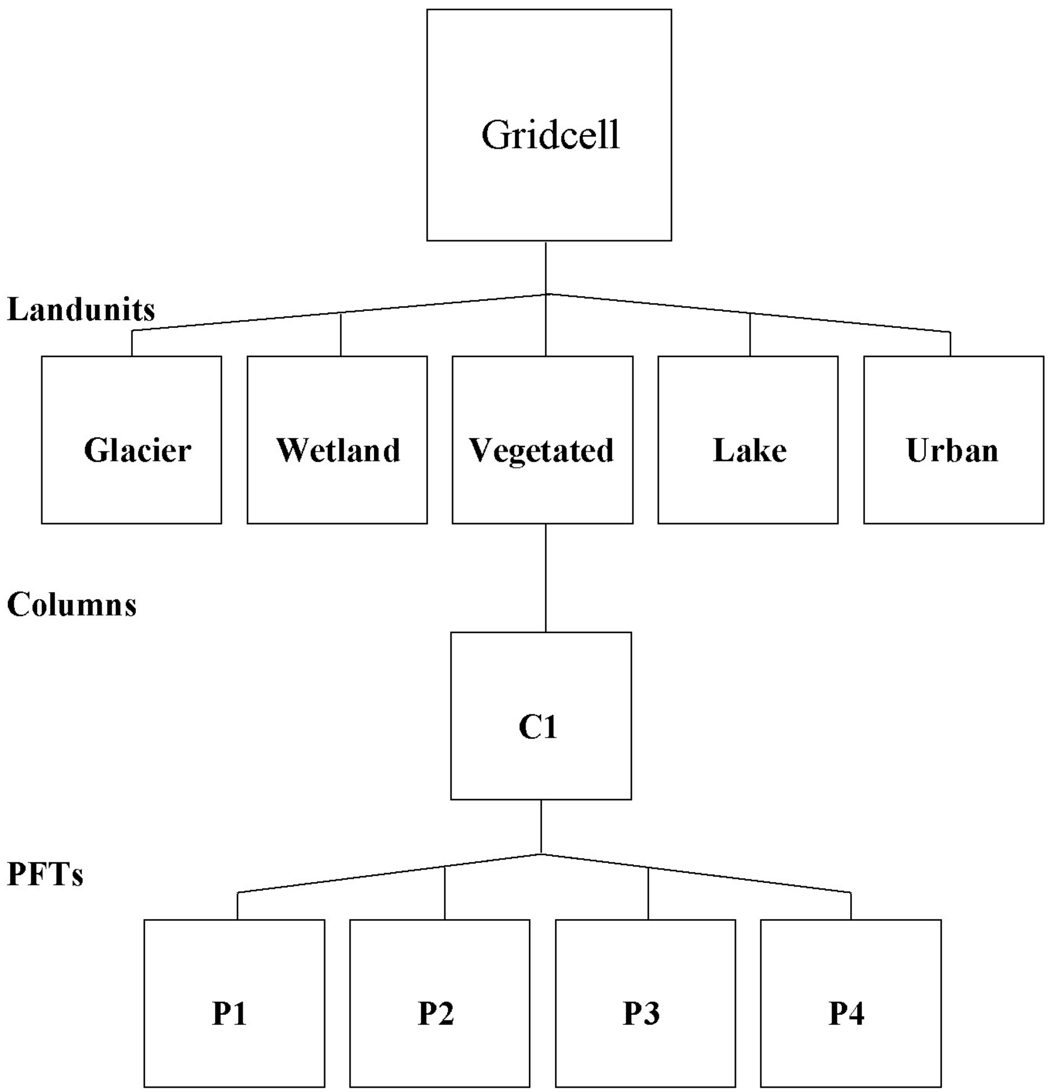

Note that the biogeophysical processes related to soil and snow require PFT level properties to be aggregated to the column level. For example, the net heat flux into the ground is required as a boundary condition for the solution of snow/soil temperatures (section 6). This column level property must be determined by aggregating the net heat flux from all PFTs sharing the column. This is generally accomplished in the model by computing a weighted sum of the desired quantity over all PFTs whose weighting depends on the PFT area relative to all PFTs, unless otherwise noted in the text.

1.1.3 Biogeophysical Processes

Biogeophysical processes are simulated for each subgrid landunit, column, and PFT independently and each subgrid unit maintains its own prognostic variables. The grid-average atmospheric forcing is used to force all subgrid units within a grid cell. The surface variables and fluxes required by the atmosphere are obtained by averaging the subgrid quantities weighted by their fractional areas. The processes simulated include (Figure 1.2):

- Vegetation composition, structure, and phenology (section 2)
- Absorption, reflection, and transmittance of solar radiation (section 3, 4)
- Absorption and emission of longwave radiation (section 4)
- Momentum, sensible heat (ground and canopy), and latent heat (ground evaporation, canopy evaporation, transpiration) fluxes (section 5)
- Heat transfer in soil and snow including phase change (section 6)
- Canopy hydrology (interception, throughfall, and drip) (section 7)
- Snow hydrology (snow accumulation and melt, compaction, water transfer between snow layers) (section 7)
- Soil hydrology (surface runoff, infiltration, sub-surface drainage, redistribution of water within the column) (section 7)
- Stomatal physiology and photosynthesis (section 8)

- Lake temperatures and fluxes (section 9)
- Routing of runoff from rivers to ocean (section 10)
- Volatile organic compounds (section 11)

Figure 1.2. Land biogeophysical and hydrologic processes simulated by CLM. Adapted from Bonan (2002).

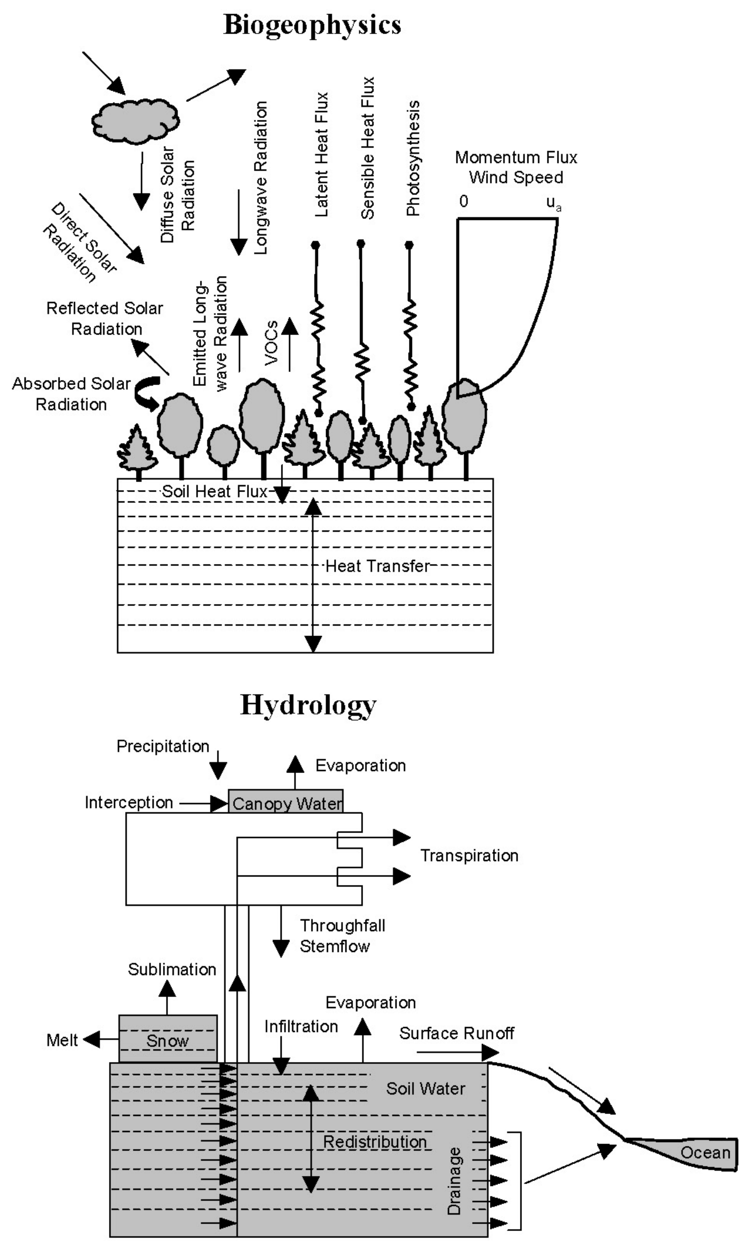

1.2 Model Requirements

1.2.1 Atmospheric Coupling

The current state of the atmosphere (Table 1.1) at a given time step is used to force the land model. This atmospheric state is provided by an atmospheric model in coupled mode. The land model then initiates a full set of calculations for surface energy, constituent, momentum, and radiative fluxes. The land model calculations are implemented in two steps. The land model proceeds with the calculation of surface energy, constituent, momentum, and radiative fluxes using the snow and soil hydrologic states from the previous time step. These fields are passed to the atmosphere (Table 1.2). The albedos sent to the atmosphere are for the solar zenith angle at the next time step but with surface conditions from the current time step. The land model then completes the soil and snow hydrology calculations. Of the variables passed to the atmosphere (Table 1.2), only the snow water equivalent changes during the soil and snow hydrology calculations.

Table 1.1. Atmospheric input to land model

[1]Reference height	z_{atm}	m
Zonal wind at z_{atm}	u_{atm}	m s^{-1}
Meridional wind at z_{atm}	v_{atm}	m s^{-1}
Potential temperature	$\overline{\theta_{atm}}$	K
Specific humidity at z_{atm}	q_{atm}	kg kg^{-1}
Pressure at z_{atm}	P_{atm}	Pa
Temperature at z_{atm}	T_{atm}	K
Incident longwave radiation	$L_{atm}\downarrow$	W m^{-2}
[2]Liquid precipitation	q_{rain}	mm s^{-1}
[2]Solid precipitation	q_{sno}	mm s^{-1}
Incident direct beam visible solar radiation	$S_{atm}\downarrow_{vis}^{\mu}$	W m^{-2}
Incident direct beam near-infrared solar radiation	$S_{atm}\downarrow_{nir}^{\mu}$	W m^{-2}
Incident diffuse visible solar radiation	$S_{atm}\downarrow_{vis}$	W m^{-2}
Incident diffuse near-infrared solar radiation	$S_{atm}\downarrow_{nir}$	W m^{-2}

[1]The reference heights for temperature, wind, and specific humidity ($z_{atm,h}$, $z_{atm,m}$, $z_{atm,w}$) are required. These are set equal to z_{atm}.

[2]The atmosphere provides convective and large-scale liquid and solid precipitation, which are added to yield total liquid precipitation q_{rain} and solid precipitation q_{sno}.

Density of air (ρ_{atm}) (kg m^{-3}) is also required but is calculated directly from $\rho_{atm} = \frac{P_{atm} - 0.378 e_{atm}}{R_{da} T_{atm}}$ where P_{atm} is atmospheric pressure (Pa), e_{atm} is atmospheric vapor pressure (Pa), R_{da} is the gas constant for dry air (J kg^{-1} K^{-1}) (Table 1.4), and T_{atm} is the atmospheric temperature (K). The atmospheric vapor pressure e_{atm} is derived from atmospheric specific humidity q_{atm} (kg kg^{-1}) as $e_{atm} = \frac{q_{atm} P_{atm}}{0.622 + 0.378 q_{atm}}$.

The CO_2 and O_2 concentrations (Pa) are required but are calculated from prescribed partial pressures and the atmospheric pressure P_{atm} as $c_a = 355 \times 10^{-6} P_{atm}$ and $o_i = 0.209 P_{atm}$.

Table 1.2. Land model output to atmospheric model

[1]Latent heat flux	$\lambda_{vap} E_v + \lambda E_g$	W m^{-2}
Sensible heat flux	$H_v + H_g$	W m^{-2}
Water vapor flux	$E_v + E_g$	mm s^{-1}
Zonal momentum flux	τ_x	kg m^{-1} s^{-2}
Meridional momentum flux	τ_y	kg m^{-1} s^{-2}
Emitted longwave radiation	$L\uparrow$	W m^{-2}
Direct beam visible albedo	$I\uparrow_{vis}^{\mu}$	-
Direct beam near-infrared albedo	$I\uparrow_{nir}^{\mu}$	-
Diffuse visible albedo	$I\uparrow_{vis}$	-
Diffuse near-infrared albedo	$I\uparrow_{nir}$	-
Absorbed solar radiation	$\vec{S}$	W m^{-2}
Radiative temperature	T_{rad}	K
Temperature at 2 meter height	T_{2m}	K
Specific humidity at 2 meter height	q_{2m}	kg kg^{-1}
Snow water equivalent	W_{sno}	m

[1] λ_{vap} is the latent heat of vaporization (J kg^{-1}) (Table 1.4) and λ is either the latent heat of vaporization λ_{vap} or latent heat of sublimation λ_{sub} (J kg^{-1}) (Table 1.4) depending on the liquid water and ice content of the top snow/soil layer (section 5.4).

1.2.2 Initialization

Initialization of the land model (i.e., providing the model with initial temperature and moisture states) depends on the type of run (initial, restart, or branch) (Vertenstein et al. 2004). An initial run starts the model from either initial conditions that are set internally in the code (referred to as arbitrary initial conditions) or from an initial conditions dataset that enables the model to start from a spun up state (i.e., where the land is in equilibrium with the simulated climate). In restart and branch runs, the model is continued from a previous simulation and initialized from a restart file that ensures that the output is bit-for-bit the same as if the previous simulation had not stopped. The fields that are required from the restart or initial conditions files can be obtained by examining the code. Arbitrary initial conditions are specified as follows.

Soil points are initialized with temperatures (vegetation T_v, ground T_g, radiative T_{rad}, and soil layers T_i, where $i = 1,\ldots,10$ is the soil layer) of 283 K, no snow or canopy water ($W_{sno} = 0$, $W_{can} = 0$), and volumetric soil water content $\theta_i = 0.3$ mm^3 mm^{-3}. Lake temperatures are initialized at 277 K and $W_{sno} = 0$. Wetlands are initialized at 277 K, θ_i =1.0, and $W_{sno} = 0$. Glacier temperatures are initialized to 250 K with a snow water equivalent $W_{sno} = 1000$ mm, snow depth $z_{sno} = \frac{W_{sno}}{\rho_{sno}}$ (m) where $\rho_{sno} = 250$ kg m^{-3} is an initial estimate for the bulk density of snow, snow age $\tau_{sno} = 0$, and θ_i =1.0. The snow layer structure (e.g., number of snow layers and layer thickness) is initialized based on the snow depth (section 6.1). The snow liquid water and ice contents (kg m^{-2}) are initialized as $w_{liq,i} = 0$ and $w_{ice,i} = \Delta z_i \rho_{sno}$, respectively, where $i = snl + 1,\ldots,0$ are the snow layers, Δz_i is the thickness of snow layer i (m), and snl is the negative of the number of snow layers (i.e., snl ranges from –5 to –1). The soil liquid water and ice contents are initialized as $w_{liq,i} = 0$ and $w_{ice,i} = \Delta z_i \rho_{ice} \theta_i$ for $T_i \le T_f$, and $w_{liq,i} = \Delta z_i \rho_{liq} \theta_i$ and $w_{ice,i} = 0$ for $T_i > T_f$, where ρ_{ice} and ρ_{liq} are the densities of ice and liquid water (kg m^{-3}) (Table 1.4), and T_f is the freezing temperature of water (K) (Table 1.4).

1.2.3 Surface Data

Required surface data for each land grid cell are listed in Table 1.3 and include the glacier, lake, wetland, and urban portions of the grid cell (vegetation occupies the remainder); the fractional cover of the 4 most abundant PFTs in the vegetated portion of the grid cell; monthly leaf and stem area index and canopy top and bottom heights for each PFT; soil color; and soil texture. These fields are aggregated to the model's grid from high-resolution surface datasets. The fractional cover of urban is currently zero pending completion of an urban parameterization.

Soil color determines dry and saturated soil albedo (section 3.2). The percent sand and clay determines soil thermal and hydrologic properties (section 6.3 and 7.4.1). The percentage of each PFT is with respect to the vegetated portion of the grid cell and the sum of the PFTs is 100%. The percent lake, wetland, glacier, and urban are specified with respect to the entire grid cell. The number of longitude points per latitude, the latitude and longitude at center of grid cell, a landmask (1-land, 0-other), and the fraction of land within grid cell (0-1) are also required. The number of longitude points should be the same for each latitude for a regular grid. The latitude and longitude (degrees) are used to determine the solar zenith angle (section 3.3).

Soil colors are from Zeng et al. (2002), which in turn are derived from Dickinson et al. (1993) with adjustments based on satellite data. The International Geosphere-Biosphere Programme (IGBP) soil dataset (Global Soil Data Task 2000) of 4931 soil mapping units and their sand and clay content for each soil layer were used to create a soil texture dataset that varies with depth (Bonan et al. 2002b). Percent lake and wetland were derived from Cogley's (1991) 1.0º by 1.0º data for perennial freshwater lakes and swamps/marshes. Glaciers were obtained from the IGBP Data and Information System Global 1-km Land Cover Data Set (IGBP DISCover) (Loveland et al. 2000). PFTs and their abundance, and leaf area index are inferred from 1-km satellite data as described in Bonan et al. (2002b). Stem area index and canopy top and bottom heights are from Bonan (1996) as described in Bonan et al. (2002b).

Table 1.3. Surface data required for CLM, their base spatial resolution, and method of aggregation to the model's grid

Surface Field	Resolution	Aggregation Method
Percent glacier	0.5°	Area average
Percent lake	1°	Area average
Percent wetland	1°	Area average
Percent sand, percent clay	5-minute	Soil mapping unit with greatest areal extent in grid cell
Soil color	2.8° (T42)	Soil color class with greatest areal extent in grid cell
PFTs (percent of vegetated land)	0.5°	Area average, choosing 4 most abundant PFTs
Monthly leaf and stem area index	0.5°	Area average
Canopy height (top, bottom)	0.5°	Area average

1.2.4 Adjustable Parameters and Physical Constants

Values of certain adjustable parameters inherent in the biogeophysical parameterizations have either been obtained from the literature or arrived at based on comparisons with observations. These are described in the text. Physical constants, shared by all of the components in the coupled modeling system, are presented in Table 1.4.

Table 1.4. Physical constants

Pi	π	3.14159265358979323846	-
Acceleration of gravity	g	9.80616	m s^{-2}
Standard pressure	P_{std}	101325	Pa
Stefan-Boltzmann constant	σ	5.67×10^{-8}	W m^{-2} K^{-4}
Boltzmann constant	κ	1.38065×10^{-23}	J K^{-1} molecule^{-1}
Avogadro's number	N_A	6.02214×10^{26}	molecule kmol^{-1}
Universal gas constant	R_{gas}	$N_A\kappa$	J K^{-1} kmol^{-1}
Molecular weight of dry air	MW_{da}	28.966	kg kmol^{-1}
Dry air gas constant	R_{da}	R_{gas}/MW_{da}	J K^{-1} kg^{-1}
Molecular weight of water vapor	MW_{wv}	18.016	kg kmol^{-1}
Water vapor gas constant	R_{wv}	R_{gas}/MW_{wv}	J K^{-1} kg^{-1}
Von Karman constant	k	0.4	-
Freezing temperature of fresh water	T_f	273.16	K
Density of liquid water	ρ_{liq}	1000	kg m^{-3}
Density of ice	ρ_{ice}	917	kg m^{-3}
Specific heat capacity of dry air	C_p	1.00464×10^{3}	J kg^{-1} K^{-1}
Specific heat capacity of water	C_{liq}	4.188×10^{3}	J kg^{-1} K^{-1}
Specific heat capacity of ice	C_{ice}	2.11727×10^{3}	J kg^{-1} K^{-1}
Latent heat of vaporization	λ_{vap}	2.501×10^{6}	J kg^{-1}
Latent heat of fusion	L_f	3.337×10^{5}	J kg^{-1}
Latent heat of sublimation	λ_{sub}	$\lambda_{vap}+L_f$	J kg^{-1}
[1]Thermal conductivity of water	λ_{liq}	0.6	W m^{-1} K^{-1}
[1]Thermal conductivity of ice	λ_{ice}	2.29	W m^{-1} K^{-1}
[1]Thermal conductivity of air	λ_{air}	0.023	W m^{-1} K^{-1}
Radius of the earth	R_e	6.37122×10^{6}	m

[1]Not shared by other components of the coupled modeling system.

2. Ecosystem Composition and Structure

2.1 Vegetation Composition

Vegetated surfaces are comprised of up to 4 of 15 possible plant functional types (PFTs) plus bare ground (Table 2.1). These PFTs differ in physiological and morphological traits along with climatic preferences (Bonan et al. 2002b). The 7 primary PFTs are needleleaf evergreen or deciduous tree, broadleaf evergreen or deciduous tree, shrub, grass, and crop. These 7 primary PFTs were expanded to 15 physiological variants based on climate rules to distinguish arctic, boreal, temperate, and tropical PFTs, C_3 and C_4 grasses, and evergreen and deciduous shrubs. These plant types differ in leaf and stem optical properties that determine reflection, transmittance, and absorption of solar radiation (Table 3.1), root distribution parameters that control the uptake of water from the soil (Table 8.1), aerodynamic parameters that determine resistance to heat, moisture, and momentum transfer (Table 5.1), and photosynthetic parameters that determine stomatal resistance, photosynthesis, and transpiration (Table 8.2). Parameter values are as in Bonan et al. (2002a) with root distribution parameters from Zeng (2001). Currently, the composition and abundance of PFTs within a grid cell are time-invariant and are prescribed from 1-km satellite data (Bonan et al. 2002a,b).

Table 2.1. Plant functional types

Plant functional type	Acronym
Needleleaf evergreen tree – temperate	NET Temperate
Needleleaf evergreen tree - boreal	NET Boreal
Needleleaf deciduous tree – boreal	NDT Boreal
Broadleaf evergreen tree – tropical	BET Tropical
Broadleaf evergreen tree – temperate	BET Temperate
Broadleaf deciduous tree – tropical	BDT Tropical
Broadleaf deciduous tree – temperate	BDT Temperate
Broadleaf deciduous tree – boreal	BDT Boreal
Broadleaf evergreen shrub - temperate	BES Temperate
Broadleaf deciduous shrub – temperate	BDS Temperate
Broadleaf deciduous shrub – boreal	BDS Boreal
C_3 arctic grass	-
C_3 grass	-
C_4 grass	-
Crop1	-
[1]Crop2	-

[1]Two types of crops are allowed to account for the different physiology of crops, but currently only the first crop type is specified in the surface dataset.

2.2 Vegetation Structure

Vegetation structure is defined by leaf and stem area indices (L, S) (section 2.3) and canopy top and bottom heights (z_{top}, z_{bot}) (Table 2.2). Separate leaf and stem area indices and canopy heights are specified for each PFT. Daily leaf and stem area indices are obtained from gridded datasets of monthly values (section 2.3). Canopy top and bottom heights are also obtained from gridded datasets. However, these are currently invariant in space and time and were obtained from PFT-specific values (Bonan et al. 2002a).

Table 2.2. Plant functional type heights

Plant functional type	z_{top} (m)	z_{bot} (m)
NET Temperate	17	8.5
NET Boreal	17	8.5
NDT Boreal	14	7
BET Tropical	35	1
BET temperate	35	1
BDT tropical	18	10
BDT temperate	20	11.5
BDT boreal	20	11.5
BES temperate	0.5	0.1
BDS temperate	0.5	0.1
BDS boreal	0.5	0.1
C_3 arctic grass	0.5	0.01
C_3 grass	0.5	0.01
C_4 grass	0.5	0.01
Crop1	0.5	0.01
Crop2	0.5	0.01

2.3 Phenology

Leaf and stem area indices (m^2 leaf area m^{-2} ground area) are updated daily by linearly interpolating between monthly values. Leaf area index is developed from 1-km AVHRR red and near-infrared reflectances obtained from the U.S. Geological Survey Earth Resources Observation System (EROS) Data Center Distributed Active Archive Center (DAAC) (Eidenshink and Faundeen 1994, DeFries et al. 2000) as described in

Bonan et al. (2002b). Stem area index is from Bonan (1996) with the data in the Southern Hemisphere being offset by six months. The leaf and stem area indices are adjusted for vertical burying by snow as

$$A = A^{*}\left(1 - f_{veg}^{sno}\right) \tag{2.1}$$

where A^{*} is the leaf or stem area before adjustment for snow, A is the remaining exposed leaf or stem area, f_{veg}^{sno} is the vertical fraction of vegetation covered by snow

$$f_{veg}^{sno} = \frac{z_{sno} - z_{bot}}{z_{top} - z_{bot}} \qquad \text{for } z_{sno} - z_{bot} \ge 0,\ 0 \le f_{veg}^{sno} \le 1, \tag{2.2}$$

and z_{sno} is the depth of snow (m) (section 7.2). For numerical reasons, exposed leaf and stem area are set to zero if less than 0.05. If the sum of exposed leaf and stem area is zero, then the surface is treated as snow-covered ground.

3. Surface Albedos

3.1 Canopy Radiative Transfer

Radiative transfer within vegetative canopies is calculated from the two-stream approximation of Dickinson (1983) and Sellers (1985) as described by Bonan (1996)

$$-\bar{\mu}\frac{dI\uparrow}{d\left(L+S\right)}+\left[1-\left(1-\beta\right)\omega\right]I\uparrow-\omega\beta I\downarrow=\omega\bar{\mu}K\beta_0 e^{-K\left(L+S\right)} \tag{3.1}$$

$$\bar{\mu}\frac{dI\downarrow}{d\left(L+S\right)}+\left[1-\left(1-\beta\right)\omega\right]I\downarrow-\omega\beta I\uparrow=\omega\bar{\mu}K\left(1-\beta_0\right)e^{-K\left(L+S\right)} \tag{3.2}$$

where $I\uparrow$ and $I\downarrow$ are the upward and downward diffuse radiative fluxes per unit incident flux, $K=G\left(\mu\right)/\mu$ is the optical depth of direct beam per unit leaf and stem area, μ is the cosine of the zenith angle of the incident beam, $G\left(\mu\right)$ is the relative projected area of leaf and stem elements in the direction $\cos^{-1}\mu$, $\bar{\mu}$ is the average inverse diffuse optical depth per unit leaf and stem area, ω is a scattering coefficient, β and β_0 are upscatter parameters for diffuse and direct beam radiation, respectively, L is the exposed leaf area index (section 2.3), and S is the exposed stem area index (section 2.3). Given the direct beam albedo $\alpha_{g,\Lambda}^{\mu}$ and diffuse albedo $\alpha_{g,\Lambda}$ of the ground (section 3.2), these equations are solved to calculate the fluxes, per unit incident flux, absorbed by the vegetation, reflected by the vegetation, and transmitted through the vegetation for direct and diffuse radiation and for visible ($<0.7\,\mu\mathrm{m}$) and near-infrared ($\geq 0.7\,\mu\mathrm{m}$) wavebands. The optical parameters $G\left(\mu\right)$, $\bar{\mu}$, ω, β, and β_0 are calculated based on work in Sellers (1985) as follows.

The relative projected area of leaves and stems in the direction $\cos^{-1}\mu$ is

$$G(\mu) = \phi_1 + \phi_2 \mu \tag{3.3}$$

where $\phi_1 = 0.5 - 0.633\chi_L - 0.33\chi_L^2$ and $\phi_2 = 0.877(1 - 2\phi_1)$ for $-0.4 \le \chi_L \le 0.6$. χ_L is the departure of leaf angles from a random distribution and equals +1 for horizontal leaves, 0 for random leaves, and –1 for vertical leaves.

The average inverse diffuse optical depth per unit leaf and stem area is

$$\bar{\mu} = \int_0^1 \frac{\mu'}{G(\mu')} d\mu' = \frac{1}{\phi_2}\left[1 - \frac{\phi_1}{\phi_2}\ln\left(\frac{\phi_1 + \phi_2}{\phi_1}\right)\right] \tag{3.4}$$

where μ' is the direction of the scattered flux.

The optical parameters ω, β, and β_0, which vary with wavelength (Λ), are weighted combinations of values for vegetation and snow. The model determines that snow is on the canopy if $T_v \le T_f$, where T_v is the vegetation temperature (K) (section 5) and T_f is the freezing temperature of water (K) (Table 1.4). In this case, the optical parameters are

$$\omega_\Lambda = \omega_\Lambda^{veg}(1 - f_{wet}) + \omega_\Lambda^{sno} f_{wet} \tag{3.5}$$

$$\omega_\Lambda \beta_\Lambda = \omega_\Lambda^{veg} \beta_\Lambda^{veg}(1 - f_{wet}) + \omega_\Lambda^{sno} \beta_\Lambda^{sno} f_{wet} \tag{3.6}$$

$$\omega_\Lambda \beta_{0,\Lambda} = \omega_\Lambda^{veg} \beta_{0,\Lambda}^{veg}(1 - f_{wet}) + \omega_\Lambda^{sno} \beta_{0,\Lambda}^{sno} f_{wet} \tag{3.7}$$

where f_{wet} is the wetted fraction of the canopy (section 7.1). The snow and vegetation weights are applied to the products $\omega_\Lambda \beta_\Lambda$ and $\omega_\Lambda \beta_{0,\Lambda}$ because these products are used in the two-stream equations. If there is no snow in the canopy,

$$\omega_\Lambda = \omega_\Lambda^{veg} \tag{3.8}$$

$$\omega_\Lambda \beta_\Lambda = \omega_\Lambda^{veg} \beta_\Lambda^{veg} \tag{3.9}$$

$$\omega_\Lambda \beta_{0,\Lambda} = \omega_\Lambda^{veg} \beta_{0,\Lambda}^{veg}. \tag{3.10}$$

For vegetation, $\omega_\Lambda^{veg} = \alpha_\Lambda + \tau_\Lambda$. α_Λ is a weighted combination of the leaf and stem reflectances ($\alpha_\Lambda^{leaf}, \alpha_\Lambda^{stem}$)

$$\alpha_\Lambda = \alpha_\Lambda^{leaf} w_{leaf} + \alpha_\Lambda^{stem} w_{stem} \tag{3.11}$$

where $w_{leaf} = L/(L+S)$ and $w_{stem} = S/(L+S)$. τ_Λ is a weighted combination of the leaf and stem transmittances ($\tau_\Lambda^{leaf}, \tau_\Lambda^{stem}$)

$$\tau_\Lambda = \tau_\Lambda^{leaf} w_{leaf} + \tau_\Lambda^{stem} w_{stem}. \tag{3.12}$$

The upscatter for diffuse radiation is

$$\omega_\Lambda^{veg} \beta_\Lambda^{veg} = \frac{1}{2}\left[\alpha_\Lambda + \tau_\Lambda + (\alpha_\Lambda - \tau_\Lambda)\left(\frac{1+\chi_L}{2}\right)^2\right] \tag{3.13}$$

and the upscatter for direct beam radiation is

$$\omega_\Lambda^{veg} \beta_{0,\Lambda}^{veg} = \frac{1+\bar{\mu}K}{\bar{\mu}K} a_s(\mu)_\Lambda \tag{3.14}$$

where the single scattering albedo is

$$\begin{aligned} a_s(\mu)_\Lambda &= \frac{\omega_\Lambda^{veg}}{2} \int_0^1 \frac{\mu' G(\mu)}{\mu G(\mu') + \mu' G(\mu)} d\mu' \\ &= \frac{\omega_\Lambda^{veg}}{2} \frac{G(\mu)}{\mu\phi_2 + G(\mu)}\left[1 - \frac{\mu\phi_1}{\mu\phi_2 + G(\mu)} \ln\left(\frac{\mu\phi_1 + \mu\phi_2 + G(\mu)}{\mu\phi_1}\right)\right]. \end{aligned} \tag{3.15}$$

The upward diffuse fluxes per unit incident direct beam and diffuse flux (i.e., the surface albedos) are

$$I\uparrow_\Lambda^\mu = \frac{h_1}{\sigma} + h_2 + h_3 \tag{3.16}$$

$$I\uparrow_\Lambda = h_7 + h_8. \tag{3.17}$$

The downward diffuse fluxes per unit incident direct beam and diffuse radiation, respectively, are

$$I\downarrow_{\Lambda}^{\mu} = \frac{h_4}{\sigma} e^{-K(L+S)} + h_5 s_1 + \frac{h_6}{s_1} \tag{3.18}$$

$$I\downarrow_{\Lambda} = h_9 s_1 + \frac{h_{10}}{s_1}. \tag{3.19}$$

The parameters h_1 to h_{10}, σ, and s_1 are from Sellers (1985) [note the error in h_4 in Sellers (1985)]:

$$b = 1 - \omega_{\Lambda} + \omega_{\Lambda}\beta_{\Lambda} \tag{3.20}$$

$$c = \omega_{\Lambda}\beta_{\Lambda} \tag{3.21}$$

$$d = \omega_{\Lambda}\bar{\mu}K\beta_{0,\Lambda} \tag{3.22}$$

$$f = \omega_{\Lambda}\bar{\mu}K\left(1 - \beta_{0,\Lambda}\right) \tag{3.23}$$

$$h = \frac{\sqrt{b^2 - c^2}}{\bar{\mu}} \tag{3.24}$$

$$\sigma = \left(\bar{\mu}K\right)^2 + c^2 - b^2 \tag{3.25}$$

$$u_1 = b - c/\alpha_{g,\Lambda}^{\mu} \text{ or } u_1 = b - c/\alpha_{g,\Lambda} \tag{3.26}$$

$$u_2 = b - c\alpha_{g,\Lambda}^{\mu} \text{ or } u_2 = b - c\alpha_{g,\Lambda} \tag{3.27}$$

$$u_3 = f + c\alpha_{g,\Lambda}^{\mu} \text{ or } u_3 = f + c\alpha_{g,\Lambda} \tag{3.28}$$

$$s_1 = \exp\left[-h\left(L + S\right)\right] \tag{3.29}$$

$$s_2 = \exp\left[-K\left(L + S\right)\right] \tag{3.30}$$

$$p_1 = b + \bar{\mu}h \tag{3.31}$$

$$p_2 = b - \bar{\mu}h \tag{3.32}$$

$$p_3 = b + \bar{\mu}K \tag{3.33}$$

$$p_4 = b - \bar{\mu}K \tag{3.34}$$

$$d_1 = \frac{p_1\left(u_1 - \bar{\mu}h\right)}{s_1} - p_2\left(u_1 + \bar{\mu}h\right)s_1 \tag{3.35}$$

$$d_2 = \frac{u_2 + \bar{\mu}h}{s_1} - \left(u_2 - \bar{\mu}h\right)s_1 \tag{3.36}$$

$$h_1 = -dp_4 - cf \tag{3.37}$$

$$h_2 = \frac{1}{d_1}\left[\left(d - \frac{h_1}{\sigma}p_3\right)\frac{\left(u_1 - \bar{\mu}h\right)}{s_1} - p_2\left(d - c - \frac{h_1}{\sigma}\left(u_1 + \bar{\mu}K\right)\right)s_2\right] \tag{3.38}$$

$$h_3 = \frac{-1}{d_1}\left[\left(d - \frac{h_1}{\sigma}p_3\right)\left(u_1 + \bar{\mu}h\right)s_1 - p_1\left(d - c - \frac{h_1}{\sigma}\left(u_1 + \bar{\mu}K\right)\right)s_2\right] \tag{3.39}$$

$$h_4 = -fp_3 - cd \tag{3.40}$$

$$h_5 = \frac{-1}{d_2}\left[\left(\frac{h_4\left(u_2 + \bar{\mu}h\right)}{\sigma s_1}\right) + \left(u_3 - \frac{h_4}{\sigma}\left(u_2 - \bar{\mu}K\right)\right)s_2\right] \tag{3.41}$$

$$h_6 = \frac{1}{d_2}\left[\frac{h_4}{\sigma}\left(u_2 - \bar{\mu}h\right)s_1 + \left(u_3 - \frac{h_4}{\sigma}\left(u_2 - \bar{\mu}K\right)\right)s_2\right] \tag{3.42}$$

$$h_7 = \frac{c\left(u_1 - \bar{\mu}h\right)}{d_1 s_1} \tag{3.43}$$

$$h_8 = \frac{-c\left(u_1 + \bar{\mu}h\right)s_1}{d_1} \tag{3.44}$$

$$h_9 = \frac{u_2 + \bar{\mu}h}{d_2 s_1} \tag{3.45}$$

$$h_{10} = \frac{-s_1\left(u_2 - \bar{\mu}h\right)}{d_2} \tag{3.46}$$

Plant functional type optical properties (Table 3.1) were taken from Dorman and Sellers (1989). Optical properties for intercepted snow (Table 3.2) were taken from Sellers et al. (1986).

Table 3.1. Plant functional type optical properties

Plant Functional Type	χ_L	α_{vis}^{leaf}	α_{nir}^{leaf}	α_{vis}^{stem}	α_{nir}^{stem}	τ_{vis}^{leaf}	τ_{nir}^{leaf}	τ_{vis}^{stem}	τ_{nir}^{stem}
NET Temperate	0.01	0.07	0.35	0.16	0.39	0.05	0.10	0.001	0.001
NET Boreal	0.01	0.07	0.35	0.16	0.39	0.05	0.10	0.001	0.001
NDT Boreal	0.01	0.07	0.35	0.16	0.39	0.05	0.10	0.001	0.001
BET Tropical	0.10	0.10	0.45	0.16	0.39	0.05	0.25	0.001	0.001
BET temperate	0.10	0.10	0.45	0.16	0.39	0.05	0.25	0.001	0.001
BDT tropical	0.01	0.10	0.45	0.16	0.39	0.05	0.25	0.001	0.001
BDT temperate	0.25	0.10	0.45	0.16	0.39	0.05	0.25	0.001	0.001
BDT boreal	0.25	0.10	0.45	0.16	0.39	0.05	0.25	0.001	0.001
BES temperate	0.01	0.07	0.35	0.16	0.39	0.05	0.10	0.001	0.001
BDS temperate	0.25	0.10	0.45	0.16	0.39	0.05	0.25	0.001	0.001
BDS boreal	0.25	0.10	0.45	0.16	0.39	0.05	0.25	0.001	0.001
C_3 arctic grass	-0.30	0.11	0.58	0.36	0.58	0.07	0.25	0.220	0.380
C_3 grass	-0.30	0.11	0.58	0.36	0.58	0.07	0.25	0.220	0.380
C_4 grass	-0.30	0.11	0.58	0.36	0.58	0.07	0.25	0.220	0.380
Crop1	-0.30	0.11	0.58	0.36	0.58	0.07	0.25	0.220	0.380
Crop2	-0.30	0.11	0.58	0.36	0.58	0.07	0.25	0.220	0.380

Table 3.2. Intercepted snow optical properties

	Waveband (Λ)	
Parameter	vis	nir
ω^{sno}	0.8	0.4
β^{sno}	0.5	0.5
β_0^{sno}	0.5	0.5

3.2 Ground Albedos

The overall direct beam $\alpha_{g,\Lambda}^{\mu}$ and diffuse $\alpha_{g,\Lambda}$ ground albedos are weighted combinations of "soil" and snow albedos

$$\alpha_{g,\Lambda}^{\mu} = \alpha_{soi,\Lambda}^{\mu} \left(1 - f_{sno}\right) + \alpha_{sno,\Lambda}^{\mu} f_{sno} \tag{3.47}$$

$$\alpha_{g,\Lambda} = \alpha_{soi,\Lambda} \left(1 - f_{sno}\right) + \alpha_{sno,\Lambda} f_{sno} \tag{3.48}$$

where f_{sno} is the fraction of the ground covered with snow which is calculated from

$$f_{sno} = \frac{z_{sno}}{10 z_{0m,g} + z_{sno}} \tag{3.49}$$

where z_{sno} is the depth of snow (m) (section 7.2), and $z_{0m,g} = 0.01$ is the momentum roughness length for soil (m) (section 5).

$\alpha_{soi,\Lambda}^{\mu}$ and $\alpha_{soi,\Lambda}$ vary with glacier, lake, wetland, and soil surfaces. Glacier albedos are from NCAR LSM (Bonan 1996)

$$\alpha_{soi,vis}^{\mu} = \alpha_{soi,vis} = 0.80$$

$$\alpha_{soi,nir}^{\mu} = \alpha_{soi,nir} = 0.55 .$$

Unfrozen lake and wetland albedos depend on the cosine of the solar zenith angle μ

$$\alpha_{soi,\Lambda}^{\mu} = \alpha_{soi,\Lambda} = 0.05\left(\mu + 0.15\right)^{-1}. \tag{3.50}$$

Frozen lake and wetland albedos are from NCAR LSM (Bonan 1996)

$$\alpha_{soi,vis}^{\mu} = \alpha_{soi,vis} = 0.60$$

$$\alpha_{soi,nir}^{\mu} = \alpha_{soi,nir} = 0.40 .$$

As in NCAR LSM (Bonan 1996), soil albedos vary with color class

$$\alpha_{soi,\Lambda}^{\mu} = \alpha_{soi,\Lambda} = \left(\alpha_{sat,\Lambda} + \Delta\right) \le \alpha_{dry,\Lambda} \tag{3.51}$$

where Δ depends on the volumetric water content of the first soil layer θ_1 (section 7.4) as $\Delta = 0.11 - 0.40\theta_1 > 0$, and $\alpha_{sat,\Lambda}$ and $\alpha_{dry,\Lambda}$ are albedos for saturated and dry soil color classes (Table 3.3).

Table 3.3. Dry and saturated soil albedos

	Dry		Saturated	
Color Class	vis	nir	vis	nir
1 = light	0.24	0.48	0.12	0.24
2	0.22	0.44	0.11	0.22
3	0.20	0.40	0.10	0.20
4	0.18	0.36	0.09	0.18
5	0.16	0.32	0.08	0.16
6	0.14	0.28	0.07	0.14
7	0.12	0.24	0.06	0.12
8 = dark	0.10	0.20	0.05	0.10

Snow albedos are taken from BATS (Dickinson et al. 1993), which are inferred from the work of Wiscombe and Warren (1980) and Anderson (1976). The direct beam albedo is

$$\alpha_{sno,\Lambda}^{\mu} = \alpha_{sno,\Lambda} + 0.4 f\left(\mu\right)\left[1 - \alpha_{sno,\Lambda}\right]. \tag{3.52}$$

The function $f\left(\mu\right)$ is a factor between 0 and 1 giving the increase of snow albedo due to solar zenith angle exceeding 60º

$$f\left(\mu\right) = \begin{cases} \left[\dfrac{1+\dfrac{1}{b}}{1+\mu 2b} - \dfrac{1}{b}\right] \geq 0 & \text{for } \mu \leq 0.5 \\ 0 & \text{for } \mu > 0.5 \end{cases} \tag{3.53}$$

The parameter $b = 2.0$ controls the solar zenith angle dependence and is based on best available data (Dickinson et al. 1993).

The diffuse albedo is

$$\alpha_{sno,\Lambda} = \left[1 - C_{\Lambda} F_{age}\right] \alpha_{sno,\Lambda,0} \tag{3.54}$$

where $\alpha_{sno,\Lambda,0}$ is the albedo of new snow for solar zenith angle less than 60º (Table 3.4) and C_{Λ} is an empirical constant (Table 3.4). The term F_{age} is a transformed snow age used to give the fractional reduction of snow albedo due to snow aging (assumed to represent increasing grain size and dirt, soot content) for solar zenith angle less than 60º

$$F_{age} = 1 - \frac{1}{1+\tau_{sno}}. \tag{3.55}$$

The non-dimensional age of snow τ_{sno} is incremented as a model prognostic variable at each time step as follows

$$\Delta \tau_{sno} = \begin{cases} \tau_0 \left(r_1 + r_2 + r_3\right) \Delta t & \text{for } 0 < W_{sno} \leq 800 \\ 0 & \text{for } W_{sno} > 800 \end{cases} \tag{3.56}$$

where Δt is the model time step (s), $\tau_0 = 1 \times 10^{-6}$ (s^{-1}), and W_{sno} is the mass of snow water (kg m^{-2}) (section 7.2).

The term r_1 represents the effect of grain growth due to vapor diffusion

$$r_1 = \exp\left[5000\left(\frac{1}{T_f} - \frac{1}{T_{snl+1}}\right)\right] \tag{3.57}$$

where T_{snl+1} is the surface temperature of the top snow layer with snl being the negative of the number of snow layers (section 6). The term r_2 represents the additional effect near and at freezing of melt water

$$r_2 = r_1^{10} \le 1. \tag{3.58}$$

The term r_3 represents the effect of dirt and soot

$$r_3 = 0.3. \tag{3.59}$$

A snowfall of 10 kg m^{-2} liquid water equivalent is assumed to restore the surface snow age, hence albedo, to that of new snow ($F_{age} = 0$). Since the precipitation in one model time step will generally be less than that required to restore the surface when it snows for a given time step, the snow age is reduced by a factor depending on the amount of fresh snow as follows:

$$\tau_{sno}^{n+1} = \left(\tau_{sno}^{n} + \Delta\tau_{sno}\right)\left[1 - 0.1\left(W_{sno}^{n+1} - W_{sno}^{n}\right)\right] \ge 0 \tag{3.60}$$

where τ_{sno}^{n+1} is the updated snow age at the current time step, τ_{sno}^{n} is the snow age at the previous time step, and $W_{sno}^{n+1} - W_{sno}^{n} \ge 0$ is the change in mass of snow water (kg m^{-2}) (section 7.2). After snow layers are combined or subdivided (section 7.2), the snow age τ_{sno} is set to zero if the number of snow layers is less than the maximum number of layers.

Table 3.4. Snow albedo parameters

	Waveband (Λ)	
Parameter	vis	nir
C_{Λ}	0.2	0.5
$\alpha_{sno,\Lambda,0}$	0.95	0.65

3.3 Solar Zenith Angle

The CLM uses the same formulation for solar zenith angle as the Community Atmosphere Model. The cosine of the solar zenith angle μ is

$$\mu = \sin\phi \sin\delta - \cos\phi \cos\delta \cos h \tag{3.61}$$

where h is the solar hour angle (radians) (24 hour periodicity), δ is the solar declination angle (radians), and ϕ is latitude (radians) (positive in Northern Hemisphere). The solar hour angle h (radians) is

$$h = 2\pi d + \theta \tag{3.62}$$

where d is calendar day ($d = 0.0$ at 0Z on January 1), and θ is longitude (radians) (positive east of the Greenwich meridian).

The solar declination angle δ is calculated as in Berger (1978a,b) and is valid for one million years past or hence, relative to 1950 A.D. The orbital parameters may be specified directly or the orbital parameters are calculated for the desired year. The required orbital parameters to be input by the user are the obliquity of the Earth ε (degrees, $-90^{\circ} < \varepsilon < 90^{\circ}$), Earth's eccentricity e ($0.0 < e < 0.1$), and the longitude of the perihelion relative to the moving vernal equinox $\tilde{\omega}$ ($0^{\circ} < \tilde{\omega} < 360^{\circ}$) (unadjusted for the apparent orbit of the Sun around the Earth (Berger et al. 1993)). The solar declination δ (radians) is

$$\delta = \sin^{-1}\left[\sin\left(\varepsilon\right)\sin\left(\lambda\right)\right] \tag{3.63}$$

where ε is Earth's obliquity and λ is the true longitude of the Earth.

The obliquity of the Earth ε (degrees) is

$$\varepsilon = \varepsilon^* + \sum_{i=1}^{i=47} A_i \cos\left(f_i t + \delta_i\right) \tag{3.64}$$

where ε^* is a constant of integration (Table 3.5), A_i, f_i, and δ_i are amplitude, mean rate, and phase terms in the cosine series expansion (Berger 1978a,b), and $t = t_0 - 1950$ where t_0 is the year. The series expansion terms are not shown here but can be found in the source code file shr_orb_mod.F90.

The true longitude of the Earth λ (radians) is counted counterclockwise from the vernal equinox ($\lambda = 0$ at the vernal equinox)

$$\lambda = \lambda_m + \left(2e - \frac{1}{4}e^3\right)\sin\left(\lambda_m - \tilde{\omega}\right) + \frac{5}{4}e^2 \sin 2\left(\lambda_m - \tilde{\omega}\right) + \frac{13}{12}e^3 \sin 3\left(\lambda_m - \tilde{\omega}\right) \tag{3.65}$$

where λ_m is the mean longitude of the Earth at the vernal equinox, e is Earth's eccentricity, and $\tilde{\omega}$ is the longitude of the perihelion relative to the moving vernal equinox. The mean longitude λ_m is

$$\lambda_m = \lambda_{m0} + \frac{2\pi\left(d - d_{ve}\right)}{365} \tag{3.66}$$

where $d_{ve} = 80.5$ is the calendar day at vernal equinox (March 21 at noon), and

$$\lambda_{m0} = 2\left[\left(\frac{1}{2}e + \frac{1}{8}e^3\right)\left(1+\beta\right)\sin\tilde{\omega} - \frac{1}{4}e^2\left(\frac{1}{2}+\beta\right)\sin 2\tilde{\omega} + \frac{1}{8}e^3\left(\frac{1}{3}+\beta\right)\sin 3\tilde{\omega}\right] \tag{3.67}$$

where $\beta = \sqrt{1-e^2}$. Earth's eccentricity e is

$$e = \sqrt{\left(e^{\cos}\right)^2 + \left(e^{\sin}\right)^2} \tag{3.68}$$

where

$$\begin{aligned} e^{\cos} &= \sum_{j=1}^{19} M_j \cos\left(g_j t + B_j\right), \\ e^{\sin} &= \sum_{j=1}^{19} M_j \sin\left(g_j t + B_j\right) \end{aligned} \tag{3.69}$$

are the cosine and sine series expansions for e, and M_j, g_j, and B_j are amplitude, mean rate, and phase terms in the series expansions (Berger 1978a,b). The longitude of the perihelion relative to the moving vernal equinox $\tilde{\omega}$ (degrees) is

$$\tilde{\omega} = \Pi \frac{180}{\pi} + \psi \tag{3.70}$$

where Π is the longitude of the perihelion measured from the reference vernal equinox (i.e., the vernal equinox at 1950 A.D.) and describes the absolute motion of the perihelion relative to the fixed stars, and ψ is the annual general precession in longitude and describes the absolute motion of the vernal equinox along Earth's orbit relative to the fixed stars. The general precession ψ (degrees) is

$$\psi = \frac{\tilde{\psi} t}{3600} + \zeta + \sum_{i=1}^{78} F_i \sin\left(f_i' t + \delta_i'\right) \tag{3.71}$$

where $\tilde{\psi}$ (arcseconds) and ζ (degrees) are constants (Table 3.5), and F_i, f_i', and δ_i' are amplitude, mean rate, and phase terms in the sine series expansion (Berger 1978a,b). The longitude of the perihelion Π (radians) depends on the sine and cosine series expansions for the eccentricity e as follows:

$$\Pi = \begin{cases} 0 & \text{for } -1\times10^{-8} \le e^{\cos} \le 1\times10^{-8} \text{ and } e^{\sin} = 0 \\ 1.5\pi & \text{for } -1\times10^{-8} \le e^{\cos} \le 1\times10^{-8} \text{ and } e^{\sin} < 0 \\ 0.5\pi & \text{for } -1\times10^{-8} \le e^{\cos} \le 1\times10^{-8} \text{ and } e^{\sin} > 0 \\ \tan^{-1}\left[\dfrac{e^{\sin}}{e^{\cos}}\right] + \pi & \text{for } e^{\cos} < -1\times10^{-8} \\ \tan^{-1}\left[\dfrac{e^{\sin}}{e^{\cos}}\right] + 2\pi & \text{for } e^{\cos} > 1\times10^{-8} \text{ and } e^{\sin} < 0 \\ \tan^{-1}\left[\dfrac{e^{\sin}}{e^{\cos}}\right] & \text{for } e^{\cos} > 1\times10^{-8} \text{ and } e^{\sin} \ge 0 \end{cases}. \quad (3.72)$$

The numerical solution for the longitude of the perihelion $\tilde{\omega}$ is constrained to be between 0 and 360 degrees (measured from the autumn equinox). A constant 180 degrees is then added to $\tilde{\omega}$ because the Sun is considered as revolving around the Earth (geocentric coordinate system) (Berger et al. 1993).

Table 3.5. Orbital parameters

Parameter	
ε^*	23.320556
$\tilde{\psi}$ (arcseconds)	50.439273
ζ (degrees)	3.392506

4. Radiative Fluxes

The net radiation at the surface is $\left(\vec{S}_v + \vec{S}_g\right) - \left(\vec{L}_v + \vec{L}_g\right)$, where $\vec{S}$ is the net solar flux absorbed by the vegetation ("v") and the ground ("g") and $\vec{L}$ is the net longwave flux (positive toward the atmosphere) (W m^{-2}).

4.1 Solar Fluxes

With reference to Figure 4.1, the direct beam flux transmitted through the canopy, per unit incident flux, is $e^{-K(L+S)}$, and the direct beam and diffuse fluxes absorbed by the vegetation, per unit incident flux, are

$$\vec{I}_{\Lambda}^{\mu} = 1 - I\uparrow_{\Lambda}^{\mu} - \left(1-\alpha_{g,\Lambda}\right) I\downarrow_{\Lambda}^{\mu} - \left(1-\alpha_{g,\Lambda}^{\mu}\right) e^{-K(L+S)} \tag{4.1}$$

$$\vec{I}_{\Lambda} = 1 - I\uparrow_{\Lambda} - \left(1-\alpha_{g,\Lambda}\right) I\downarrow_{\Lambda}. \tag{4.2}$$

$I\uparrow_{\Lambda}^{\mu}$ and $I\uparrow_{\Lambda}$ are the upward diffuse fluxes, per unit incident direct beam and diffuse flux (section 3.1). $I\downarrow_{\Lambda}^{\mu}$ and $I\downarrow_{\Lambda}$ are the downward diffuse fluxes below the vegetation per unit incident direct beam and diffuse radiation (section 3.1). $\alpha_{g,\Lambda}^{\mu}$ and $\alpha_{g,\Lambda}$ are the direct beam and diffuse ground albedos (section 3.2). L and S are the exposed leaf area index and stem area index (section 2.3).

Figure 4.1. Schematic diagram of (a) direct beam radiation, (b) diffuse solar radiation, and (c) longwave radiation absorbed, transmitted, and reflected by vegetation and ground. For clarity, terms involving $T^{n+1} - T^{n}$ are not shown in (c).

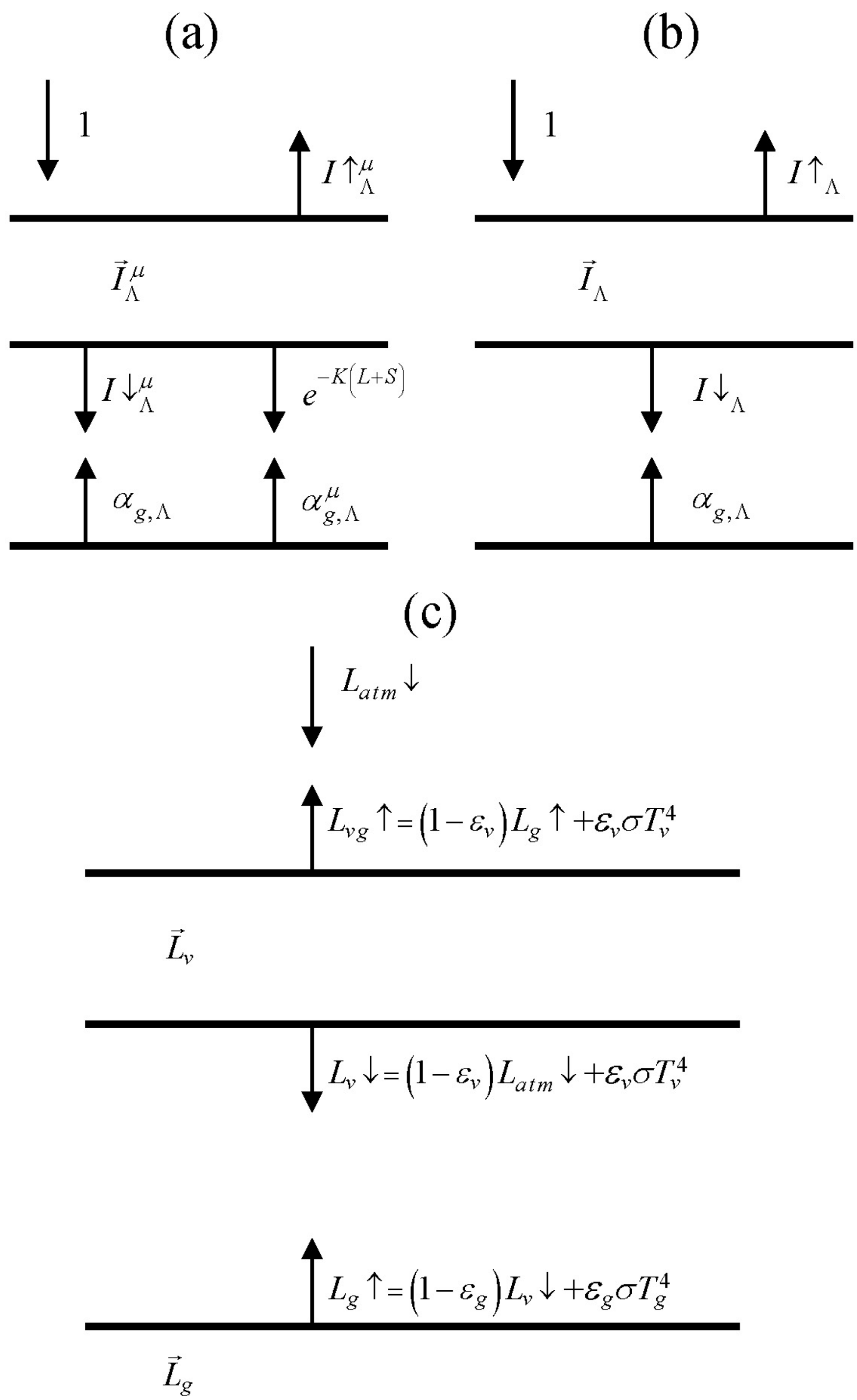

The total solar radiation absorbed by the vegetation and ground is

$$\vec{S}_v = \sum_{\Lambda} S_{atm} \downarrow^{\mu}_{\Lambda} \vec{I}^{\mu}_{\Lambda} + S_{atm} \downarrow_{\Lambda} \vec{I}_{\Lambda} \tag{4.3}$$

$$\begin{aligned} \vec{S}_g = \sum_{\Lambda} S_{atm} \downarrow^{\mu}_{\Lambda} e^{-K(L+S)} \left(1-\alpha^{\mu}_{g,\Lambda}\right) + \\ \left(S_{atm} \downarrow^{\mu}_{\Lambda} I \downarrow^{\mu}_{\Lambda} + S_{atm} \downarrow_{\Lambda} I \downarrow_{\Lambda}\right)\left(1-\alpha_{g,\Lambda}\right) \end{aligned} \tag{4.4}$$

where $S_{atm} \downarrow^{\mu}_{\Lambda}$ and $S_{atm} \downarrow_{\Lambda}$ are the incident direct beam and diffuse solar fluxes (W m^{-2}).

For non-vegetated surfaces, $e^{-K(L+S)} = 1$, $\vec{I}^{\mu}_{\Lambda} = \vec{I}_{\Lambda} = 0$, $I \downarrow^{\mu}_{\Lambda} = 0$, and $I \downarrow_{\Lambda} = 1$, so that

$$\begin{aligned} \vec{S}_g &= \sum_{\Lambda} S_{atm} \downarrow^{\mu}_{\Lambda} \left(1-\alpha^{\mu}_{g,\Lambda}\right) + S_{atm} \downarrow_{\Lambda} \left(1-\alpha_{g,\Lambda}\right) \\ \vec{S}_v &= 0 \end{aligned} . \tag{4.5}$$

Solar radiation is conserved as

$$\sum_{\Lambda} \left(S_{atm} \downarrow^{\mu}_{\Lambda} + S_{atm} \downarrow_{\Lambda}\right) = \left(\vec{S}_v + \vec{S}_g\right) + \sum_{\Lambda} \left(S_{atm} \downarrow^{\mu}_{\Lambda} I \uparrow^{\mu}_{\Lambda} + S_{atm} \downarrow_{\Lambda} I \uparrow_{\Lambda}\right) \tag{4.6}$$

where the latter term in parentheses is reflected solar radiation.

Photosynthesis and transpiration depend non-linearly on solar radiation, via the light response of stomata. Here, sunlit leaves are assumed to absorb all of the visible and diffuse solar radiation absorbed by the vegetation (excluding that which is absorbed by stems). The sunlit fraction of the canopy is

$$f_{sun} = \frac{\int_0^{L+S} e^{-K'x} dx}{L+S} = \frac{1-e^{-K'(L+S)}}{K'(L+S)} \tag{4.7}$$

where $e^{-K'(L+S)}$ is the fractional area of sunflecks on a horizontal plane below the leaf and stem area index $L+S$ (section 2.3). The shaded fraction is $f_{sha} = 1 - f_{sun}$, and the sunlit and shaded leaf area indices are $L^{sun} = f_{sun} L$ and $L^{sha} = f_{sha} L$. In calculating f_{sun},

$$K' = \frac{G(\mu)}{\mu}\sqrt{1-\omega_{vis}^{veg}}\,, \tag{4.8}$$

where $\sqrt{1-\omega_{vis}^{veg}}$ accounts for scattering within the canopy (Sellers 1985) and ω_{vis}^{veg}, $G(\mu)$, and μ are parameters in the two-stream approximation (section 3.1). To prevent numerical instabilities, $f_{sun} = 0$ when the sunlit fraction is less than 0.01.

The solar radiation absorbed by the sunlit and shaded leaves in the visible waveband ($< 0.7\mu\text{m}$) is, for $f_{sun} > 0$,

$$\begin{aligned} \phi^{sun} &= \left(S_{atm}\downarrow_{vis}^{\mu}\ \vec{I}_{vis}^{\mu} + S_{atm}\downarrow_{vis}\ \vec{I}_{vis}\right)\frac{L}{L+S}. \\ \phi^{sha} &= 0 \end{aligned} \tag{4.9}$$

These equations assume the sunlit leaves absorb $L/(L+S)$ of the solar radiation absorbed by the vegetation.

4.2 Longwave Fluxes

The net longwave radiation (W m^{-2}) (positive toward the atmosphere) at the surface is

$$\vec{L} = L\uparrow - L_{atm}\downarrow \tag{4.10}$$

where $L\uparrow$ is the upward longwave radiation from the surface and $L_{atm}\downarrow$ is the downward atmospheric longwave radiation (W m^{-2}). The radiative temperature T_{rad} (K) is defined from the upward longwave radiation as

$$T_{rad} = \left(\frac{L\uparrow}{\sigma}\right)^{1/4} \tag{4.11}$$

where σ is the Stefan-Boltzmann constant (W m^{-2} K^{-4}) (Table 1.4). With reference to Figure 4.1, the upward longwave radiation from the surface to the atmosphere is

$$L\uparrow = \delta_{veg} L_{vg}\uparrow + \left(1-\delta_{veg}\right)\left(1-\varepsilon_g\right) L_{atm}\downarrow + \left(1-\delta_{veg}\right)\varepsilon_g \sigma \left(T_g^n\right)^4 + 4\varepsilon_g \sigma \left(T_g^n\right)^3 \left(T_g^{n+1} - T_g^n\right) \tag{4.12}$$

where $L_{vg}\uparrow$ is the upward longwave radiation from the vegetation/soil system for exposed leaf and stem area $L+S \geq 0.05$, δ_{veg} is a step function and is zero for $L+S < 0.05$ and one otherwise, ε_g is the ground emissivity, and T_g^{n+1} and T_g^n are the snow/soil surface temperatures at the current and previous time steps, respectively (section 6).

For non-vegetated surfaces, the above equation reduces to

$$L\uparrow = \left(1-\varepsilon_g\right) L_{atm}\downarrow + \varepsilon_g \sigma \left(T_g^n\right)^4 + 4\varepsilon_g \sigma \left(T_g^n\right)^3 \left(T_g^{n+1} - T_g^n\right) \tag{4.13}$$

where the first term is the atmospheric longwave radiation reflected by the ground, the second term is the longwave radiation emitted by the ground, and the last term is the increase (decrease) in longwave radiation emitted by the ground due to an increase (decrease) in ground temperature.

For vegetated surfaces, the upward longwave radiation from the surface reduces to

$$L\uparrow = L_{vg}\uparrow + 4\varepsilon_g \sigma \left(T_g^n\right)^3 \left(T_g^{n+1} - T_g^n\right) \tag{4.14}$$

where

$$
\begin{aligned}
L_{vg}\uparrow &= \left(1-\varepsilon_g\right)\left(1-\varepsilon_v\right)\left(1-\varepsilon_v\right)L_{atm}\downarrow \\
&\quad +\varepsilon_v\left[1+\left(1-\varepsilon_g\right)\left(1-\varepsilon_v\right)\right]\sigma\left(T_v^n\right)^3\left[T_v^n+4\left(T_v^{n+1}-T_v^n\right)\right] \\
&\quad +\varepsilon_g\left(1-\varepsilon_v\right)\sigma\left(T_g^n\right)^4 \\
&= \left(1-\varepsilon_g\right)\left(1-\varepsilon_v\right)\left(1-\varepsilon_v\right)L_{atm}\downarrow \\
&\quad +\varepsilon_v\sigma\left(T_v^n\right)^4 \\
&\quad +\varepsilon_v\left(1-\varepsilon_g\right)\left(1-\varepsilon_v\right)\sigma\left(T_v^n\right)^4 \\
&\quad +4\varepsilon_v\sigma\left(T_v^n\right)^3\left(T_v^{n+1}-T_v^n\right) \\
&\quad +4\varepsilon_v\left(1-\varepsilon_g\right)\left(1-\varepsilon_v\right)\sigma\left(T_v^n\right)^3\left(T_v^{n+1}-T_v^n\right) \\
&\quad +\varepsilon_g\left(1-\varepsilon_v\right)\sigma\left(T_g^n\right)^4
\end{aligned}
\tag{4.15}
$$

where ε_v is the vegetation emissivity and T_v^{n+1} and T_v^n are the vegetation temperatures at the current and previous time steps, respectively (section 5). The first term in the equation above is the atmospheric longwave radiation that is transmitted through the canopy, reflected by the ground, and transmitted through the canopy to the atmosphere. The second term is the longwave radiation emitted by the canopy directly to the atmosphere. The third term is the longwave radiation emitted downward from the canopy, reflected by the ground, and transmitted through the canopy to the atmosphere. The fourth term is the increase (decrease) in longwave radiation due to an increase (decrease) in canopy temperature that is emitted by the canopy directly to the atmosphere. The fifth term is the increase (decrease) in longwave radiation due to an increase (decrease) in canopy temperature that is emitted downward from the canopy, reflected from the ground, and transmitted through the canopy to the atmosphere. The last term is the longwave radiation emitted by the ground and transmitted through the canopy to the atmosphere.

The upward longwave radiation from the ground is

$$L_g \uparrow = \left(1-\varepsilon_g\right) L_v \downarrow + \varepsilon_g \sigma \left(T_g^n\right)^4 \tag{4.16}$$

where $L_v \downarrow$ is the downward longwave radiation below the vegetation

$$L_v \downarrow = \left(1-\varepsilon_v\right) L_{atm} \downarrow + \varepsilon_v \sigma \left(T_v^n\right)^4 + 4\varepsilon_v \sigma \left(T_v^n\right)^3 \left(T_v^{n+1} - T_v^n\right). \tag{4.17}$$

The net longwave radiation flux for the ground is (positive toward the atmosphere)

$$\vec{L}_g = \varepsilon_g \sigma \left(T_g^n\right)^4 - \delta_{veg} \varepsilon_g L_v \downarrow - \left(1-\delta_{veg}\right) \varepsilon_g L_{atm} \downarrow . \tag{4.18}$$

The above expression for $\vec{L}_g$ is the net longwave radiation forcing that is used in the soil temperature calculation (section 6). Once updated soil temperatures have been obtained, the term $4\varepsilon_g \sigma \left(T_g^n\right)^3 \left(T_g^{n+1} - T_g^n\right)$ is added to $\vec{L}_g$ to calculate the ground heat flux (section 5.4)

The net longwave radiation flux for vegetation is (positive toward the atmosphere)

$$\vec{L}_v = \left[2 - \varepsilon_v \left(1-\varepsilon_g\right)\right] \varepsilon_v \sigma \left(T_v\right)^4 - \varepsilon_v \varepsilon_g \sigma \left(T_g^n\right)^4 - \varepsilon_v \left[1 + \left(1-\varepsilon_g\right)\left(1-\varepsilon_v\right)\right] L_{atm} \downarrow . \tag{4.19}$$

These equations assume that absorptivity equals emissivity. The emissivity of the ground is $\varepsilon_g = \varepsilon_{soi}$, where $\varepsilon_{soi} = 0.96$ for soil, 0.97 for glacier, 0.96 for wetland, and 0.97 for snow-covered surfaces (snow water equivalent (kg m^{-2}) $W_{sno} > 0$). The vegetation emissivity is

$$\varepsilon_v = 1 - e^{-(L+S)/\bar{\mu}} \tag{4.20}$$

where L and S are the leaf and stem area indices (section 2.3) and $\bar{\mu} = 1$ is the average inverse optical depth for longwave radiation.

5. Momentum, Sensible Heat, and Latent Heat Fluxes

The zonal τ_x and meridional τ_y momentum fluxes (kg m^{-1} s^{-2}), sensible heat flux H (W m^{-2}), and water vapor flux E (kg m^{-2} s^{-1}) between the atmosphere at reference height $z_{atm,x}$ (m) [where x is height for wind (momentum) (m), temperature (sensible heat) (h), and humidity (water vapor) (w); with zonal and meridional winds u_{atm} and v_{atm} (m s^{-1}), potential temperature θ_{atm} (K), and specific humidity q_{atm} (kg kg^{-1})] and the surface [with u_s, v_s, θ_s, and q_s] are

$$\tau_x = -\rho_{atm} \frac{\left(u_{atm} - u_s\right)}{r_{am}} \tag{5.1}$$

$$\tau_y = -\rho_{atm} \frac{\left(v_{atm} - v_s\right)}{r_{am}} \tag{5.2}$$

$$H = -\rho_{atm} C_p \frac{\left(\theta_{atm} - \theta_s\right)}{r_{ah}} \tag{5.3}$$

$$E = -\rho_{atm} \frac{\left(q_{atm} - q_s\right)}{r_{aw}}. \tag{5.4}$$

These fluxes are derived in the next section from Monin-Obukhov similarity theory developed for the surface layer (i.e., the nearly constant flux layer above the surface sublayer). In this derivation, u_s and v_s are defined to equal zero at height $z_{0m} + d$ (the apparent sink for momentum) so that r_{am} is the aerodynamic resistance (s m^{-1}) for momentum between the atmosphere at height $z_{atm,m}$ and the surface at height $z_{0m} + d$. Thus, the momentum fluxes become

$$\tau_x = -\rho_{atm} \frac{u_{atm}}{r_{am}} \tag{5.5}$$

$$\tau_y = -\rho_{atm} \frac{v_{atm}}{r_{am}}. \tag{5.6}$$

Likewise, θ_s and q_s are defined at heights $z_{0h} + d$ and $z_{0w} + d$ (the apparent sinks for heat and water vapor, respectively). Consequently, r_{ah} and r_{aw} are the aerodynamic resistances (s m^{-1}) to sensible heat and water vapor transfer between the atmosphere at heights $z_{atm,h}$ and $z_{atm,w}$ and the surface at heights $z_{0h} + d$ and $z_{0w} + d$, respectively. The specific heat capacity of air C_p (J kg^{-1} K^{-1}) is a constant (Table 1.4). The atmospheric potential temperature is

$$\theta_{atm} = T_{atm} + \Gamma_d z_{atm,h} \tag{5.7}$$

where T_{atm} is the air temperature (K) at height $z_{atm,h}$ and $\Gamma_d = 0.0098$ K m^{-1} is the negative of the dry adiabatic lapse rate [this expression is first-order equivalent to $\theta_{atm} = T_{atm} \left(P_{srf} / P_{atm} \right)^{R_{da}/C_p}$ (Stull 1988), where P_{srf} is the surface pressure (Pa), P_{atm} is the atmospheric pressure (Pa), and R_{da} is the gas constant for dry air (J kg^{-1} K^{-1}) (Table 1.4)]. By definition, $\theta_s = T_s$. The density of moist air (kg m^{-3}) is

$$\rho_{atm} = \frac{P_{atm} - 0.378 e_{atm}}{R_{da} T_{atm}} \tag{5.8}$$

where the atmospheric vapor pressure e_{atm} (Pa) is derived from the atmospheric specific humidity q_{atm}

$$e_{atm} = \frac{q_{atm} P_{atm}}{0.622 + 0.378 q_{atm}}. \tag{5.9}$$

5.1 Monin-Obukhov Similarity Theory

The surface vertical kinematic fluxes of momentum $\overline{u'w'}$ and $\overline{v'w'}$ (m^2 s^{-2}), sensible heat $\overline{\theta'w'}$ (K m s^{-1}), and latent heat $\overline{q'w'}$ (kg kg^{-1} m s^{-1}), where u', v', w', θ', and q' are zonal horizontal wind, meridional horizontal wind, vertical velocity, potential temperature, and specific humidity turbulent fluctuations about the mean, are defined from Monin-Obukhov similarity applied to the surface layer. This theory states that when scaled appropriately, the dimensionless mean horizontal wind speed, mean potential temperature, and mean specific humidity profile gradients depend on unique functions of $\zeta = \frac{z-d}{L}$ (Zeng et al. 1998) as

$$\frac{k\left(z-d\right)}{u_*}\frac{\partial\left|\boldsymbol{u}\right|}{\partial z} = \phi_m\left(\zeta\right) \tag{5.10}$$

$$\frac{k\left(z-d\right)}{\theta_*}\frac{\partial\theta}{\partial z} = \phi_h\left(\zeta\right) \tag{5.11}$$

$$\frac{k\left(z-d\right)}{q_*}\frac{\partial q}{\partial z} = \phi_w\left(\zeta\right) \tag{5.12}$$

where z is height in the surface layer (m), d is the displacement height (m), L is the Monin-Obukhov length scale (m) that accounts for buoyancy effects resulting from vertical density gradients (i.e., the atmospheric stability), k is the von Karman constant (Table 1.4), and $\left|\boldsymbol{u}\right|$ is the atmospheric wind speed (m s^{-1}). ϕ_m, ϕ_h, and ϕ_w are universal (over any surface) similarity functions of ζ that relate the constant fluxes of momentum, sensible heat, and latent heat to the mean profile gradients of $\left|\boldsymbol{u}\right|$, θ, and q in the surface layer. In neutral conditions, $\phi_m = \phi_h = \phi_w = 1$. The velocity (i.e., friction velocity) u_* (m s^{-1}), temperature θ_* (K), and moisture q_* (kg kg^{-1}) scales are

$$u_*^2 = \sqrt{\left(\overline{u'w'}\right)^2 + \left(\overline{v'w'}\right)^2} = \frac{|\tau|}{\rho_{atm}} \tag{5.13}$$

$$\theta_* u_* = -\overline{\theta' w'} = -\frac{H}{\rho_{atm} C_p} \tag{5.14}$$

$$q_* u_* = -\overline{q' w'} = -\frac{E}{\rho_{atm}} \tag{5.15}$$

where $|\tau|$ is the shearing stress (kg m^{-1} s^{-2}), with zonal and meridional components $\overline{u'w'} = -\frac{\tau_x}{\rho_{atm}}$ and $\overline{v'w'} = -\frac{\tau_y}{\rho_{atm}}$, respectively, H is the sensible heat flux (W m^{-2}) and E is the water vapor flux (kg m^{-2} s^{-1}).

The dimensionless length scale L is the Monin-Obukhov length defined as

$$L = -\frac{u_*^3}{k\left(\frac{g}{\overline{\theta_{v,atm}}}\right)\theta_v' w'} = \frac{u_*^2 \overline{\theta_{v,atm}}}{kg\theta_{v*}} \tag{5.16}$$

where g is the acceleration of gravity (m s^{-2}) (Table 1.4), and $\overline{\theta_{v,atm}} = \overline{\theta_{atm}}\left(1 + 0.61 q_{atm}\right)$ is the reference virtual potential temperature. $L > 0$ indicates stable conditions. $L < 0$ indicates unstable conditions. $L = \infty$ for neutral conditions. The temperature scale θ_{v*} is defined as

$$\theta_{v*} u_* = \left[\theta_*\left(1 + 0.61 q_{atm}\right) + 0.61 \overline{\theta_{atm}} q_*\right] u_* \tag{5.17}$$

where $\overline{\theta_{atm}}$ is the atmospheric potential temperature.

Following Panofsky and Dutton (1984), the differential equations for $\phi_m\left(\zeta\right)$, $\phi_h\left(\zeta\right)$, and $\phi_w\left(\zeta\right)$ can be integrated formally without commitment to their exact forms. Integration between two arbitrary heights in the surface layer z_2 and z_1 ($z_2 > z_1$) with horizontal winds $|\boldsymbol{u}|_1$ and $|\boldsymbol{u}|_2$, potential temperatures θ_1 and θ_2, and specific humidities q_1 and q_2 results in

$$|\boldsymbol{u}|_2 - |\boldsymbol{u}|_1 = \frac{u_*}{k}\left[\ln\left(\frac{z_2 - d}{z_1 - d}\right) - \psi_m\left(\frac{z_2 - d}{L}\right) + \psi_m\left(\frac{z_1 - d}{L}\right)\right] \tag{5.18}$$

$$\theta_2 - \theta_1 = \frac{\theta_*}{k}\left[\ln\left(\frac{z_2 - d}{z_1 - d}\right) - \psi_h\left(\frac{z_2 - d}{L}\right) + \psi_h\left(\frac{z_1 - d}{L}\right)\right] \tag{5.19}$$

$$q_2 - q_1 = \frac{q_*}{k}\left[\ln\left(\frac{z_2 - d}{z_1 - d}\right) - \psi_w\left(\frac{z_2 - d}{L}\right) + \psi_w\left(\frac{z_1 - d}{L}\right)\right]. \tag{5.20}$$

The functions $\psi_m(\zeta)$, $\psi_h(\zeta)$, and $\psi_w(\zeta)$ are defined as

$$\psi_m(\zeta) = \int_{z_{0m}/L}^{\zeta} \frac{\left[1 - \phi_m(x)\right]}{x} dx \tag{5.21}$$

$$\psi_h(\zeta) = \int_{z_{0h}/L}^{\zeta} \frac{\left[1 - \phi_h(x)\right]}{x} dx \tag{5.22}$$

$$\psi_w(\zeta) = \int_{z_{0w}/L}^{\zeta} \frac{\left[1 - \phi_w(x)\right]}{x} dx \tag{5.23}$$

where z_{0m}, z_{0h}, and z_{0w} are the roughness lengths (m) for momentum, sensible heat, and water vapor, respectively.

Defining the surface values

$|\boldsymbol{u}|_1 = 0$ at $z_1 = z_{0m} + d$,

$\theta_1 = \theta_s$ at $z_1 = z_{0h} + d$, and

$q_1 = q_s$ at $z_1 = z_{0w} + d$,

and the atmospheric values at $z_2 = z_{atm,x}$

$$|\boldsymbol{u}|_2 = V_a = \sqrt{u_{atm}^2 + v_{atm}^2 + U_c^2} \geq 1, \tag{5.24}$$

$\theta_2 = \theta_{atm}$, and

$q_2 = q_{atm}$,

the integral forms of the flux-gradient relations are

$$V_a = \frac{u_*}{k}\left[\ln\left(\frac{z_{atm,m} - d}{z_{0m}}\right) - \psi_m\left(\frac{z_{atm,m} - d}{L}\right) + \psi_m\left(\frac{z_{0m}}{L}\right)\right] \tag{5.25}$$

$$\theta_{atm} - \theta_s = \frac{\theta_*}{k}\left[\ln\left(\frac{z_{atm,h} - d}{z_{0h}}\right) - \psi_h\left(\frac{z_{atm,h} - d}{L}\right) + \psi_h\left(\frac{z_{0h}}{L}\right)\right] \tag{5.26}$$

$$q_{atm} - q_s = \frac{q_*}{k}\left[\ln\left(\frac{z_{atm,w} - d}{z_{0w}}\right) - \psi_w\left(\frac{z_{atm,w} - d}{L}\right) + \psi_w\left(\frac{z_{0w}}{L}\right)\right]. \tag{5.27}$$

The constraint $V_a \ge 1$ is required simply for numerical reasons to prevent H and E from becoming small with small wind speeds. The convective velocity U_c accounts for the contribution of large eddies in the convective boundary layer to surface fluxes as follows

$$\begin{array}{lll} U_c = 0 & \zeta \ge 0 & \text{(stable)} \\ U_c = \beta w_* & \zeta < 0 & \text{(unstable)} \end{array} \tag{5.28}$$

where w_* is the convective velocity scale

$$w_* = \left(\frac{-g u_* \theta_{v*} z_i}{\overline{\theta_{v,atm}}}\right)^{1/3}, \tag{5.29}$$

$z_i = 1000$ is the convective boundary layer height (m), and $\beta = 1$.

The momentum flux gradient relations are (Zeng et al. 1998)

$$\begin{array}{ll} \phi_m(\zeta) = 0.7k^{2/3}(-\zeta)^{1/3} & \text{for } \zeta < -1.574 \text{ (very unstable)} \\ \phi_m(\zeta) = (1 - 16\zeta)^{-1/4} & \text{for } -1.574 \le \zeta < 0 \text{ (unstable)} \\ \phi_m(\zeta) = 1 + 5\zeta & \text{for } 0 \le \zeta \le 1 \text{ (stable)} \\ \phi_m(\zeta) = 5 + \zeta & \text{for } \zeta > 1 \text{ (very stable).} \end{array} \tag{5.30}$$

The sensible and latent heat flux gradient relations are (Zeng et al. 1998)

$$\begin{aligned}
&\phi_h(\zeta) = \phi_w(\zeta) = 0.9k^{4/3}(-\zeta)^{-1/3} && \text{for } \zeta < -0.465 \text{ (very unstable)} \\
&\phi_h(\zeta) = \phi_w(\zeta) = (1-16\zeta)^{-1/2} && \text{for } -0.465 \le \zeta < 0 \text{ (unstable)} \\
&\phi_h(\zeta) = \phi_w(\zeta) = 1+5\zeta && \text{for } 0 \le \zeta \le 1 \text{ (stable)} \\
&\phi_h(\zeta) = \phi_w(\zeta) = 5+\zeta && \text{for } \zeta > 1 \text{ (very stable).}
\end{aligned} \tag{5.31}$$

To ensure continuous functions of $\phi_m(\zeta)$, $\phi_h(\zeta)$, and $\phi_w(\zeta)$, the simplest approach (i.e., without considering any transition regimes) is to match the relations for very unstable and unstable conditions at $\zeta_m = -1.574$ for $\phi_m(\zeta)$ and $\zeta_h = \zeta_w = -0.465$ for $\phi_h(\zeta) = \phi_w(\zeta)$ (Zeng et al. 1998). The flux gradient relations can be integrated to yield wind profiles for the following conditions:

Very unstable $(\zeta < -1.574)$

$$V_a = \frac{u_*}{k}\left\{\left[\ln\frac{\zeta_m L}{z_{0m}} - \psi_m(\zeta_m)\right] + 1.14\left[(-\zeta)^{1/3} - (-\zeta_m)^{1/3}\right] + \psi_m\left(\frac{z_{0m}}{L}\right)\right\} \tag{5.32}$$

Unstable $(-1.574 \le \zeta < 0)$

$$V_a = \frac{u_*}{k}\left\{\left[\ln\frac{z_{atm,m} - d}{z_{0m}} - \psi_m(\zeta)\right] + \psi_m\left(\frac{z_{0m}}{L}\right)\right\} \tag{5.33}$$

Stable $(0 \le \zeta \le 1)$

$$V_a = \frac{u_*}{k}\left\{\left[\ln\frac{z_{atm,m} - d}{z_{0m}} + 5\zeta\right] - 5\frac{z_{0m}}{L}\right\} \tag{5.34}$$

Very stable $(\zeta > 1)$

$$V_a = \frac{u_*}{k}\left\{\left[\ln\frac{L}{z_{0m}} + 5\right] + \left[5\ln\zeta + \zeta - 1\right] - 5\frac{z_{0m}}{L}\right\} \tag{5.35}$$

where

$$\psi_m(\zeta) = 2\ln\left(\frac{1+x}{2}\right) + \ln\left(\frac{1+x^2}{2}\right) - 2\tan^{-1}x + \frac{\pi}{2} \tag{5.36}$$

and $x = (1-16\zeta)^{1/4}$.

The potential temperature profiles are:

Very unstable $(\zeta < -0.465)$

$$\theta_{atm} - \theta_s = \frac{\theta_*}{k}\left\{\left[\ln\frac{\zeta_h L}{z_{0h}} - \psi_h(\zeta_h)\right] + 0.8\left[(-\zeta_h)^{-1/3} - (-\zeta)^{-1/3}\right] + \psi_h\left(\frac{z_{0h}}{L}\right)\right\} \tag{5.37}$$

Unstable $(-0.465 \le \zeta < 0)$

$$\theta_{atm} - \theta_s = \frac{\theta_*}{k}\left\{\left[\ln\frac{z_{atm,h}-d}{z_{0h}} - \psi_h(\zeta)\right] + \psi_h\left(\frac{z_{0h}}{L}\right)\right\} \tag{5.38}$$

Stable $(0 \le \zeta \le 1)$

$$\theta_{atm} - \theta_s = \frac{\theta_*}{k}\left\{\left[\ln\frac{z_{atm,h}-d}{z_{0h}} + 5\zeta\right] - 5\frac{z_{0h}}{L}\right\} \tag{5.39}$$

Very stable $(\zeta > 1)$

$$\theta_{atm} - \theta_s = \frac{\theta_*}{k}\left\{\left[\ln\frac{L}{z_{0h}} + 5\right] + \left[5\ln\zeta + \zeta - 1\right] - 5\frac{z_{0h}}{L}\right\}. \tag{5.40}$$

The specific humidity profiles are:

Very unstable $(\zeta < -0.465)$

$$q_{atm} - q_s = \frac{q_*}{k}\left\{\left[\ln\frac{\zeta_w L}{z_{0w}} - \psi_w(\zeta_w)\right] + 0.8\left[(-\zeta_w)^{-1/3} - (-\zeta)^{-1/3}\right] + \psi_w\left(\frac{z_{0w}}{L}\right)\right\} \tag{5.41}$$

Unstable $(-0.465 \le \zeta < 0)$

$$q_{atm} - q_s = \frac{q_*}{k}\left\{\left[\ln\frac{z_{atm,w} - d}{z_{0w}} - \psi_w\left(\zeta\right)\right] + \psi_w\left(\frac{z_{0w}}{L}\right)\right\} \tag{5.42}$$

Stable $\left(0 \le \zeta \le 1\right)$

$$q_{atm} - q_s = \frac{q_*}{k}\left\{\left[\ln\frac{z_{atm,w} - d}{z_{0w}} + 5\zeta\right] - 5\frac{z_{0w}}{L}\right\} \tag{5.43}$$

Very stable $\left(\zeta > 1\right)$

$$q_{atm} - q_s = \frac{q_*}{k}\left\{\left[\ln\frac{L}{z_{0w}} + 5\right] + \left[5\ln\zeta + \zeta - 1\right] - 5\frac{z_{0w}}{L}\right\} \tag{5.44}$$

where

$$\psi_h\left(\zeta\right) = \psi_w\left(\zeta\right) = 2\ln\left(\frac{1 + x^2}{2}\right). \tag{5.45}$$

Using the definitions of u_*, θ_*, and q_*, an iterative solution of these equations can be used to calculate the surface momentum, sensible heat, and water vapor flux using atmospheric and surface values for $\left|\boldsymbol{u}\right|$, θ, and q except that L depends on u_*, θ_*, and q_*. However, the bulk Richardson number

$$R_{iB} = \frac{\theta_{v,atm} - \theta_{v,s}}{\overline{\theta_{v,atm}}}\frac{g\left(z_{atm,m} - d\right)}{V_a^2} \tag{5.46}$$

is related to ζ (Arya 2001) as

$$R_{iB} = \zeta\left[\ln\left(\frac{z_{atm,h} - d}{z_{0h}}\right) - \psi_h\left(\zeta\right)\right]\left[\ln\left(\frac{z_{atm,m} - d}{z_{0m}}\right) - \psi_m\left(\zeta\right)\right]^{-2}. \tag{5.47}$$

Using $\phi_h = \phi_m^2 = \left(1-16\zeta\right)^{-1/2}$ for unstable conditions and $\phi_h = \phi_m = 1+5\zeta$ for stable conditions to determine $\psi_m\left(\zeta\right)$ and $\psi_h\left(\zeta\right)$, the inverse relationship $\zeta = f\left(R_{iB}\right)$ can be solved to obtain a first guess for ζ and thus L from

$$\begin{array}{lll} \zeta = \dfrac{R_{iB} \ln\left(\dfrac{z_{atm,m} - d}{z_{0m}}\right)}{1-5\min\left(R_{iB}, 0.19\right)} & 0.01 \le \zeta \le 2 & \text{for } R_{iB} \ge 0 \text{ (neutral or stable)} \\ \zeta = R_{iB} \ln\left(\dfrac{z_{atm,m} - d}{z_{0m}}\right) & -100 \le \zeta \le -0.01 & \text{for } R_{iB} < 0 \text{ (unstable)} \end{array} . \qquad (5.48)$$

Upon iteration (section 5.3.2), the following is used to determine ζ and thus L

$$\zeta = \frac{\left(z_{atm,m} - d\right) k g \theta_{v*}}{u_*^2 \overline{\theta_{v,atm}}} \qquad (5.49)$$

where

$$\begin{array}{ll} 0.01 \le \zeta \le 2 & \text{for } \zeta \ge 0 \text{ (neutral or stable)} \\ \text{-}100 \le \zeta \le \text{-}0.01 & \text{for } \zeta < 0 \text{ (unstable)} \end{array} .$$

The difference in virtual potential air temperature between the reference height and the surface is

$$\theta_{v,atm} - \theta_{v,s} = \left(\theta_{atm} - \theta_s\right)\left(1+0.61 q_{atm}\right) + 0.61 \overline{\theta_{atm}} \left(q_{atm} - q_s\right). \qquad (5.50)$$

The momentum, sensible heat, and water vapor fluxes between the surface and the atmosphere can also be written in the form

$$\tau_x = -\rho_{atm} \frac{\left(u_{atm} - u_s\right)}{r_{am}} \qquad (5.51)$$

$$\tau_y = -\rho_{atm} \frac{\left(v_{atm} - v_s\right)}{r_{am}} \qquad (5.52)$$

$$H = -\rho_{atm} C_p \frac{(\theta_{atm} - \theta_s)}{r_{ah}} \tag{5.53}$$

$$E = -\rho_{atm} \frac{(q_{atm} - q_s)}{r_{aw}} \tag{5.54}$$

where the aerodynamic resistances (s m^{-1}) are

$$r_{am} = \frac{V_a}{u_*^2} = \frac{1}{k^2 V_a}\left[\ln\left(\frac{z_{atm,m} - d}{z_{0m}}\right) - \psi_m\left(\frac{z_{atm,m} - d}{L}\right) + \psi_m\left(\frac{z_{0m}}{L}\right)\right]^2 \tag{5.55}$$

$$\begin{aligned} r_{ah} = \frac{\theta_{atm} - \theta_s}{\theta_* u_*} = \frac{1}{k^2 V_a}&\left[\ln\left(\frac{z_{atm,m} - d}{z_{0m}}\right) - \psi_m\left(\frac{z_{atm,m} - d}{L}\right) + \psi_m\left(\frac{z_{0m}}{L}\right)\right] \\ &\left[\ln\left(\frac{z_{atm,h} - d}{z_{0h}}\right) - \psi_h\left(\frac{z_{atm,h} - d}{L}\right) + \psi_h\left(\frac{z_{0h}}{L}\right)\right] \end{aligned} \tag{5.56}$$

$$\begin{aligned} r_{aw} = \frac{q_{atm} - q_s}{q_* u_*} = \frac{1}{k^2 V_a}&\left[\ln\left(\frac{z_{atm,m} - d}{z_{0m}}\right) - \psi_m\left(\frac{z_{atm,m} - d}{L}\right) + \psi_m\left(\frac{z_{0m}}{L}\right)\right] \\ &\left[\ln\left(\frac{z_{atm,w} - d}{z_{0w}}\right) - \psi_w\left(\frac{z_{atm,w} - d}{L}\right) + \psi_w\left(\frac{z_{0w}}{L}\right)\right]. \end{aligned} \tag{5.57}$$

A 2-m height "screen" temperature is useful for comparison with observations

$$T_{2m} = \theta_s + \frac{\theta_*}{k}\left[\ln\left(\frac{2 + z_{0h}}{z_{0h}}\right) - \psi_h\left(\frac{2 + z_{0h}}{L}\right) + \psi_h\left(\frac{z_{0h}}{L}\right)\right] \tag{5.58}$$

where for convenience, "2-m" is defined as 2 m above the apparent sink for sensible heat ($z_{0h} + d$). Similarly, a 2-m height specific humidity is defined

$$q_{2m} = q_s + \frac{q_*}{k}\left[\ln\left(\frac{2 + z_{0w}}{z_{0w}}\right) - \psi_w\left(\frac{2 + z_{0w}}{L}\right) + \psi_w\left(\frac{z_{0w}}{L}\right)\right]. \tag{5.59}$$

5.2 Sensible and Latent Heat Fluxes for Non-Vegetated Surfaces

Surfaces are considered non-vegetated for the surface flux calculations if leaf plus stem area index $L+S<0.05$ (section 2.3). By definition, this includes bare soil, wetlands, and glaciers. The solution for lakes is described in section 9. For these surfaces, the surface temperature $\theta_s = T_s$ is also the ground surface temperature T_g (this can be either the soil or snow surface) so that the sensible heat flux H_g (W m^{-2}) is, with reference to Figure 5.1,

$$H_g = -\rho_{atm} C_p \frac{\left(\theta_{atm} - T_g\right)}{r_{ah}} \tag{5.60}$$

where ρ_{atm} is the density of atmospheric air (kg m^{-3}), C_p is the specific heat capacity of air (J kg^{-1} K^{-1}) (Table 1.4), θ_{atm} is the atmospheric potential temperature (K), and r_{ah} is the aerodynamic resistance to sensible heat transfer (s m^{-1}).

The water vapor flux E_g (kg m^{-2} s^{-1}) is, with reference to Figure 5.2,

$$E_g = -\frac{\rho_{atm}\left(q_{atm} - q_g\right)}{r_{aw}} \tag{5.61}$$

where q_{atm} is the atmospheric specific humidity (kg kg^{-1}), q_g is the specific humidity of the soil surface (kg kg^{-1}), and r_{aw} is the aerodynamic resistance to water vapor transfer (s m^{-1}). The specific humidity of the soil surface q_g is assumed to be proportional to the saturation specific humidity

$$q_g = \alpha q_{sat}^{T_g} \tag{5.62}$$

where $q_{sat}^{T_g}$ is the saturated specific humidity at the ground surface temperature T_g (section 5.5). The factor α is a weighted combination of values for soil and snow

$$\alpha = \alpha_{soi,1}\left(1 - f_{sno}\right) + \alpha_{sno} f_{sno} \tag{5.63}$$

where f_{sno} is the fraction of ground covered by snow (section 3.2), and $\alpha_{sno} = 1.0$. $\alpha = 1.0$ for wetlands and glaciers. $\alpha_{soi,1}$ refers to the surface soil layer and is a function of the surface soil water matric potential ψ as in Philip (1957)

$$\alpha_{soi,1} = \exp\left(\frac{\psi_1 g}{1\times 10^3 R_{wv} T_g}\right) \tag{5.64}$$

where R_{wv} is the gas constant for water vapor (J kg^{-1} K^{-1}) (Table 1.4), g is the gravitational acceleration (m s^{-2}) (Table 1.4), and ψ_1 is the soil water matric potential of the top soil layer (mm). The soil water matric potential ψ_1 is

$$\psi_1 = \psi_{sat,1} s_1^{-B_1} \geq -1\times 10^8 \tag{5.65}$$

where $\psi_{sat,1}$ is the saturated matric potential (mm) (section 7.4.1), B_1 is the Clapp and Hornberger (1978) parameter (section 7.4.1), and s_1 is the wetness of the top soil layer with respect to saturation. The surface wetness s_1 is a function of the liquid water and ice content

$$s_1 = \frac{1}{\Delta z_1 \theta_{sat,1}}\left[\frac{w_{liq,1}}{\rho_{liq}} + \frac{w_{ice,1}}{\rho_{ice}}\right] \qquad 0.01 \leq s_1 \leq 1.0 \tag{5.66}$$

where Δz_1 is the thickness of the top soil layer (m), ρ_{liq} and ρ_{ice} are the density of liquid water and ice (kg m^{-3}) (Table 1.4), $w_{liq,1}$ and $w_{ice,1}$ are the mass of liquid water and ice of the top soil layer (kg m^{-2}) (section 7), and $\theta_{sat,1}$ is the saturated volumetric water content (i.e., porosity) of the top soil layer (mm^3 mm^{-3}) (section 7.4.1). If $q_{sat}^{T_g} > q_{atm}$ and $q_{atm} > q_g$, then $q_g = q_{atm}$ and $\frac{dq_g}{dT_g} = 0$. This prevents large increases (decreases) in q_g for small increases (decreases) in soil moisture in very dry soils.

The roughness lengths used to calculate r_{am}, r_{ah}, and r_{aw} are $z_{0m} = z_{0m,g}$, $z_{0h} = z_{0h,g}$, and $z_{0w} = z_{0w,g}$. The displacement height $d = 0$. The momentum roughness length $z_{0m,g} = 0.01$ for soil, glaciers, and wetland, and $z_{0m,g} = 0.0024$ for snow-covered surfaces ($f_{sno} > 0$). In general, z_{0m} is different from z_{0h} because the transfer of momentum is affected by pressure fluctuations in the turbulent waves behind the roughness elements, while for heat and water vapor transfer no such dynamical mechanism exists. Rather, heat and water vapor must be transferred by molecular diffusion across the interfacial sublayer. The following relation from Zilitinkevich (1970) is adopted by Zeng and Dickinson (1998)

$$z_{0h,g} = z_{0w,g} = z_{0m,g} e^{-a\left(u_* z_{0m,g}/\upsilon\right)^{0.45}} \tag{5.67}$$

where the quantity $u_* z_{0m,g} \big/ \upsilon$ is the roughness Reynolds number (and may be interpreted as the Reynolds number of the smallest turbulent eddy in the flow) with the kinematic viscosity of air $\upsilon = 1.5 \times 10^{-5}$ m^2 s^{-1} and $a = 0.13$.

The numerical solution for the fluxes of momentum, sensible heat, and water vapor flux from non-vegetated surfaces proceeds as follows:

1. An initial guess for the wind speed V_a is obtained from eq. (5.24) assuming an initial convective velocity $U_c = 0$ m s^{-1} for stable conditions ($\theta_{v,atm} - \theta_{v,s} \geq 0$ as evaluated from eq. (5.50)) and $U_c = 0.5$ for unstable conditions ($\theta_{v,atm} - \theta_{v,s} < 0$).
2. An initial guess for the Monin-Obukhov length L is obtained from the bulk Richardson number using equations (5.46) and (5.48).
3. The following system of equations is iterated three times:
   - Friction velocity u_* (eqs. (5.32), (5.33), (5.34), (5.35))
   - Potential temperature scale θ_* (eqs. (5.37), (5.38), (5.39), (5.40))
   - Humidity scale q_* (eqs. (5.41), (5.42), (5.43), (5.44))
   - Roughness lengths for sensible $z_{0h,g}$ and latent heat $z_{0w,g}$ (eq. (5.67))
   - Virtual potential temperature scale θ_{v*} (eq. (5.17))
   - Wind speed including the convective velocity, V_a (eq. (5.24))
   - Monin-Obukhov length L (eq. (5.49))
4. Aerodynamic resistances r_{am}, r_{ah}, and r_{aw} (eqs. (5.55), (5.56), (5.57))
5. Momentum fluxes τ_x, τ_y (eqs. (5.5), (5.6))
6. Sensible heat flux H_g (eq. (5.60))
7. Water vapor flux E_g (eq. (5.61))
8. 2-m height air temperature T_{2m} and specific humidity q_{2m} (eqs. (5.58), (5.59))

The partial derivatives of the soil surface fluxes with respect to ground temperature, which are needed for the soil temperature calculations (section 6.1) and to update the soil surface fluxes (section 5.4), are

$$\frac{\partial H_g}{\partial T_g} = \frac{\rho_{atm} C_p}{r_{ah}} \tag{5.68}$$

$$\frac{\partial E_g}{\partial T_g} = \frac{\rho_{atm}}{r_{aw}} \frac{dq_g}{dT_g} \tag{5.69}$$

where

$$\frac{dq_g}{dT_g} = \alpha \frac{dq_{sat}^{T_g}}{dT_g}. \tag{5.70}$$

The partial derivatives $\frac{\partial r_{ah}}{\partial T_g}$ and $\frac{\partial r_{aw}}{\partial T_g}$, which cannot be determined analytically, are ignored for $\frac{\partial H_g}{\partial T_g}$ and $\frac{\partial E_g}{\partial T_g}$.

5.3 Sensible and Latent Heat Fluxes and Temperature for Vegetated Surfaces

In the case of a vegetated surface, the sensible heat H and water vapor flux E are partitioned into vegetation and ground fluxes that depend on vegetation T_v and ground T_g temperatures in addition to surface temperature T_s and specific humidity q_s. Because of the coupling between vegetation temperature and fluxes, Newton-Raphson iteration is used to solve for the vegetation temperature and the sensible heat and water vapor fluxes from vegetation simultaneously using the ground temperature from the previous time step. In section 5.3.1, the equations used in the iteration scheme are derived. Details on the numerical scheme are provided in section 5.3.2.

5.3.1 Theory

The air within the canopy is assumed to have negligible capacity to store heat so that the sensible heat flux H between the surface at height $z_{0h} + d$ and the atmosphere at height $z_{atm,h}$ must be balanced by the sum of the sensible heat from the vegetation H_v and the ground H_g

$$H = H_v + H_g \tag{5.71}$$

where, with reference to Figure 5.1,

$$H = -\rho_{atm} C_p \frac{\left(\theta_{atm} - T_s\right)}{r_{ah}} \tag{5.72}$$

$$H_v = -\rho_{atm} C_p \left(T_s - T_v\right) \frac{\left(L + S\right)}{r_b} \tag{5.73}$$

$$H_g = -\rho_{atm} C_p \frac{\left(T_s - T_g\right)}{r_{ah}{}'} \tag{5.74}$$

where ρ_{atm} is the density of atmospheric air (kg m^{-3}), C_p is the specific heat capacity of air (J kg^{-1} K^{-1}) (Table 1.4), θ_{atm} is the atmospheric potential temperature (K), and r_{ah} is the aerodynamic resistance to sensible heat transfer (s m^{-1}).

Here, T_s is the surface temperature at height $z_{0h} + d$, also referred to as the canopy air temperature. L and S are the exposed leaf and stem area indices (section 2.3), r_b is the leaf boundary layer resistance (s m^{-1}), and $r_{ah}{}'$ is the aerodynamic resistance (s m^{-1}) to heat transfer between the ground at height $z_{0h}{}'$ and the canopy air at height $z_{0h} + d$.

Figure 5.1. Schematic diagram of sensible heat fluxes for (a) non-vegetated surfaces and (b) vegetated surfaces.

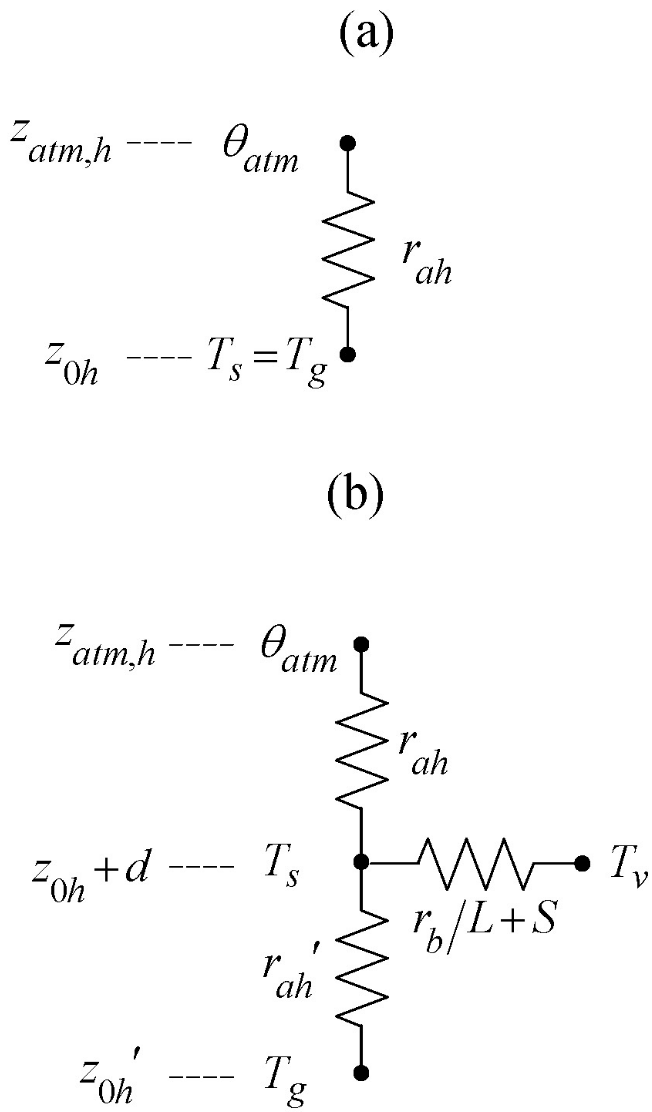

Figure 5.2. Schematic diagram of water vapor fluxes for (a) non-vegetated surfaces and (b) vegetated surfaces.

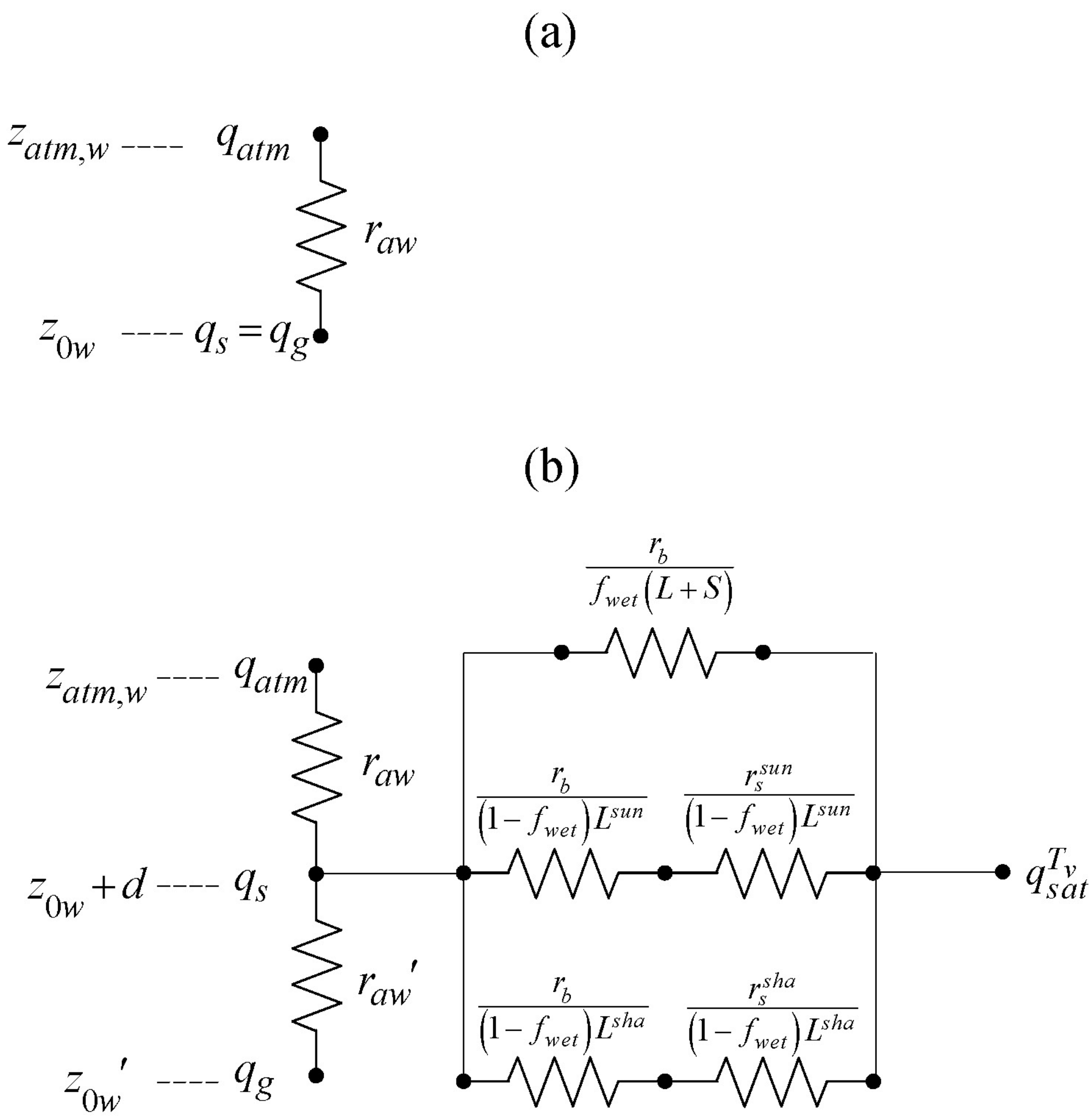

Equations (5.71)-(5.74) can be solved for the canopy air temperature T_s

$$T_s = \frac{c_a^h \theta_{atm} + c_g^h T_g + c_v^h T_v}{c_a^h + c_g^h + c_v^h} \tag{5.75}$$

where

$$c_a^h = \frac{1}{r_{ah}} \tag{5.76}$$

$$c_g^h = \frac{1}{r_{ah}{}'} \tag{5.77}$$

$$c_v^h = \frac{\left(L+S\right)}{r_b} \tag{5.78}$$

are the sensible heat conductances from the canopy air to the atmosphere, the ground to canopy air, and leaf surface to canopy air, respectively (m s^{-1}).

When the expression for T_s is substituted into equation (5.73), the sensible heat flux from vegetation H_v is a function of θ_{atm}, T_g, and T_v

$$H_v = -\rho_{atm} C_p \left[c_a^h \theta_{atm} + c_g^h T_g - \left(c_a^h + c_g^h \right) T_v \right] \frac{c_v^h}{c_a^h + c_v^h + c_g^h}. \tag{5.79}$$

Similarly, the expression for T_s can be substituted into equation (5.74) to obtain the sensible heat flux from ground H_g

$$H_g = -\rho_{atm} C_p \left[c_a^h \theta_{atm} + c_v^h T_v - \left(c_a^h + c_v^h \right) T_g \right] \frac{c_g^h}{c_a^h + c_v^h + c_g^h}. \tag{5.80}$$

The air within the canopy is assumed to have negligible capacity to store water vapor so that the water vapor flux E between the surface at height $z_{0w} + d$ and the atmosphere at height $z_{atm,w}$ must be balanced by the sum of the water vapor flux from the vegetation E_v and the ground E_g

$$E = E_v + E_g \tag{5.81}$$

where, with reference to Figure 5.2,

$$E = -\rho_{atm} \frac{\left(q_{atm} - q_s\right)}{r_{aw}} \tag{5.82}$$

$$E_v = -\rho_{atm} \frac{\left(q_s - q_{sat}^{T_v}\right)}{r_{total}} \tag{5.83}$$

$$E_g = -\rho_{atm} \frac{\left(q_s - q_g\right)}{r_{aw}'} \tag{5.84}$$

where q_{atm} is the atmospheric specific humidity (kg kg^{-1}), r_{aw} is the aerodynamic resistance to water vapor transfer (s m^{-1}), $q_{sat}^{T_v}$ (kg kg^{-1}) is the saturation water vapor specific humidity at the vegetation temperature (section 5.5), q_g is the specific humidity at the ground surface (section 5.2), and r_{aw}' is the aerodynamic resistance (s m^{-1}) to water vapor transfer between the ground at height z_{0w}' and the canopy air at height $z_{0w} + d$. r_{total} is the total resistance to water vapor transfer from the canopy to the canopy air and includes contributions from leaf boundary layer and sunlit and shaded stomatal resistances r_b, r_s^{sun}, and r_s^{sha} (Figure 5.2).

The water vapor flux from vegetation is the sum of water vapor flux from wetted leaf and stem area E_v^w (evaporation of water intercepted by the canopy) and transpiration from dry leaf surfaces E_v^t

$$E_v = E_v^w + E_v^t \tag{5.85}$$

where, with reference to Figure 5.2,

$$E_v^w = -\rho_{atm} f_{wet} \left(L + S\right) \frac{\left(q_s - q_{sat}^{T_v}\right)}{r_b} \tag{5.86}$$

and

$$\begin{array}{ll} E_v^t = E_v^{pot} r_{dry}'' & E_v^{pot} > 0 \text{ and } \beta_t > 1\times 10^{-10} \\ E_v^t = 0 & E_v^{pot} \le 0 \text{ or } \beta_t \le 1\times 10^{-10} \end{array}. \tag{5.87}$$

where E_v^{pot} is the potential transpiration

$$E_v^{pot} = -\frac{\rho_{atm}\left(q_s - q_{sat}^{T_v}\right)}{r_b}, \tag{5.88}$$

r_{dry}'' is the fraction of potential transpiration

$$r_{dry}'' = \frac{f_{dry} r_b}{L}\left(\frac{L^{sun}}{r_b + r_s^{sun}} + \frac{L^{sha}}{r_b + r_s^{sha}}\right), \tag{5.89}$$

and β_t is a soil moisture function limiting transpiration (section 8). The term f_{wet} is the fraction of leaves and stems that are wet (section 7.1), f_{dry} is the fraction of leaves that are dry (section 7.1), L^{sun} and L^{sha} are the sunlit and shaded leaf area indices (section 4.1), and r_s^{sun} and r_s^{sha} are the sunlit and shaded stomatal resistances (s m^{-1}) (section 8).

Equations (5.81)-(5.84) can be solved for the canopy specific humidity q_s

$$q_s = \frac{c_a^w q_{atm} + c_g^w q_g + c_v^w q_{sat}^{T_v}}{c_a^w + c_v^w + c_g^w} \tag{5.90}$$

where

$$c_a^w = \frac{1}{r_{aw}} \tag{5.91}$$

$$c_v^w = \frac{\left(L+S\right)}{r_b} r'' \tag{5.92}$$

$$c_g^w = \frac{1}{r_{aw}{}'} \tag{5.93}$$

are the water vapor conductances from the canopy air to the atmosphere, the leaf to canopy air, and ground to canopy air, respectively. The term r'' is the fraction of potential evapotranspiration and varies as

$$\begin{array}{ll} r'' = f_{wet} + r_{dry}'' & E_v^{pot} > 0, \beta_t > 1\times 10^{-10} \\ r'' = f_{wet} & E_v^{pot} > 0, \beta_t \le 1\times 10^{-10} \\ r'' = 1 & E_v^{pot} \le 0 \end{array} \tag{5.94}$$

with the restriction that r'' cannot exceed water availability

$$r'' \le \frac{E_v^t + \frac{W_{can}}{\Delta t}}{E_v^{pot}} \tag{5.95}$$

where W_{can} is canopy water (kg m^{-2}) (section 7.1), and Δt is the time step (s).

When the expression for q_s is substituted into equation (5.83), the water vapor flux from vegetation E_v is a function of q_{atm}, q_g, and $q_{sat}^{T_v}$

$$E_v = -\rho_{atm}\left[c_a^w q_{atm} + c_g^w q_g - \left(c_a^w + c_g^w\right) q_{sat}^{T_v}\right]\frac{c_v^w}{c_a^w + c_v^w + c_g^w}. \tag{5.96}$$

Similarly, the expression for q_s can be substituted into equation (5.84) to obtain the water vapor flux from the ground beneath the canopy E_g

$$E_g = -\rho_{atm}\left[c_a^w q_{atm} + c_v^w q_{sat}^{T_v} - \left(c_a^w + c_v^w\right) q_g\right]\frac{c_g^w}{c_a^w + c_v^w + c_g^w}. \tag{5.97}$$

The aerodynamic resistances to heat (moisture) transfer between the ground at height z_{0h}' (z_{0w}') and the canopy air at height $z_{0h} + d$ ($z_{0w} + d$) are

$$r_{ah}' = r_{aw}' = \frac{1}{C_s U_{av}} \tag{5.98}$$

where

$$U_{av} = V_a \sqrt{\frac{1}{r_{am} V_a}} = u_* \tag{5.99}$$

is the magnitude of the wind velocity incident on the leaves (equivalent here to friction velocity) (m s^{-1}) and C_s is the turbulent transfer coefficient between the underlying soil and the canopy air. C_s is obtained by interpolation between values for dense canopy and bare soil (Zeng et al., 2004)

$$C_s = C_{s,bare} W + C_{s,dense}(1 - W) \tag{5.100}$$

where the weight W is

$$W = e^{-(L+S)}. \tag{5.101}$$

$C_{s,dense} = 0.004$ is the value for a dense canopy (Dickinson et al., 1993) and $C_{s,bare}$ is the value for bare soil

$$C_{s,bare} = \frac{k}{a}\left(\frac{z_{0m,g} U_{av}}{\upsilon}\right)^{-0.45} \tag{5.102}$$

where the kinematic viscosity of air $\upsilon = 1.5 \times 10^{-5}$ m^2 s^{-1} and $a = 0.13$.

The leaf boundary layer resistance r_b is

$$r_b = \frac{1}{C_v}\left(U_{av} / d_{leaf}\right)^{-1/2} \tag{5.103}$$

where $C_v = 0.01$ m s$^{-1/2}$ is the turbulent transfer coefficient between the canopy surface and canopy air, and d_{leaf} is the characteristic dimension of the leaves in the direction of wind flow (Table 5.1).

The partial derivatives of the fluxes from the soil beneath the canopy with respect to ground temperature, which are needed for the soil temperature calculations (section 6.1) and to update the soil surface fluxes (section 5.4), are

$$\frac{\partial H_g}{\partial T_g} = \frac{\rho_{atm} C_p}{r'_{ah}} \frac{c_a^h + c_v^h}{c_a^h + c_v^h + c_g^h} \tag{5.104}$$

$$\frac{\partial E_g}{\partial T_g} = \frac{\rho_{atm}}{r'_{aw}} \frac{c_a^w + c_v^w}{c_a^w + c_v^w + c_g^w} \frac{dq_g}{dT_g}. \tag{5.105}$$

The partial derivatives $\frac{\partial r'_{ah}}{\partial T_g}$ and $\frac{\partial r'_{aw}}{\partial T_g}$, which cannot be determined analytically, are ignored for $\frac{\partial H_g}{\partial T_g}$ and $\frac{\partial E_g}{\partial T_g}$.

The roughness lengths used to calculate r_{am}, r_{ah}, and r_{aw} from equations (5.55), (5.56), and (5.57) are $z_{0m} = z_{0m,v}$, $z_{0h} = z_{0h,v}$, and $z_{0w} = z_{0w,v}$. The vegetation displacement height d and the roughness lengths are a function of plant height

$$z_{0m,v} = z_{0h,v} = z_{0w,v} = z_{top} R_{z0m} \tag{5.106}$$

$$d = z_{top} R_d \tag{5.107}$$

where z_{top} is canopy top height (m) (Table 2.2), and R_{z0m} and R_d are the ratio of momentum roughness length and displacement height to canopy top height, respectively (Table 5.1).

Table 5.1. Plant functional type aerodynamic parameters

Plant functional type	R_{z0m}	R_d	d_{leaf} (m)
NET Temperate	0.055	0.67	0.04
NET Boreal	0.055	0.67	0.04
NDT Boreal	0.055	0.67	0.04
BET Tropical	0.075	0.67	0.04
BET temperate	0.075	0.67	0.04
BDT tropical	0.055	0.67	0.04
BDT temperate	0.055	0.67	0.04
BDT boreal	0.055	0.67	0.04
BES temperate	0.120	0.68	0.04
BDS temperate	0.120	0.68	0.04
BDS boreal	0.120	0.68	0.04
C_3 arctic grass	0.120	0.68	0.04
C_3 grass	0.120	0.68	0.04
C_4 grass	0.120	0.68	0.04
Crop1	0.120	0.68	0.04
Crop2	0.120	0.68	0.04

5.3.2 Numerical Implementation

Canopy energy conservation gives

$$-\vec{S}_v + \vec{L}_v\left(T_v\right) + H_v\left(T_v\right) + \lambda E_v\left(T_v\right) = 0 \tag{5.108}$$

where $\vec{S}_v$ is the solar radiation absorbed by the vegetation (section 4.1), $\vec{L}_v$ is the net longwave radiation absorbed by vegetation (section 4.2), and H_v and λE_v are the sensible and latent heat fluxes from vegetation, respectively. The term λ is taken to be the latent heat of vaporization λ_{vap} (Table 1.4).

$\vec{L}_v$, H_v, and λE_v depend on the vegetation temperature T_v. The Newton-Raphson method for finding roots of non-linear systems of equations can be applied to iteratively solve for T_v as

$$\Delta T_v = \frac{\vec{S}_v - \vec{L}_v - H_v - \lambda E_v}{\frac{\partial \vec{L}_v}{\partial T_v} + \frac{\partial H_v}{\partial T_v} + \frac{\partial \lambda E_v}{\partial T_v}} \tag{5.109}$$

where $\Delta T_v = T_v^{n+1} - T_v^n$ and the subscript "n" indicates the iteration.

The partial derivatives are

$$\frac{\partial \vec{L}_v}{\partial T_v} = 4\varepsilon_v \sigma \left[2 - \varepsilon_v \left(1 - \varepsilon_g \right) \right] T_v^3 \tag{5.110}$$

$$\frac{\partial H_v}{\partial T_v} = \rho_{atm} C_p \left(c_a^h + c_g^h \right) \frac{c_v^h}{c_a^h + c_v^h + c_g^h} \tag{5.111}$$

$$\frac{\partial \lambda E_v}{\partial T_v} = \lambda \rho_{atm} \left(c_a^w + c_g^w \right) \frac{c_v^w}{c_a^w + c_v^w + c_g^w} \frac{dq_{sat}^{T_v}}{dT_v} . \tag{5.112}$$

The partial derivatives $\frac{\partial r_{ah}}{\partial T_v}$ and $\frac{\partial r_{aw}}{\partial T_v}$, which cannot be determined analytically, are ignored for $\frac{\partial H_v}{\partial T_v}$ and $\frac{\partial \lambda E_v}{\partial T_v}$. However, if ζ changes sign more than four times during the temperature iteration, $\zeta = -0.01$. This helps prevent "flip-flopping" between stable and unstable conditions. The water vapor flux E_v, transpiration flux E_v^t, and sensible heat flux H_v are updated for changes in leaf temperature as

$$E_v = -\rho_{atm}\left[c_a^w q_{atm} + c_g^w q_g - \left(c_a^w + c_g^w\right)\left(q_{sat}^{T_v} + \frac{dq_{sat}^{T_v}}{dT_v}\Delta T_v\right)\right]\frac{c_v^w}{c_a^w + c_v^w + c_g^w} \tag{5.113}$$

$$E_v^t = -r_{dry}{''}\rho_{atm}\left[c_a^w q_{atm} + c_g^w q_g - \left(c_a^w + c_g^w\right)\left(q_{sat}^{T_v} + \frac{dq_{sat}^{T_v}}{dT_v}\Delta T_v\right)\right]\frac{c_v^h}{c_a^w + c_v^w + c_g^w} \tag{5.114}$$

$$H_v = -\rho_{atm} C_p\left[c_a^h \theta_{atm} + c_g^h T_g - \left(c_a^h + c_g^h\right)\left(T_v + \Delta T_v\right)\right]\frac{c_v^h}{c_a^h + c_v^h + c_g^h}. \tag{5.115}$$

The numerical solution for vegetation temperature and the fluxes of momentum, sensible heat, and water vapor flux from vegetated surfaces proceeds as follows:

1. Initial values for canopy air temperature and specific humidity are obtained from

$$T_s = \frac{T_g + \theta_{atm}}{2} \tag{5.116}$$

$$q_s = \frac{q_g + q_{atm}}{2}. \tag{5.117}$$

2. An initial guess for the wind speed V_a is obtained from eq. (5.24) assuming an initial convective velocity $U_c = 0$ m s^{-1} for stable conditions ($\theta_{v,atm} - \theta_{v,s} \ge 0$ as evaluated from eq. (5.50)) and $U_c = 0.5$ for unstable conditions ($\theta_{v,atm} - \theta_{v,s} < 0$).
3. An initial guess for the Monin-Obukhov length L is obtained from the bulk Richardson number using equation (5.46) and (5.48).
4. Iteration proceeds on the following system of equations:
   - Friction velocity u_* (eqs. (5.32), (5.33), (5.34), (5.35))
   - Ratio $\dfrac{\theta_*}{\theta_{atm} - \theta_s}$ (eqs. (5.37), (5.38), (5.39), (5.40))
   - Ratio $\dfrac{q_*}{q_{atm} - q_s}$ (eqs. (5.41), (5.42), (5.43), (5.44))

- Aerodynamic resistances r_{am}, r_{ah}, and r_{aw} (eqs. (5.55), (5.56), (5.57))
- Magnitude of the wind velocity incident on the leaves U_{av} (eq. (5.99))
- Leaf boundary layer resistance r_b (eq. (5.103))
- Aerodynamic resistances $r_{ah}{}'$ and $r_{aw}{}'$ (eq. (5.98))
- Sunlit and shaded stomatal resistances r_s^{sun} and r_s^{sha} (section 8)
- Sensible heat conductances c_a^h, c_g^h, and c_v^h (eqs. (5.76), (5.77), (5.78))
- Transpiration E_v^t (eq. (5.87)). This is an initial calculation to check for water limitations on r'' (eqs. (5.94) and (5.95)).
- Latent heat conductances c_a^w, c_v^w, and c_g^w (eqs. (5.91), (5.92), (5.93))
- Sensible heat flux from vegetation H_v (eq. (5.79))
- Latent heat flux from vegetation λE_v (eq. (5.96))
- If the latent heat flux has changed sign from the latent heat flux computed at the previous iteration ($\lambda E_v{}^{n+1} \times \lambda E_v{}^{n} < 0$), the latent heat flux is constrained to be 10% of the computed value. The difference between the constrained and computed value ($\Delta_1 = 0.1\lambda E_v{}^{n+1} - \lambda E_v{}^{n+1}$) is added to the sensible heat flux later.
- Change in vegetation temperature ΔT_v (eq. (5.109)) and update the vegetation temperature as $T_v^{n+1} = T_v^n + \Delta T_v$. T_v is constrained to change by no more than 1º in one iteration. If this limit is exceeded, the energy error is

$$\Delta_2 = \vec{S}_v - \vec{L}_v - \frac{\partial \vec{L}_v}{\partial T_v}\Delta T_v - H_v - \frac{\partial H_v}{\partial T_v}\Delta T_v - \lambda E_v - \frac{\partial \lambda E_v}{\partial T_v}\Delta T_v \tag{5.118}$$

where $\Delta T_v = 1$ or -1. The error Δ_2 is added to the sensible heat flux later.

- Water vapor flux E_v (eq. (5.113))
- Transpiration E_v^t (eq. (5.114))
- The water vapor flux E_v is constrained to be less than or equal to the sum of transpiration E_v^t and the water available from wetted leaves and stems. The energy error due to this constraint is

$$\Delta_3 = \max\left(0, E_v - E_v^t - \frac{W_{can}}{\Delta t}\right). \tag{5.119}$$

  The error $\lambda\Delta_3$ is added to the sensible heat flux later.

- Sensible heat flux H_v (eq. (5.115)). The three energy error terms, Δ_1, Δ_2, and Δ_3 are also added to the sensible heat flux.
- The saturated vapor pressure e_i (section 8), saturated specific humidity $q_{sat}^{T_v}$ and its derivative $\frac{dq_{sat}^{T_v}}{dT_v}$ at the leaf surface (section 5.5), are re-evaluated based on the new T_v.
- Canopy air temperature T_s (eq. (5.75))
- Canopy air specific humidity q_s (eq. (5.90))
- Temperature difference $\theta_{atm} - \theta_s$
- Specific humidity difference $q_{atm} - q_s$
- Potential temperature scale $\theta_* = \frac{\theta_*}{\theta_{atm} - \theta_s}\left(\theta_{atm} - \theta_s\right)$ where $\frac{\theta_*}{\theta_{atm} - \theta_s}$ was calculated earlier in the iteration

- Humidity scale $q_* = \frac{q_*}{q_{atm} - q_s}(q_{atm} - q_s)$ where $\frac{q_*}{q_{atm} - q_s}$ was calculated earlier in the iteration
- Virtual potential temperature scale θ_{v*} (eq. (5.17))
- Wind speed including the convective velocity, V_a (eq. (5.24))
- Monin-Obukhov length L (eq. (5.49))
- The iteration is stopped after two or more steps if $\tilde{\Delta} T_v < 0.01$ and $\left|\lambda E_v^{n+1} - \lambda E_v^n\right| < 0.1$ where $\tilde{\Delta} T_v = \max\left(\left|T_v^{n+1} - T_v^n\right|, \left|T_v^n - T_v^{n-1}\right|\right)$, or after forty iterations have been carried out.

5. Momentum fluxes τ_x, τ_y (eqs. (5.5), (5.6))
6. Sensible heat flux from ground H_g (eq. (5.74))
7. Water vapor flux from ground E_g (eq. (5.84))
8. 2-m height air temperature T_{2m} and specific humidity q_{2m} (eqs. (5.58), (5.59))

5.4 Update of Ground Sensible and Latent Heat Fluxes

The sensible and water vapor heat fluxes derived above for bare soil and soil beneath canopy are based on the ground surface temperature from the previous time step T_g^n and are used as the surface forcing for the solution of the soil temperature equations (section 6.1). This solution yields a new ground surface temperature T_g^{n+1}. The ground sensible and water vapor fluxes are then updated for T_g^{n+1} as

$$H_g' = H_g + \left(T_g^{n+1} - T_g^n\right)\frac{\partial H_g}{\partial T_g} \tag{5.120}$$

$$E'_g = E_g + \left(T_g^{n+1} - T_g^n\right)\frac{\partial E_g}{\partial T_g} \tag{5.121}$$

where H_g and E_g are the sensible heat and water vapor fluxes derived from equations (5.60) and (5.61) for non-vegetated surfaces and equations (5.74) and (5.84) for vegetated surfaces using T_g^n. One further adjustment is made to H'_g and E'_g. If the soil moisture in the top snow/soil layer is not sufficient to support the updated ground evaporation, i.e., if $E'_g > 0$ and $f_{evap} < 1$ where

$$f_{evap} = \frac{\left(w_{ice,\,snl+1} + w_{liq,snl+1}\right)/\Delta t}{\sum_{j=1}^{npft}\left(E'_g\right)_j\left(wt\right)_j} \le 1, \tag{5.122}$$

an adjustment is made to reduce the ground evaporation accordingly as

$$E''_g = f_{evap} E'_g. \tag{5.123}$$

The term $\sum_{j=1}^{npft}\left(E'_g\right)_j\left(wt\right)_j$ is the sum of E'_g over all evaporating PFTs where $\left(E'_g\right)_j$ is the ground evaporation from the j^{th} PFT on the column, $\left(wt\right)_j$ is the relative area of the j^{th} PFT with respect to the column, and $npft$ is the number of PFTs on the column. $w_{ice,snl+1}$ and $w_{liq,snl+1}$ are the ice and liquid water contents (kg m^{-2}) of the top snow/soil layer (section 7). The resulting energy deficit is assigned to sensible heat as

$$H''_g = H_g + \lambda\left(E'_g - E''_g\right). \tag{5.124}$$

The ground water vapor flux E''_g is partitioned into evaporation of liquid water from snow/soil q_{seva} (kg m^{-2} s^{-1}), sublimation from snow/soil ice q_{subl} (kg m^{-2} s^{-1}), liquid dew on snow/soil q_{sdew} (kg m^{-2} s^{-1}), or frost on snow/soil q_{frost} (kg m^{-2} s^{-1}) as

$$q_{seva} = \min\left(\frac{E'_g}{\sum_{j=1}^{npft}\left(E'_g\right)_j\left(wt\right)_j}\frac{w_{liq,snl+1}}{\Delta t}, E''_g\right) \qquad E''_g \ge 0 \tag{5.125}$$

$$q_{subl} = E''_g - q_{seva} \qquad E''_g \ge 0 \tag{5.126}$$

$$q_{sdew} = \left|E''_g\right| \qquad E''_g < 0 \text{ and } T_g \ge T_f \tag{5.127}$$

$$q_{frost} = \left|E''_g\right| \qquad E''_g < 0 \text{ and } T_g < T_f . \tag{5.128}$$

The loss or gain in snow mass due to q_{seva}, q_{subl}, q_{sdew}, and q_{frost} on a snow surface are accounted for during the snow hydrology calculations (section 7.2). The loss of soil surface water due to q_{seva} is accounted for in the calculation of infiltration (section 7.3), while losses or gains due to q_{subl}, q_{sdew}, and q_{frost} on a soil surface are accounted for following the sub-surface drainage calculations (section 7.5).

The ground heat flux G is calculated as

$$G = \vec{S}_g - \vec{L}_g - H_g - \lambda E_g \tag{5.129}$$

where $\vec{S}_g$ is the solar radiation absorbed by the ground (section 4.1), $\vec{L}_g$ is the net longwave radiation absorbed by the ground (section 4.2)

$$\vec{L}_g = \varepsilon_g \sigma \left(T_g^n\right)^4 - \delta_{veg}\varepsilon_g L_v \downarrow - \left(1-\delta_{veg}\right)\varepsilon_g L_{atm} \downarrow + 4\varepsilon_g \sigma \left(T_g^n\right)^3 \left(T_g^{n+1} - T_g^n\right), \tag{5.130}$$

and H_g and λE_g are the sensible and latent heat fluxes after the adjustments described above.

When converting ground water vapor flux to an energy flux, the term λ is arbitrarily assumed to be

$$\lambda = \left\{ \begin{array}{ll} \lambda_{sub} & \text{if } w_{liq,snl+1} = 0 \text{ and } w_{ice,snl+1} > 0 \\ \lambda_{vap} & \text{otherwise} \end{array} \right\} \tag{5.131}$$

where λ_{sub} and λ_{vap} are the latent heat of sublimation and vaporization, respectively (J kg^{-1}) (Table 1.4). When converting vegetation water vapor flux to an energy flux, λ_{vap} is used.

The system balances energy as

$$\vec{S}_g + \vec{S}_v + L_{atm} \downarrow - L \uparrow - H_v - H_g - \lambda_{vap} E_v - \lambda E_g - G = 0. \tag{5.132}$$

5.5 Saturation Vapor Pressure

Saturation vapor pressure e_{sat}^T (Pa) and its derivative $\frac{de_{sat}^T}{dT}$, as a function of temperature T (ºC), are calculated from the eighth-order polynomial fits of Flatau et al. (1992)

$$e_{sat}^T = 100\left[a_0 + a_1 T + \cdots + a_n T^n\right] \tag{5.133}$$

$$\frac{de_{sat}^T}{dT} = 100\left[b_0 + b_1 T + \cdots + b_n T^n\right] \tag{5.134}$$

where the coefficients for ice are valid for $-75\,^{\circ}\text{C} \le T < 0\,^{\circ}\text{C}$ and the coefficients for water are valid for $0\,^{\circ}\text{C} \le T \le 100\,^{\circ}\text{C}$ (Table 5.2 and 5.3). The saturated water vapor specific humidity q_{sat}^T and its derivative $\frac{dq_{sat}^T}{dT}$ are

$$q_{sat}^T = \frac{0.622 e_{sat}^T}{P_{atm} - 0.378 e_{sat}^T} \tag{5.135}$$

$$\frac{dq_{sat}^T}{dT} = \frac{0.622 P_{atm}}{\left(P_{atm} - 0.378 e_{sat}^T\right)^2} \frac{de_{sat}^T}{dT}. \tag{5.136}$$

Table 5.2. Coefficients for e_{sat}^{T}

	water	ice
a_0	6.11213476	6.11123516
a_1	4.44007856×10^{-1}	5.03109514×10^{-1}
a_2	1.43064234×10^{-2}	1.88369801×10^{-2}
a_3	2.64461437×10^{-4}	4.20547422×10^{-4}
a_4	3.05903558×10^{-6}	6.14396778×10^{-6}
a_5	1.96237241×10^{-8}	6.02780717×10^{-8}
a_6	8.92344772×10^{-11}	3.87940929×10^{-10}
a_7	$-3.73208410\times10^{-13}$	1.49436277×10^{-12}
a_8	2.09339997×10^{-16}	2.62655803×10^{-15}

Table 5.3. Coefficients for $\frac{de_{sat}^{T}}{dT}$

	water	ice
b_0	4.44017302×10^{-1}	5.03277922×10^{-1}
b_1	2.86064092×10^{-2}	3.77289173×10^{-2}
b_2	7.94683137×10^{-4}	1.26801703×10^{-3}
b_3	1.21211669×10^{-5}	2.49468427×10^{-5}
b_4	1.03354611×10^{-7}	3.13703411×10^{-7}
b_5	4.04125005×10^{-10}	2.57180651×10^{-9}
b_6	$-7.88037859\times10^{-13}$	1.33268878×10^{-11}
b_7	$-1.14596802\times10^{-14}$	3.94116744×10^{-14}
b_8	3.81294516×10^{-17}	4.98070196×10^{-17}

6. Soil and Snow Temperatures

The first law of heat conduction is

$$F = -\lambda \nabla T \tag{6.1}$$

where F is the amount of heat conducted across a unit cross-sectional area in unit time (W m^{-2}), λ is thermal conductivity (W m^{-1} K^{-1}), and ∇T is the spatial gradient of temperature (K m^{-1}). In one-dimensional form

$$F_z = -\lambda \frac{\partial T}{\partial z} \tag{6.2}$$

where z is in the vertical direction (m) and is positive downward and F_z is positive upward. To account for non-steady or transient conditions, the principle of energy conservation in the form of the continuity equation is invoked as

$$c\frac{\partial T}{\partial t} = -\frac{\partial F_z}{\partial z} \tag{6.3}$$

where c is the volumetric snow/soil heat capacity (J m^{-3} K^{-1}) and t is time (s). Combining equations (6.2) and (6.3) yields the second law of heat conduction in one-dimensional form

$$c\frac{\partial T}{\partial t} = \frac{\partial}{\partial z}\left[\lambda \frac{\partial T}{\partial z}\right]. \tag{6.4}$$

This equation is solved numerically to calculate the soil and snow temperatures for a ten-layer soil column with up to five overlaying layers of snow with the boundary conditions of h as the heat flux into the surface snow/soil layer from the overlying atmosphere and zero heat flux at the bottom of the soil column. The temperature profile is calculated first without phase change and then readjusted for phase change (section 6.2).

6.1 Numerical Solution

The soil column is discretized into ten layers where the depth of soil layer i, or node depth, z_i (m), is

$$z_i = f_s \left\{ \exp\left[0.5\left(i - 0.5\right)\right] - 1 \right\} \tag{6.5}$$

where $f_s = 0.025$ is a scaling factor. The thickness of each layer Δz_i (m) is

$$\Delta z_i = \left\{ \begin{array}{ll} 0.5\left(z_1 + z_2\right) & i = 1 \\ 0.5\left(z_{i+1} - z_{i-1}\right) & i = 2,3,\ldots,N-1 \\ z_N - z_{N-1} & i = N \end{array} \right\} \tag{6.6}$$

where $N = 10$ is the number of soil layers. The depths at the layer interfaces $z_{h,i}$ (m) are

$$z_{h,i} = \left\{ \begin{array}{ll} 0.5\left(z_i + z_{i+1}\right) & i = 1,2,\ldots,N-1 \\ z_N + 0.5\Delta z_N & i = N \end{array} \right\}. \tag{6.7}$$

The exponential form of equation (6.5) is to obtain more soil layers near the soil surface where the soil water gradient is generally strong (section 7.4).

The overlying snow pack is modeled with up to five layers depending on the total snow depth. The layers from top to bottom are indexed in the fortran code as $i = -4, -3, -2, -1, 0$, which permits the accumulation or ablation of snow at the top of the snow pack without renumbering the layers. Layer $i = 0$ is the snow layer next to the soil surface and layer $i = snl + 1$ is the top layer, where the variable snl is the negative of the number of snow layers. The number of snow layers and the thickness of each layer is a function of snow depth z_{sno} (m) as follows.

$$\left\{ \begin{array}{ll} snl = -1 & \\ \Delta z_0 = z_{sno} & \text{for } 0.01 \le \mathrm{z_{sno}} \le 0.03 \end{array} \right\},$$

$$\left\{\begin{array}{ll} snl = -2 & \\ \Delta z_{-1} = z_{sno}/2 & \text{for } 0.03 < \mathrm{z_{sno}} \le 0.04 \\ \Delta z_0 = \Delta z_{-1} & \end{array}\right\},$$

$$\left\{\begin{array}{ll} snl = -2 & \\ \Delta z_{-1} = 0.02 & \text{for } 0.04 < \mathrm{z_{sno}} \le 0.07 \\ \Delta z_0 = z_{sno} - \Delta z_{-1} & \end{array}\right\},$$

$$\left\{\begin{array}{ll} snl = -3 & \\ \Delta z_{-2} = 0.02 & \\ \Delta z_{-1} = \left(z_{sno} - 0.02\right)/2 & \text{for } 0.07 < \mathrm{z_{sno}} \le 0.12 \\ \Delta z_0 = \Delta z_{-1} & \end{array}\right\},$$

$$\left\{\begin{array}{ll} snl = -3 & \\ \Delta z_{-2} = 0.02 & \\ \Delta z_{-1} = 0.05 & \text{for } 0.12 < \mathrm{z_{sno}} \le 0.18 \\ \Delta z_0 = z_{sno} - \Delta z_{-2} - \Delta z_{-1} & \end{array}\right\},$$

$$\left\{\begin{array}{ll} snl = -4 & \\ \Delta z_{-3} = 0.02 & \\ \Delta z_{-2} = 0.05 & \text{for } 0.18 < \mathrm{z_{sno}} \le 0.29 \\ \Delta z_{-1} = \left(z_{sno} - \Delta z_{-3} - \Delta z_{-2}\right)/2 & \\ \Delta z_0 = \Delta z_{-1} & \end{array}\right\},$$

$$\left\{\begin{array}{ll} snl = -4 & \\ \Delta z_{-3} = 0.02 & \\ \Delta z_{-2} = 0.05 & \text{for } 0.29 < \mathrm{z_{sno}} \le 0.41 \\ \Delta z_{-1} = 0.11 & \\ \Delta z_0 = z_{sno} - \Delta z_{-3} - \Delta z_{-2} - \Delta z_{-1} & \end{array}\right\},$$

$$\left\{\begin{array}{ll} snl = -5 & \\ \Delta z_{-4} = 0.02 & \\ \Delta z_{-3} = 0.05 & \text{for } 0.41 < \mathrm{z_{sno}} \le 0.64 \\ \Delta z_{-2} = 0.11 & \\ \Delta z_{-1} = \left(z_{sno} - \Delta z_{-4} - \Delta z_{-3} - \Delta z_{-2}\right)/2 & \\ \Delta z_0 = \Delta z_{-1} & \end{array}\right\},$$

$$\left\{\begin{array}{ll} snl = -5 & \\ \Delta z_{-4} = 0.02 & \\ \Delta z_{-3} = 0.05 & \text{for } 0.64 < \mathrm{z_{sno}} \\ \Delta z_{-2} = 0.11 & \\ \Delta z_{-1} = 0.23 & \\ \Delta z_{0} = z_{sno} - \Delta z_{-4} - \Delta z_{-3} - \Delta z_{-2} - \Delta z_{-1} & \end{array}\right\}.$$

The node depths, which are located at the midpoint of the snow layers, and the layer interfaces are both referenced from the soil surface and are defined as negative values

$$z_i = z_{h,i} - 0.5\Delta z_i \qquad i = snl + 1, \ldots, 0 \tag{6.8}$$

$$z_{h,i} = z_{h,i+1} - \Delta z_{i+1} \qquad i = snl, \ldots, -1 . \tag{6.9}$$

Note that $z_{h,0}$, the interface between the bottom snow layer and the top soil layer, is zero. Thermal properties (i.e., temperature T_i [K]; thermal conductivity λ_i [W m^{-1} K^{-1}]; volumetric heat capacity c_i [J m^{-3} K^{-1}]) are defined for soil layers at the node depths (Figure 6.1) and for snow layers at the layer midpoints.

The heat flux F_i (W m^{-2}) from layer i to layer $i+1$ is

$$F_i = -\lambda\left[z_{h,i}\right]\left(\frac{T_i - T_{i+1}}{z_{i+1} - z_i}\right) \tag{6.10}$$

where the thermal conductivity at the interface $\lambda\left[z_{h,i}\right]$ is

$$\lambda\left[z_{h,i}\right] = \left\{\begin{array}{ll} \dfrac{\lambda_i \lambda_{i+1}\left(z_{i+1} - z_i\right)}{\lambda_i\left(z_{i+1} - z_{h,i}\right) + \lambda_{i+1}\left(z_{h,i} - z_i\right)} & i = snl + 1, \ldots, N - 1 \\ 0 & i = N \end{array}\right\}. \tag{6.11}$$

These equations are derived, with reference to Figure 6.1, assuming that the heat flux from i (depth z_i) to the interface between i and $i+1$ (depth $z_{h,i}$) equals the heat flux from the interface to $i+1$ (depth z_{i+1}), i.e.,

$$-\lambda_i \frac{T_i - T_m}{z_{h,i} - z_i} = -\lambda_{i+1} \frac{T_m - T_{i+1}}{z_{i+1} - z_{h,i}} \tag{6.12}$$

where T_m is the temperature at the interface of layers i and $i+1$. Solving equation (6.12) for T_m and substituting T_m back into the left side of equation (6.12) yields equations (6.10) and (6.11).

Figure 6.1. Schematic diagram of numerical scheme used to solve for soil temperature. Shown are three soil layers, $i-1$, i, and $i+1$. The thermal conductivity λ, specific heat capacity c, and temperature T are defined at the layer node depth z. T_m is the interface temperature. The thermal conductivity $\lambda\left[z_h\right]$ is defined at the interface of two layers z_h. The layer thickness is Δz. The heat fluxes F_{i-1} and F_i are defined as positive upwards.

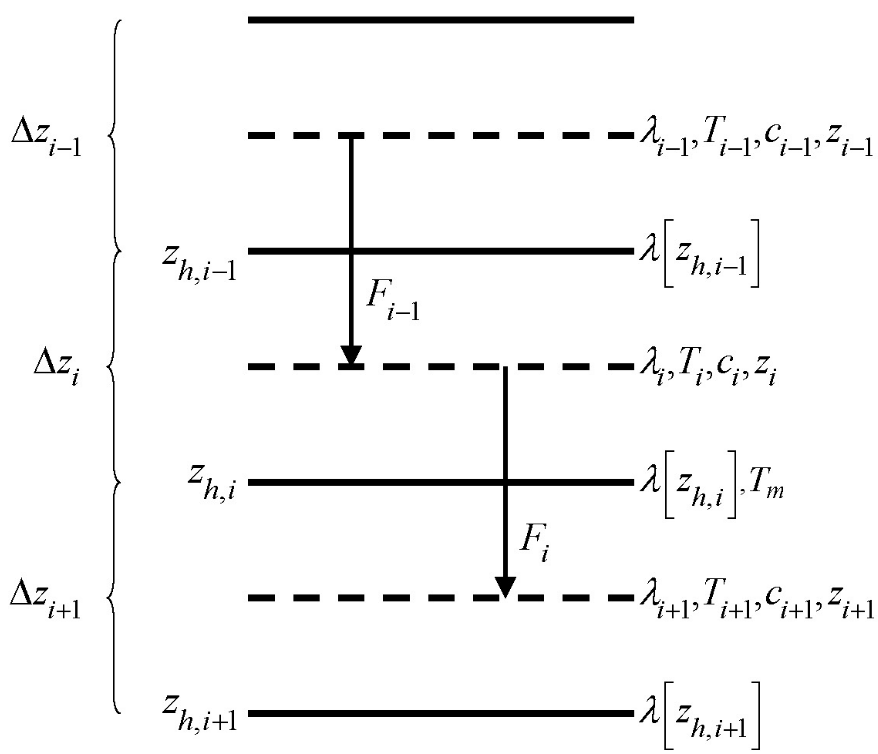

The energy balance for the i^{th} layer is

$$\frac{c_i \Delta z_i}{\Delta t}\left(T_i^{n+1} - T_i^n\right) = -F_{i-1} + F_i \tag{6.13}$$

where the superscripts n and $n+1$ indicate values at the beginning and end of the time step, respectively, and Δt is the time step (s). This equation is solved using the Crank-Nicholson method, which combines the explicit method with fluxes evaluated at n (F_{i-1}^n, F_i^n) and the implicit method with fluxes evaluated at $n+1$ (F_{i-1}^{n+1}, F_i^{n+1})

$$\frac{c_i \Delta z_i}{\Delta t}\left(T_i^{n+1} - T_i^n\right) = \alpha\left(-F_{i-1}^n + F_i^n\right) + \left(1-\alpha\right)\left(-F_{i-1}^{n+1} + F_i^{n+1}\right) \tag{6.14}$$

where $\alpha = 0.5$, resulting in a tridiagonal system of equations

$$r_i = a_i T_{i-1}^{n+1} + b_i T_i^{n+1} + c_i T_{i+1}^{n+1} \tag{6.15}$$

where a_i, b_i, and c_i are the subdiagonal, diagonal, and superdiagonal elements in the tridiagonal matrix and r_i is a column vector of constants.

For the top snow/soil layer $i = snl + 1$, the heat flux from the overlying atmosphere into the surface snow/soil layer h (W m^{-2}, defined as positive into the soil) is

$$h^{n+1} = -\alpha F_{i-1}^n - \left(1-\alpha\right) F_{i-1}^{n+1}. \tag{6.16}$$

The energy balance for layer $i = snl + 1$ is then

$$\frac{c_i \Delta z_i}{\Delta t}\left(T_i^{n+1} - T_i^n\right) = h^{n+1} + \alpha F_i^n + \left(1-\alpha\right) F_i^{n+1}. \tag{6.17}$$

The heat flux h at $n+1$ may be approximated as follows

$$h^{n+1} = h^n + \frac{\partial h}{\partial T_i}\left(T_i^{n+1} - T_i^n\right). \tag{6.18}$$

The resulting equations are then

$$\frac{c_i \Delta z_i}{\Delta t}\left(T_i^{n+1} - T_i^n\right) = h^n + \frac{\partial h}{\partial T_i}\left(T_i^{n+1} - T_i\right)$$
$$-\alpha \frac{\lambda\left[z_{h,i}\right]\left(T_i^n - T_{i+1}^n\right)}{z_{i+1} - z_i} - \left(1-\alpha\right)\frac{\lambda\left[z_{h,i}\right]\left(T_i^{n+1} - T_{i+1}^{n+1}\right)}{z_{i+1} - z_i} \tag{6.19}$$

$$a_i = 0 \tag{6.20}$$

$$b_i = 1 + \frac{\Delta t}{c_i \Delta z_i}\left[\left(1-\alpha\right)\frac{\lambda\left[z_{h,i}\right]}{z_{i+1} - z_i} - \frac{\partial h}{\partial T_i}\right] \tag{6.21}$$

$$c_i = -\left(1-\alpha\right)\frac{\Delta t}{c_i \Delta z_i}\frac{\lambda\left[z_{h,i}\right]}{z_{i+1} - z_i} \tag{6.22}$$

$$r_i = T_i^n + \frac{\Delta t}{c_i \Delta z_i}\left[h^n - \frac{\partial h}{\partial T_i}T_i^n + \alpha F_i\right] \tag{6.23}$$

where

$$F_i = -\lambda\left[z_{h,i}\right]\left(\frac{T_i^n - T_{i+1}^n}{z_{i+1} - z_i}\right). \tag{6.24}$$

The heat flux into the snow/soil surface from the overlying atmosphere h is

$$h = \vec{S}_g - \vec{L}_g - H_g - \lambda E_g \tag{6.25}$$

where $\vec{S}_g$ is the solar radiation absorbed by the ground (section 4.1), $\vec{L}_g$ is the longwave radiation absorbed by the ground (positive toward the atmosphere) (section 4.2), H_g is the sensible heat flux from the ground (section 5), and λE_g is the latent heat flux from the ground (section 5). The partial derivative of the heat flux h with respect to ground temperature is

$$\frac{\partial h}{\partial T_g} = -\frac{\partial \vec{L}_g}{\partial T_g} - \frac{\partial H_g}{\partial T_g} - \frac{\partial \lambda E_g}{\partial T_g} \tag{6.26}$$

where the partial derivative of the net longwave radiation is

$$\frac{\partial \vec{L}_g}{\partial T_g} = -4\varepsilon_g \sigma \left(T_g^n\right)^3 \tag{6.27}$$

and the partial derivatives of the sensible and latent heat fluxes are given by equations (5.68) and (5.69) for non-vegetated surfaces, and by equations (5.104) and (5.105) for vegetated surfaces. σ is the Stefan-Boltzmann constant (W m^{-2} K^{-4}) (Table 1.4) and ε_g is the ground emissivity (section 4.2). For purposes of computing h and $\frac{\partial h}{\partial T_g}$, the term λ is arbitrarily assumed to be

$$\lambda = \begin{cases} \lambda_{sub} & \text{if } w_{liq,snl+1} = 0 \text{ and } w_{ice,snl+1} > 0 \\ \lambda_{vap} & \text{otherwise} \end{cases} \tag{6.28}$$

where λ_{sub} and λ_{vap} are the latent heat of sublimation and vaporization, respectively (J kg^{-1}) (Table 1.4), and $w_{liq,snl+1}$ and $w_{ice,snl+1}$ are the liquid water and ice contents of the top snow/soil layer, respectively (kg m^{-2}) (section 7).

The surface snow/soil layer temperature computed in this way is the layer-averaged temperature and hence has a somewhat reduced diurnal amplitude compared with surface temperature. An accurate surface temperature is provided that compensates for this effect and numerical error by tuning the heat capacity of the top layer (through adjustment of the layer thickness) to give an exact match to the analytic solution for diurnal heating. The top layer thickness for $i = snl + 1$ is given by

$$\Delta z_{i*} = 0.5\left[z_i - z_{h,i-1} + c_a\left(z_{i+1} - z_{h,i-1}\right)\right] \tag{6.29}$$

where c_a is a tunable parameter, varying from 0 to 1, and is taken as 0.34 by comparing the numerical solution with the analytic solution (Z.-L. Yang 1998, unpublished manuscript). Δz_{i*} is used in place of Δz_i for $i = snl + 1$ in equations (6.19)-(6.24). The top snow/soil layer temperature computed in this way is the ground surface temperature T_g^{n+1}.

The boundary condition at the bottom of the snow/soil column is zero heat flux, $F_i = 0$, resulting in, for $i = N$,

$$\frac{c_i \Delta z_i}{\Delta t}\left(T_i^{n+1} - T_i^n\right) = \alpha \frac{\lambda\left[z_{h,i-1}\right]\left(T_{i-1}^n - T_i^n\right)}{z_i - z_{i-1}} + \left(1-\alpha\right)\frac{\lambda\left[z_{h,i-1}\right]\left(T_{i-1}^{n+1} - T_i^{n+1}\right)}{z_i - z_{i-1}} \tag{6.30}$$

$$a_i = -\left(1-\alpha\right)\frac{\Delta t}{c_i \Delta z_i}\frac{\lambda\left[z_{h,i-1}\right]}{z_i - z_{i-1}} \tag{6.31}$$

$$b_i = 1 + \left(1-\alpha\right)\frac{\Delta t}{c_i \Delta z_i}\frac{\lambda\left[z_{h,i-1}\right]}{z_i - z_{i-1}} \tag{6.32}$$

$$c_i = 0 \tag{6.33}$$

$$r_i = T_i^n - \alpha \frac{\Delta t}{c_i \Delta z_i} F_{i-1} \tag{6.34}$$

where

$$F_{i-1} = -\frac{\lambda\left[z_{h,i-1}\right]}{z_i - z_{i-1}}\left(T_{i-1}^n - T_i^n\right). \tag{6.35}$$

For the interior snow/soil layers, $snl + 1 < i < N$,

$$\begin{aligned}\frac{c_i \Delta z_i}{\Delta t}\left(T_i^{n+1} - T_i^n\right) = &-\alpha \frac{\lambda\left[z_{h,i}\right]\left(T_i^n - T_{i+1}^n\right)}{z_{i+1} - z_i} + \alpha \frac{\lambda\left[z_{h,i-1}\right]\left(T_{i-1}^n - T_i^n\right)}{z_i - z_{i-1}} \\ &-\left(1-\alpha\right)\frac{\lambda\left[z_{h,i}\right]\left(T_i^{n+1} - T_{i+1}^{n+1}\right)}{z_{i+1} - z_i} + \left(1-\alpha\right)\frac{\lambda\left[z_{h,i-1}\right]\left(T_{i-1}^{n+1} - T_i^{n+1}\right)}{z_i - z_{i-1}}\end{aligned} \tag{6.36}$$

$$a_i = -\left(1-\alpha\right)\frac{\Delta t}{c_i \Delta z_i}\frac{\lambda\left[z_{h,i-1}\right]}{z_i - z_{i-1}} \tag{6.37}$$

$$b_i = 1 + \left(1-\alpha\right)\frac{\Delta t}{c_i \Delta z_i}\left[\frac{\lambda\left[z_{h,i-1}\right]}{z_i - z_{i-1}} + \frac{\lambda\left[z_{h,i}\right]}{z_{i+1} - z_i}\right] \tag{6.38}$$

$$c_i = -\left(1-\alpha\right)\frac{\Delta t}{c_i \Delta z_i}\frac{\lambda\left[z_{h,i}\right]}{z_{i+1} - z_i} \tag{6.39}$$

$$r_i = T_i^n + \alpha \frac{\Delta t}{c_i \Delta z_i}\left(F_i - F_{i-1}\right). \tag{6.40}$$

6.2 Phase Change

Upon solution of the tridiagonal equation set (Press et al. 1992), the snow/soil temperatures are evaluated to determine if phase change will take place as

$$\begin{array}{lll} T_i^{n+1} > T_f \text{ and } w_{ice,i} > 0 & & \text{melting} \\ T_i^{n+1} < T_f \text{ and } w_{liq,i} > 0 & & \text{freezing} \end{array} \tag{6.41}$$

where T_i^{n+1} is the soil layer temperature after solution of the tridiagonal equation set, $w_{ice,i}$ and $w_{liq,i}$ are the mass of ice and liquid water (kg m^{-2}) in each snow/soil layer, respectively, and T_f is the freezing temperature of water (K) (Table 1.4). For the special case when snow is present (snow mass $W_{sno} > 0$) but there are no explicit snow layers ($snl = 0$) (i.e., there is not enough snow present to meet the minimum snow depth requirement of 0.01 m), snow melt will take place for soil layer $i = 1$ if the soil layer temperature is greater than the freezing temperature ($T_1^{n+1} > T_f$).

The rate of phase change is assessed from the energy excess (or deficit) needed to change T_i to freezing temperature, T_f. The excess or deficit of energy H_i (W m^{-2}) is determined as follows

$$H_i = \begin{Bmatrix} h + \frac{\partial h}{\partial T}\left(T_f - T_i^n\right) + \alpha F_i^n + (1-\alpha) F_i^{n+1} - \frac{c_i \Delta z_i}{\Delta t}\left(T_f - T_i^n\right) & i = snl+1 \\ \alpha\left(F_i^n - F_{i-1}^n\right) + (1-\alpha)\left(F_i^{n+1} - F_{i-1}^{n+1}\right) - \frac{c_i \Delta z_i}{\Delta t}\left(T_f - T_i^n\right) & i = snl+2,\ldots,N \end{Bmatrix} \quad (6.42)$$

where F_i^{n+1} and F_{i-1}^{n+1} are calculated from equations (6.24) and (6.35) using T_i^{n+1}. If the melting or freezing criteria are met (eq. (6.41)) and $|H_i| > 0$, then the ice mass is readjusted as

$$w_{ice,i}^{n+1} = \begin{Bmatrix} w_{ice,i}^n - \frac{H_i \Delta t}{L_f} \ge 0 & \frac{H_i \Delta t}{L_f} > 0 \\ \min\left(w_{liq,i}^n + w_{ice,i}^n,\, w_{ice,i}^n - \frac{H_i \Delta t}{L_f}\right) & \frac{H_i \Delta t}{L_f} < 0 \end{Bmatrix} \quad (6.43)$$

where L_f is the latent heat of fusion (J kg^{-1}) (Table 1.4). Liquid water mass is readjusted as

$$w_{liq,i}^{n+1} = w_{liq,i}^n + w_{ice,i}^n - w_{ice,i}^{n+1} \ge 0. \quad (6.44)$$

Because part of the energy H_i may not be consumed in melting or released in freezing, the energy is recalculated as

$$H_{i*} = H_i - \frac{L_f\left(w_{ice,i}^n - w_{ice,i}^{n+1}\right)}{\Delta t} \quad (6.45)$$

and this energy is used to cool or warm the snow/soil layer (if $|H_{i*}| > 0$) as

$$T_i^{n+1} = \begin{Bmatrix} T_f + \frac{\Delta t}{c_i \Delta z_i} H_{i*} \Big/ \left(1 - \frac{\Delta t}{c_i \Delta z_i} \frac{\partial h}{\partial T}\right) & i = snl+1 \\ T_f + \frac{\Delta t}{c_i \Delta z_i} H_{i*} & i = snl+2,\ldots N \end{Bmatrix}. \quad (6.46)$$

For the special case when snow is present ($W_{sno} > 0$), there are no explicit snow layers ($snl = 0$), and $\frac{H_1 \Delta t}{L_f} > 0$ (melting), the snow mass W_{sno} (kg m^{-2}) is reduced according to

$$W_{sno}^{n+1} = W_{sno}^{n} - \frac{H_1 \Delta t}{L_f} \geq 0 . \tag{6.47}$$

The snow depth is reduced proportionally

$$z_{sno}^{n+1} = \frac{W_{sno}^{n+1}}{W_{sno}^{n}} z_{sno}^{n} . \tag{6.48}$$

Again, because part of the energy may not be consumed in melting, the energy for the surface soil layer $i = 1$ is recalculated as

$$H_{1*} = H_1 - \frac{L_f \left(W_{sno}^{n} - W_{sno}^{n+1} \right)}{\Delta t} . \tag{6.49}$$

If there is excess energy ($H_{1*} > 0$), this energy becomes available to the top soil layer as

$$H_1 = H_{1*} . \tag{6.50}$$

The ice mass, liquid water content, and temperature of the top soil layer are then determined from equations (6.43), (6.44), and (6.46) using the recalculated energy from equation (6.50). Snow melt M_{1S} (kg m^{-2} s^{-1}) and phase change energy $E_{p,1S}$ (W m^{-2}) for this special case are

$$M_{1S} = \frac{W_{sno}^{n} - W_{sno}^{n+1}}{\Delta t} \geq 0 \tag{6.51}$$

$$E_{p,1S} = L_f M_{1S} . \tag{6.52}$$

The total energy of phase change E_p (W m^{-2}) for the snow/soil column is

$$E_p = E_{p,1S} + \sum_{i=snl+1}^{N} E_{p,i} \tag{6.53}$$

where

$$E_{p,i} = L_f \frac{\left(w_{ice,i}^{n} - w_{ice,i}^{n+1}\right)}{\Delta t}. \tag{6.54}$$

The total snow melt M (kg m^{-2} s^{-1}) is

$$M = M_{1S} + \sum_{i=snl+1}^{i=0} M_i \tag{6.55}$$

where

$$M_i = \frac{\left(w_{ice,i}^{n} - w_{ice,i}^{n+1}\right)}{\Delta t} \geq 0. \tag{6.56}$$

The solution for snow/soil temperatures conserves energy as

$$G - E_p - \sum_{i=snl+1}^{i=N} \frac{c_i \Delta z_i}{\Delta t}\left(T_i^{n+1} - T_i^{n}\right) = 0 \tag{6.57}$$

where G is the ground heat flux (section 5.4).

6.3 Soil and Snow Thermal Properties

Soil thermal conductivity λ_i (W m^{-1} K^{-1}) is from Farouki (1981)

$$\lambda_i = \begin{Bmatrix} K_{e,i}\lambda_{sat,i} + \left(1 - K_{e,i}\right)\lambda_{dry,i} & S_{r,i} > 1\times 10^{-7} \\ \lambda_{dry,i} & S_{r,i} \leq 1\times 10^{-7} \end{Bmatrix} \tag{6.58}$$

where $\lambda_{sat,i}$ is the saturated thermal conductivity, $\lambda_{dry,i}$ is the dry thermal conductivity, $K_{e,i}$ is the Kersten number, and $S_{r,i}$ is the wetness of the soil with respect to saturation. For glaciers and wetlands,

$$\lambda_i = \begin{Bmatrix} \lambda_{liq,i} & T_i \geq T_f \\ \lambda_{ice,i} & T_i < T_f \end{Bmatrix} \tag{6.59}$$

where λ_{liq} and λ_{ice} are the thermal conductivities of liquid water and ice, respectively (Table 1.4). The saturated thermal conductivity $\lambda_{sat,i}$ (W m^{-1} K^{-1}) depends on the thermal conductivities of the soil solid, liquid water, and ice constituents

$$\lambda_{sat,i} = \begin{Bmatrix} \lambda_{s,i}^{1-\theta_{sat,i}} \lambda_{liq}^{\theta_{sat,i}} & T_i \geq T_f \\ \lambda_{s,i}^{1-\theta_{sat,i}} \lambda_{liq}^{\theta_{sat,i}} \lambda_{ice}^{\theta_{sat,i}-\theta_{liq,i}} & T_i < T_f \end{Bmatrix} \tag{6.60}$$

where the thermal conductivity of soil solids $\lambda_{s,i}$ varies with the sand and clay content

$$\lambda_{s,i} = \frac{8.80\ (\%sand)_i + 2.92\ (\%clay)_i}{(\%sand)_i + (\%clay)_i}, \tag{6.61}$$

and $\theta_{sat,i}$ is the volumetric water content at saturation (porosity) (section 7.4.1). The thermal conductivity of dry natural soil $\lambda_{dry,i}$ (W m^{-1} K^{-1}) depends on the bulk density $\rho_{d,i} = 2700\left(1-\theta_{sat,i}\right)$ kg m^{-3} as

$$\lambda_{dry,i} = \frac{0.135\rho_{d,i} + 64.7}{2700 - 0.947\rho_{d,i}}. \tag{6.62}$$

The Kersten number $K_{e,i}$ is a function of the degree of saturation S_r and phase of water

$$K_{e,i} = \begin{Bmatrix} \log\left(S_{r,i}\right) + 1 \geq 0 & T_i \geq T_f \\ S_{r,i} & T_i < T_f \end{Bmatrix} \tag{6.63}$$

where

$$S_{r,i} = \left(\frac{w_{liq,i}}{\rho_{liq}\Delta z_i} + \frac{w_{ice,i}}{\rho_{ice}\Delta z_i}\right)\frac{1}{\theta_{sat,i}} = \frac{\theta_{liq,i} + \theta_{ice,i}}{\theta_{sat,i}} \leq 1. \tag{6.64}$$

Thermal conductivity λ_i (W m^{-1} K^{-1}) for snow is from Jordan (1991)

$$\lambda_i = \lambda_{air} + \left(7.75\times10^{-5}\rho_{sno,i} + 1.105\times10^{-6}\rho_{sno,i}^2\right)\left(\lambda_{ice} - \lambda_{air}\right) \tag{6.65}$$

where λ_{air} is the thermal conductivity of air (Table 1.4) and $\rho_{sno,i}$ is the bulk density of snow (kg m^{-3})

$$\rho_{sno,i} = \frac{w_{ice,i} + w_{liq,i}}{\Delta z_i}. \tag{6.66}$$

The volumetric heat capacity c_i (J m^{-3} K^{-1}) for soil is from de Vries (1963) and depends on the heat capacities of the soil solid, liquid water, and ice constituents

$$c_i = c_{s,i}\left(1 - \theta_{sat,i}\right) + \frac{w_{ice,i}}{\Delta z_i} C_{ice} + \frac{w_{liq,i}}{\Delta z_i} C_{liq} \tag{6.67}$$

where the heat capacity of soil solids $c_{s,i}$ (J m^{-3} K^{-1}) is

$$c_{s,i} = \left(\frac{2.128\ (\%sand)_i + 2.385\ (\%clay)_i}{(\%sand)_i + (\%clay)_i}\right) \times 10^6 \tag{6.68}$$

and C_{liq} and C_{ice} are the specific heat capacities (J kg^{-1} K^{-1}) of liquid water and ice, respectively (Table 1.4). For glaciers, wetlands, and snow

$$c_i = \frac{w_{ice,i}}{\Delta z_i} C_{ice} + \frac{w_{liq,i}}{\Delta z_i} C_{liq}. \tag{6.69}$$

For the special case when snow is present ($W_{sno} > 0$) but there are no explicit snow layers ($snl = 0$), the heat capacity of the top layer is a blend of ice and soil heat capacity

$$c_1 = c_{1,soil} + \frac{C_{ice} W_{sno}}{\Delta z_1} \tag{6.70}$$

where $c_{1,soil}$ is calculated from equation (6.67) or (6.69).

7. Hydrology

The model parameterizes interception, throughfall, canopy drip, snow accumulation and melt, water transfer between snow layers, infiltration, surface runoff, sub-surface drainage, and redistribution within the soil column to simulate changes in canopy water ΔW_{can}, snow water ΔW_{sno}, soil water $\Delta w_{liq,i}$, and soil ice $\Delta w_{ice,i}$ (all in kg m^{-2} or mm of H_2O).

The total water balance of the system is

$$\Delta W_{can} + \Delta W_{sno} + \sum_{i=1}^{N} \left(\Delta w_{liq,i} + \Delta w_{ice,i} \right) = \left(q_{rain} + q_{sno} - E_v - E_g - q_{over} - q_{drai} - q_{rgwl} \right) \Delta t \quad (7.1)$$

where q_{rain} is liquid part of precipitation, q_{sno} is solid part of precipitation, E_v is evapotranspiration from vegetation (section 5), E_g is ground evaporation (section 5), q_{over} is surface runoff (section 7.3), q_{drai} is sub-surface drainage (section 7.5), q_{rgwl} is runoff from glaciers, wetlands, and lakes, and runoff from other surface types due to snow capping (section 7.6) (all in kg m^{-2} s^{-1}), N is the number of soil layers, and Δt is the time step (s).

7.1 Canopy Water

Precipitation is either intercepted by the canopy, falls directly through to the snow/soil surface (throughfall), or drips off the vegetation (canopy drip). Interception by vegetation q_{intr} (kg m^{-2} s^{-1}) does not distinguish between liquid and solid phases

$$q_{intr} = \left(q_{rain} + q_{sno} \right) \left[1 - \exp\left(-0.5 \left(L + S \right) \right) \right] \quad (7.2)$$

where L and S are the exposed leaf and stem area index, respectively (section 2.3). Throughfall (kg m^{-2} s^{-1}), however, is divided into liquid and solid phases reaching the ground (soil or snow surface) as

$$q_{thru,liq} = q_{rain} \exp\left[-0.5\left(L+S\right)\right] \tag{7.3}$$

$$q_{thru,ice} = q_{sno} \exp\left[-0.5\left(L+S\right)\right]. \tag{7.4}$$

Similarly, the canopy drip is

$$q_{drip,liq} = \frac{W_{can}^{intr} - W_{can,\max}}{\Delta t} \frac{q_{rain}}{q_{rain} + q_{sno}} \ge 0 \tag{7.5}$$

$$q_{drip,ice} = \frac{W_{can}^{intr} - W_{can,\max}}{\Delta t} \frac{q_{sno}}{q_{rain} + q_{sno}} \ge 0 \tag{7.6}$$

where

$$W_{can}^{intr} = W_{can}^{n} + q_{intr} \Delta t \ge 0 \tag{7.7}$$

is the canopy water after accounting for interception, W_{can}^{n} is the canopy water from the previous time step, and $W_{can,\max}$ (kg m^{-2}) is the maximum amount of water the canopy can hold

$$W_{can,\max} = p\left(L+S\right). \tag{7.8}$$

The maximum storage of solid water is assumed to be the same as that of liquid water, $p = 0.1$ kg m^{-2} (Dickinson et al. 1993). The canopy water is updated as

$$W_{can}^{n+1} = W_{can}^{n} + q_{intr} \Delta t - \left(q_{drip,liq} + q_{drip,ice}\right) \Delta t - E_{v}^{w} \Delta t \ge 0. \tag{7.9}$$

where E_{v}^{w} is the flux of water vapor from stem and leaf surfaces (section 5).

The total rate of liquid and solid precipitation reaching the ground is then

$$q_{grnd,liq} = q_{thru,liq} + q_{drip,liq} \tag{7.10}$$

$$q_{grnd,ice} = q_{thru,ice} + q_{drip,ice} . \tag{7.11}$$

Solid precipitation reaching the soil or snow surface, $q_{grnd,ice}\Delta t$, is added immediately to the snow pack (section 7.2). The liquid part, $q_{grnd,liq}\Delta t$ is added after surface fluxes (section 5) and snow/soil temperatures (section 6) have been determined.

The wetted fraction of the canopy (stems plus leaves), which is required for the surface albedo (section 3.1) and surface flux (section 5) calculations is (Dickinson et al. 1993)

$$f_{wet} = \left\{ \begin{array}{ll} \left[\dfrac{W_{can}}{p\left(L+S\right)} \right]^{2/3} \le 1 & L+S>0 \\ 0 & L+S=0 \end{array} \right\} \tag{7.12}$$

while the fraction of the canopy that is dry and transpiring is

$$f_{dry} = \left\{ \begin{array}{ll} \dfrac{\left(1-f_{wet}\right)L}{L+S} & L+S>0 \\ 0 & L+S=0 \end{array} \right\} . \tag{7.13}$$

7.2 Snow

The parameterizations for snow are based primarily on Anderson (1976), Jordan (1991), and Dai and Zeng (1997). Snow can have up to five layers. These layers are indexed in the fortran code as $i=-4,-3,-2,-1,0$ where layer $i=0$ is the snow layer next to the top soil layer and layer $i=-4$ is the top layer of a five-layer snow pack. Since the number of snow layers varies according to the snow depth, we use the notation $snl+1$ to describe the top layer of snow for the variable layer snow pack, where snl is the negative of the number of snow layers. Refer to Figure 7.1 for an example of the snow layer structure for a three layer snow pack.

Figure 7.1. Example of three layer snow pack ($snl = -3$).

Shown are three snow layers, $i = -2$, $i = -1$, and $i = 0$. The layer node depth is z, the layer interface is z_h, and the layer thickness is Δz.

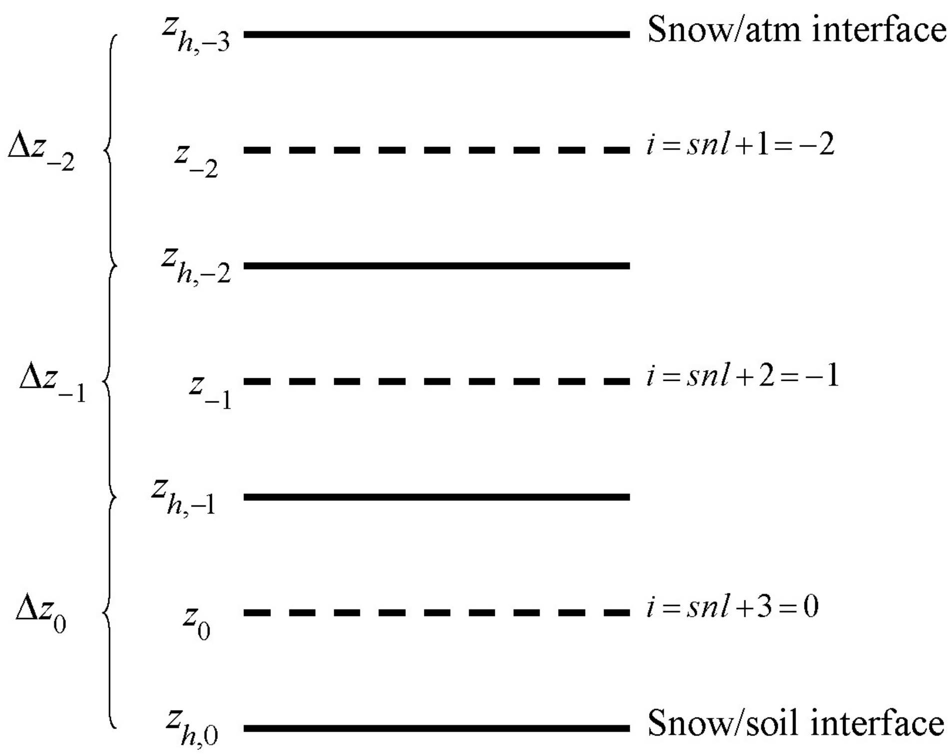

The state variables for snow are the mass of water $w_{liq,i}$ (kg m^{-2}), mass of ice $w_{ice,i}$ (kg m^{-2}), layer thickness Δz_i (m), and temperature T_i (section 6). The water vapor phase is neglected. Snow can also exist in the model without being represented by explicit snow layers. This occurs when the snow pack is less than a specified minimum snow depth ($z_{sno} < 0.01$ m). In this case, the state variable is the mass of snow W_{sno} (kg m^{-2}).

The next two sections (7.2.1 and 7.2.2) describe the ice and water content of the snow pack assuming that at least one snow layer exists. See section 7.2.3 for a description of how a snow layer is initialized.

7.2.1 Ice Content

The conservation equation for mass of ice in snow layers is

$$\frac{\partial w_{ice,i}}{\partial t} = \left\{ \begin{array}{ll} q_{ice,i-1} - \frac{\left(\Delta w_{ice,i}\right)_p}{\Delta t} & i = snl+1 \\ -\frac{\left(\Delta w_{ice,i}\right)_p}{\Delta t} & i = snl+2,\ldots,0 \end{array} \right\} \tag{7.14}$$

where $q_{ice,i-1}$ is the rate of ice accumulation from precipitation or frost or the rate of ice loss from sublimation (kg m^{-2} s^{-1}) in the top layer and $\left(\Delta w_{ice,i}\right)_p / \Delta t$ is the change in ice due to phase change (melting rate) (section 6.2). The term $q_{ice,i-1}$ is computed in two steps as

$$q_{ice,i-1} = q_{grnd,ice} + \left(q_{frost} - q_{subl}\right) \tag{7.15}$$

where $q_{grnd,ice}$ is the rate of solid precipitation reaching the ground (section 7.1) and q_{frost} and q_{subl} are gains due to frost and losses due to sublimation, respectively (section 5.4). In the first step, immediately after $q_{grnd,ice}$ has been determined after accounting for interception (section 7.1), a new snow depth z_{sno} (m) is calculated from

$$z_{sno}^{n+1} = z_{sno}^{n} + \Delta z_{sno} \tag{7.16}$$

where

$$\Delta z_{sno} = \frac{q_{grnd,ice} \Delta t}{\rho_{sno}} \tag{7.17}$$

and ρ_{sno} is the bulk density of newly fallen snow (kg m^{-3}) (Anderson 1976)

$$\rho_{sno} = \left\{ \begin{array}{ll} 50 + 1.7(17)^{1.5} & T_{atm} > T_f + 2 \\ 50 + 1.7\left(T_{atm} - T_f + 15\right)^{1.5} & T_f - 15 < T_{atm} \le T_f + 2 \\ 50 & T_{atm} \le T_f - 15 \end{array} \right\} \tag{7.18}$$

where T_{atm} is the atmospheric temperature (K), and T_f is the freezing temperature of water (K) (Table 1.4). The mass of snow W_{sno} is

$$W_{sno}^{n+1} = W_{sno}^{n} + q_{grnd,ice} \Delta t \,. \tag{7.19}$$

The ice content of the top layer and the layer thickness are updated as

$$w_{ice,snl+1}^{n+1} = w_{ice,snl+1}^{n} + q_{grnd,ice} \Delta t \tag{7.20}$$

$$\Delta z_{snl+1}^{n+1} = \Delta z_{snl+1}^{n} + \Delta z_{sno} \,. \tag{7.21}$$

Since wetlands are modeled as columns of water (no soil), snow is not allowed to accumulate if the surface temperature is above freezing ($T_g > T_f$). In this case, the incoming solid precipitation is assigned to the runoff term q_{rgwl} (section 7.6).

In the second step, after surface fluxes and snow/soil temperatures have been determined (sections 5 and 6), $w_{ice,snl+1}$ is updated for frost or sublimation as

$$w_{ice,snl+1}^{n+1} = w_{ice,snl+1}^{n} + \left(q_{frost} - q_{subl}\right) \Delta t \,. \tag{7.22}$$

If $w_{ice,snl+1}^{n+1} < 0$ upon solution of equation (7.22), the ice content is reset to zero and the liquid water content $w_{liq,snl+1}$ is reduced by the amount required to bring $w_{ice,snl+1}^{n+1}$ up to zero.

The snow water equivalent W_{sno} is capped to not exceed 1000 kg m^{-2}. If the addition of q_{frost} were to result in $W_{sno} > 1000$ kg m^{-2}, the frost term q_{frost} is instead added to the runoff term q_{rgwl} (section 7.6).

7.2.2 Water Content

The conservation equation for mass of water in snow layers is

$$\frac{\partial w_{liq,i}}{\partial t} = \left(q_{liq,i-1} - q_{liq,i}\right) + \frac{\left(\Delta w_{liq,i}\right)_p}{\Delta t} \tag{7.23}$$

where $q_{liq,i-1}$ is the flow of liquid water into layer i from the layer above, $q_{liq,i}$ is the flow of water out of layer i to the layer below, $\left(\Delta w_{liq,i}\right)_p / \Delta t$ is the change in liquid water due to phase change (melting rate) (section 6.2). For the top snow layer only,

$$q_{liq,i-1} = q_{grnd,liq} + \left(q_{sdew} - q_{seva}\right) \tag{7.24}$$

where $q_{grnd,liq}$ is the rate of liquid precipitation reaching the snow (section 7.1), q_{seva} is the evaporation of liquid water and q_{sdew} is the liquid dew (section 5.4). After surface fluxes and snow/soil temperatures have been determined (sections 5 and 6), $w_{liq,snl+1}$ is updated for the liquid precipitation reaching the ground and dew or evaporation as

$$w_{liq,snl+1}^{n+1} = w_{liq,snl+1}^{n} + \left(q_{grnd,liq} + q_{sdew} - q_{seva}\right)\Delta t . \tag{7.25}$$

When the liquid water within a snow layer exceeds the layer's holding capacity, the excess water is added to the underlying layer, limited by the effective porosity ($1-\theta_{ice}$) of the layer. Thus, water flow between layers, $q_{liq,i}$, for layers other than the layer next to the soil surface, is

$$q_{liq,i} = \frac{\rho_{liq}\left[\theta_{liq,i} - S_r\left(1-\theta_{ice,i}\right)\right]\Delta z_i}{\Delta t} \ge 0 \quad 1-\theta_{ice,i} \ge \theta_{imp} \text{ and } 1-\theta_{ice,i+1} \ge \theta_{imp} \tag{7.26}$$

where the volumetric liquid water $\theta_{liq,i}$ and ice $\theta_{ice,i}$ contents are

$$\theta_{ice,i} = \frac{w_{ice,i}}{\Delta z_i \rho_{ice}} \le 1 \tag{7.27}$$

$$\theta_{liq,i} = \frac{w_{liq,i}}{\Delta z_i \rho_{liq}} \le 1-\theta_{ice,i}\,, \tag{7.28}$$

$\theta_{imp} = 0.05$ is the water impermeable volumetric water content, and $S_r = 0.033$ is the irreducible water saturation (snow holds a certain amount of liquid water due to capillary retention after drainage has ceased (Anderson 1976)). The water holding capacity of the underlying layer limits the flow of water as

$$q_{liq,i} \le \frac{\rho_{liq}\left[1-\theta_{ice,i+1} - \theta_{liq,i+1}\right]\Delta z_{i+1}}{\Delta t} \qquad i = snl+1,\ldots,-1\,. \tag{7.29}$$

Furthermore, the flow of water is assumed to be zero ($q_{liq,i} = 0$) if the effective porosity of either of the two layers is less than θ_{imp}. The flow of water from the snow layer above the soil surface is

$$q_{liq,i} = \frac{\rho_{liq}\left[\theta_{liq,i} - S_r\left(1-\theta_{ice,i}\right)\right]\Delta z_i}{\Delta t} \ge 0\,. \tag{7.30}$$

Water from this layer is allowed to pond on the soil surface. The above set of equations is solved for every snow layer in a single time step. The total flow of liquid water reaching the soil surface is then $q_{liq,0}$ which is used in the calculation of surface runoff and infiltration (section 7.3).

7.2.3 Initialization of snow layer

If there are no existing snow layers ($snl+1=1$) but $z_{sno} \geq 0.01$ m after accounting for solid precipitation q_{sno}, then a snow layer is initialized ($snl=-1$) as follows

$$
\begin{aligned}
&\Delta z_0 = z_{sno} \\
&z_o = -0.5\Delta z_0 \\
&z_{h,-1} = -\Delta z_0 \\
&\tau_{sno} = 0 \\
&T_0 = \min\left(T_f, T_{atm}\right) \\
&w_{ice,0} = W_{sno} \\
&w_{liq,0} = 0
\end{aligned}
\tag{7.31}
$$

where τ_{sno} is the non-dimensional snow age (section 3.2).

7.2.4 Snow Compaction

Snow compaction is initiated after the soil hydrology calculations [surface runoff (section 7.3), infiltration (section 7.3), soil water movement (section 7.4), sub-surface drainage (section 7.5)] are complete. Compaction of snow includes three types of processes: destructive metamorphism of new snow (crystal breakdown due to wind or thermodynamic stress); snow load or overburden (pressure); and melting (changes in snow structure due to melt-freeze cycles plus changes in crystals due to liquid water). The total fractional compaction rate for each snow layer $C_{R,i}$ (s^{-1}) is the sum of the three compaction processes

$$C_{R,i} = \frac{1}{\Delta z_i}\frac{\partial \Delta z_i}{\partial t} = C_{R1,i} + C_{R2,i} + C_{R3,i}. \tag{7.32}$$

Compaction is not allowed if the layer is saturated

$$1-\left(\frac{w_{ice,i}}{\Delta z_i \rho_{ice}} + \frac{w_{liq,i}}{\Delta z_i \rho_{liq}}\right) \leq 0.001 \tag{7.33}$$

or if the ice content is below a minimum value ($w_{ice,i} \le 0.1$).

Compaction as a result of destructive metamorphism $C_{R1,i}$ (s^{-1}) is temperature dependent (Anderson 1976)

$$C_{R1,i} = \left[\frac{1}{\Delta z_i}\frac{\partial \Delta z_i}{\partial t}\right]_{metamorphism} = -c_3 c_1 c_2 \exp\left[-c_4\left(T_f - T_i\right)\right] \tag{7.34}$$

where $c_3 = 2.777\times10^{-6}$ (s^{-1}) is the fractional compaction rate for $T_i = T_f$, $c_4 = 0.04$ K^{-1}, and

$$\begin{aligned}
&c_1 = 1 && \frac{w_{ice,i}}{\Delta z_i} \le 100 \text{ kg m}^{-3} \\
&c_1 = \exp\left[-0.046\left(\frac{w_{ice,i}}{\Delta z_i} - 100\right)\right] && \frac{w_{ice,i}}{\Delta z_i} > 100 \text{ kg m}^{-3} \\
&c_2 = 2 && \frac{w_{liq,i}}{\Delta z_i} > 0.01 \\
&c_2 = 1 && \frac{w_{liq,i}}{\Delta z_i} \le 0.01
\end{aligned} \tag{7.35}$$

where $w_{ice,i}/\Delta z_i$ and $w_{liq,i}/\Delta z_i$ are the bulk densities of liquid water and ice (kg m^{-3}).

The compaction rate as a result of overburden $C_{R2,i}$ (s^{-1}) is a linear function of the snow load pressure $P_{s,i}$ (kg m^{-2}) (Anderson 1976)

$$C_{R2,i} = \left[\frac{1}{\Delta z_i}\frac{\partial \Delta z_i}{\partial t}\right]_{overburden} = -\frac{P_{s,i}}{\eta} \tag{7.36}$$

where η is a viscocity coefficient (kg s m^{-2}) that varies with density and temperature as

$$\eta = \eta_0 \exp\left[c_5\left(T_f - T_i\right) + c_6 \frac{w_{ice,i}}{\Delta z_i}\right] \tag{7.37}$$

where $\eta_0 = 9\times10^5$ kg s m^{-2}, and $c_5 = 0.08$ K^{-1}, $c_6 = 0.023$ m^3 kg^{-1} are constants. The snow load pressure $P_{s,i}$ is calculated for each layer as the sum of the ice $w_{ice,i}$ and liquid water contents $w_{liq,i}$ of the layers above

$$P_{s,i} = \sum_{j=i-1}^{snl+1} \left(w_{ice,j} + w_{liq,j} \right). \tag{7.38}$$

The compaction rate due to melting $C_{R3,i}$ (s^{-1}) is taken to be the ratio of the change in snow ice fraction after the melting to the fraction before melting

$$C_{R3,i} = \left[\frac{1}{\Delta z_i} \frac{\partial \Delta z_i}{\partial t} \right]_{melt} = -\frac{1}{\Delta t} \max\left(0, \frac{f_{ice,i}^{n} - f_{ice,i}^{n+1}}{f_{ice,i}^{n}} \right) \tag{7.39}$$

where the fraction of ice $f_{ice,i}$ is

$$f_{ice,i} = \frac{w_{ice,i}}{w_{ice,i} + w_{liq,i}} \tag{7.40}$$

and melting is identified during the phase change calculations (section 6.2).

The snow layer thickness after compaction is then

$$\Delta z_i^{n+1} = \Delta z_i^{n} \left(1 + C_{R,i} \Delta t \right). \tag{7.41}$$

7.2.5 Snow Layer Combination and Subdivision

After the determination of snow temperature including phase change (section 6), snow hydrology (sections 7.2.1, 7.2.2, and 7.2.3), and the compaction calculations (7.2.4), the number of snow layers is adjusted by either combining or subdividing layers. The combination and subdivision of snow layers is based on Jordan (1991).

7.2.5.1 Combination

If a snow layer has nearly melted or if its thickness Δz_i is less than the prescribed minimum thickness $\Delta z_{i,\min}$ (Table 7.1), the layer is combined with a neighboring layer. The overlying or underlying layer is selected as the neighboring layer according to the following rules

- If the surface layer is being removed, it is combined with the underlying layer
- If the underlying layer is not snow (i.e., it is the top soil layer), the layer is combined with the overlying layer
- If the layer is nearly completely melted, the layer is combined with the underlying layer
- If none of the above rules apply, the layer is combined with the thinnest neighboring layer.

A first pass is made through all snow layers to determine if any layer is nearly melted ($w_{ice,i} \le 0.01$). If so, the remaining liquid water and ice content of layer i is combined with the underlying neighbor $i+1$ as

$$w_{liq,i+1} = w_{liq,i+1} + w_{liq,i} \tag{7.42}$$

$$w_{ice,i+1} = w_{ice,i+1} + w_{ice,i} . \tag{7.43}$$

This includes the snow layer directly above the top soil layer. In this case, the liquid water and ice content of the melted snow layer is added to the contents of the top soil layer. The layer properties, T_i, $w_{ice,i}$, $w_{liq,i}$, Δz_i, are then re-indexed so that the layers above the eliminated layer are shifted down by one and the number of snow layers is decremented accordingly.

At this point, if there are no explicit snow layers remaining ($snl = 0$), the snow water equivalent W_{sno} and snow depth z_{sno} are set to zero, otherwise, W_{sno} and z_{sno} are re-calculated as

$$W_{sno} = \sum_{i=0}^{snl+1} \left(w_{ice,i} + w_{liq,i} \right) \tag{7.44}$$

$$z_{sno} = \sum_{i=0}^{snl+1} \Delta z_i \ . \tag{7.45}$$

If the snow depth z_{sno} is less than 0.01 m, the number of snow layers is set to zero, the total ice content of the snow pack $\sum_{i=0}^{snl+1} w_{ice,i}$ is assigned to W_{sno}, and the total liquid water $\sum_{i=0}^{snl+1} w_{liq,i}$ is assigned to the top soil layer. Otherwise, the layers are combined according the rules above.

When two snow layers are combined (denoted here as 1 and 2), their thickness combination (c) is

$$\Delta z_c = \Delta z_1 + \Delta z_2 , \tag{7.46}$$

their mass combination is

$$w_{liq,c} = w_{liq,1} + w_{liq,2} \tag{7.47}$$

$$w_{ice,c} = w_{ice,1} + w_{ice,2} , \tag{7.48}$$

and their temperatures are combined as

$$T_c = \left\{ \begin{array}{ll} T_f + \dfrac{h_c}{C_{ice} w_{ice,c} + C_{liq} w_{liq,c}} & h_c < 0 \\ T_f & 0 \le h_c \le L_f w_{liq,c} \\ T_f + \dfrac{h_c - L_f w_{liq,c}}{C_{ice} w_{ice,c} + C_{liq} w_{liq,c}} & h_c > L_f w_{liq,c} \end{array} \right\} \tag{7.49}$$

where $h_c = h_1 + h_2$ is the combined enthalpy h_i of the two layers where

$$h_i = \left(C_{ice} w_{ice,i} + C_{liq} w_{liq,i}\right)\left(T_i - T_f\right) + L_f w_{liq,i} . \tag{7.50}$$

In these equations, L_f is the latent heat of fusion (J kg^{-1}) and C_{liq} and C_{ice} are the specific heat capacities (J kg^{-1} K^{-1}) of liquid water and ice, respectively (Table 1.4). After layer combination, the node depths and layer interfaces (Figure 7.1) are recalculated from

$$z_i = z_{h,i} - 0.5\Delta z_i \qquad i = snl + 1, \ldots, 0 \tag{7.51}$$

$$z_{h,i-1} = z_{h,i} - \Delta z_i \qquad i = snl + 1, \ldots, 0 \tag{7.52}$$

where Δz_i is the layer thickness.

Table 7.1. Minimum and maximum thickness of snow layers (m)

Layer i	$\Delta z_{i,\min}$	$\Delta z_{i,\max}$
-4 (top)	0.010	0.02[1]
-3	0.015	0.05
-2	0.025	0.11
-1	0.055	0.23
0 (bottom)	0.115	-

[1]If there is only one snow layer, the layer is not subdivided until $\Delta z_i > 0.03$.

7.2.5.2 Subdivision

The snow layers are subdivided when the layer thickness exceeds the prescribed maximum thickness $\Delta z_{i,\max}$ (Table 7.1). The scheme for subdivision is summarized in section 6.1. If there is an existing layer below the layer to be subdivided, the thickness Δz_i, liquid water and ice contents, $w_{liq,i}$ and $w_{ice,i}$, and temperature T_i of the excess snow are combined with the underlying layer according to equations (7.46)-(7.49). If there is no underlying layer after adjusting the layer for the excess snow, the layer is subdivided into two layers of equal thickness, liquid water and ice contents, and temperature. After layer subdivision, the node depths and layer interfaces are recalculated from equations (7.51) and (7.52).

7.3 Surface Runoff and Infiltration

A conceptual form of TOPMODEL (Beven and Kirkby 1979) is used to parameterize runoff. The approach involves the determination of a water table level from which saturated and unsaturated fractions are calculated. The saturated fraction f_{sat} (i.e., the partial contributing area) is

$$f_{sat} = w_{fact} \min\left[1, \exp\left(-z_w\right)\right] \tag{7.53}$$

where $w_{fact} = 0.3$ is a parameter determined by the distribution of the topographic index and z_w is the mean water table depth (dimensionless) given by

$$z_w = f_z \left(z_{h,10} - \sum_{i=1}^{10} s_i \Delta z_i \right) \tag{7.54}$$

where $f_z = 1$ m^{-1} is a water table depth scale parameter, $z_{h,10}$ is the bottom depth of the lowest soil layer (currently, the bottom of the tenth layer is about 3.44 m), s_i is the soil wetness for layer i, and Δz_i is the soil layer thickness (m). The soil wetness s_i is

$$s_i = \frac{\theta_{ice,i} + \theta_{liq,i}}{\theta_{sat,i}} \le 1 \tag{7.55}$$

where $\theta_{sat,i}$ is the saturated volumetric water content (section 7.4.1), and $\theta_{ice,i}$ and $\theta_{liq,i}$ are the volumetric ice and liquid water contents

$$\theta_{ice,i} = \frac{w_{ice,i}}{\Delta z_i \rho_{ice}} \le \theta_{sat,i} \tag{7.56}$$

$$\theta_{liq,i} = \frac{w_{liq,i}}{\Delta z_i \rho_{liq}} \le \theta_{sat,i} - \theta_{ice,i} \tag{7.57}$$

and ρ_{liq} and ρ_{ice} are the density of liquid water and ice (kg m^{-3}, Table 1.4). The unsaturated fraction is $1 - f_{sat}$.

If the top soil layer is impermeable ($\theta_{sat,1} - \theta_{ice,1} < \theta_{imp}$ where $\theta_{imp} = 0.05$ is the water impermeable volumetric water content), then all of the water reaching the soil surface runs off

$$q_{over} = q_{liq,0} \tag{7.58}$$

where $q_{liq,0}$ is melt water from the snow pack plus any liquid precipitation reaching the ground. Specifically, if there is at least one snow layer, no liquid precipitation reaches the soil and $q_{liq,0}$ is simply the melt water from the snow pack (section 7.2.2). If the snow pack is less than a minimum depth then there are no explicit snow layers. However, some residual snow may still exist, in which case $q_{liq,0} = q_{grnd,liq} + M_{1S}$ where $q_{grnd,liq}$ is the liquid precipitation reaching the ground (section 7.1) and M_{1S} is melt water from the residual snow (section 6.2).

If the top soil layer is not impermeable, the surface runoff is the sum of runoff from saturated and unsaturated areas

$$q_{over} = f_{sat} q_{liq,0} + \left(1 - f_{sat}\right) \overline{w}_s^{\,4} q_{liq,0} \tag{7.59}$$

where $\overline{w}_s$ is the soil layer thickness weighted wetness in the top three layers

$$\bar{w}_s = \frac{\sum_{i=1}^{3} s_i \Delta z_i}{\sum_{i=1}^{3} \Delta z_i}. \tag{7.60}$$

Infiltration into the surface soil layer is defined as the residual of the surface water balance

$$q_{infl} = q_{liq,0} - q_{over} - q_{seva} \tag{7.61}$$

when no snow layers exist, and

$$q_{infl} = q_{liq,0} - q_{over} \tag{7.62}$$

when at least one snow layer is present. q_{seva} is the evaporation of liquid water from the top soil layer (section 5.4). Infiltration q_{infl} and explicit surface runoff q_{over} are not allowed for glaciers and wetlands.

7.4 Soil Water

Soil water is predicted from a ten-layer model (as with soil temperature), in which the vertical soil moisture transport is governed by infiltration, surface and sub-surface runoff, gradient diffusion, gravity, and root extraction through canopy transpiration. The following derivation closely follows that of Z.-L. Yang (1998, unpublished manuscript). For one-dimensional vertical water flow in soils, the conservation of mass is stated as

$$\frac{\partial \theta}{\partial t} = -\frac{\partial q}{\partial z} - e \tag{7.63}$$

where θ is the volumetric soil water content (mm^3 of water mm^{-3} of soil), t is time (s), and z is height above some datum in the soil column (mm) (positive upwards), q is soil water flux (kg m^{-2} s^{-1} or mm s^{-1}) (positive upwards), and e is a soil moisture sink term (s^{-1}) (evapotranspiration loss). This equation is solved numerically by dividing the soil column into ten layers in the vertical and integrating downward over each layer with boundary conditions of the infiltration flux into the top soil layer q_{infl} and gravitational drainage at the bottom of the soil column (specified here as the hydraulic conductivity k of the tenth soil layer).

The soil water flux q can be described by Darcy's law

$$q = -k \frac{\partial \psi_h}{\partial z} \tag{7.64}$$

where k is the hydraulic conductivity (mm s^{-1}), and ψ_h is the hydraulic potential (mm). The hydraulic potential is

$$\psi_h = \psi_m + \psi_z \tag{7.65}$$

where ψ_m is the soil matric potential (mm) (which is related to the adsorptive and capillary forces within the soil matrix), and ψ_z is the gravitational potential (mm) (the vertical distance from an arbitrary reference elevation to a point in the soil). If the reference elevation is the soil surface, then $\psi_z = z$. Letting $\psi = \psi_m$, Darcy's law becomes

$$q = -k \left[\frac{\partial \left(\psi + z \right)}{\partial z} \right]. \tag{7.66}$$

For soil layer i, this can be approximated as

$$q_i = -k\left[z_{h,i} \right] \left[\frac{\left(\psi_i - \psi_{i+1} \right) + \left(z_{i+1} - z_i \right)}{z_{i+1} - z_i} \right] \tag{7.67}$$

where $k\left[z_{h,i} \right]$ is the hydraulic conductivity at the depth of the interface of two adjacent layers ($z_{h,i}$) and z_i is the node depth of layer i (Figure 7.1).

Darcy's equation can be further manipulated to yield

$$q = -k\left[\frac{\partial\left(\psi + z\right)}{\partial z}\right] = -k\left(\frac{\partial \psi}{\partial z} + 1\right) = -k\left(\frac{\partial \theta}{\partial z}\frac{\partial \psi}{\partial \theta} + 1\right). \tag{7.68}$$

Substitution of this equation into the equation for conservation of mass, with $e = 0$, yields Richard's law

$$\frac{\partial \theta}{\partial t} = \frac{\partial}{\partial z}\left[k\left(\frac{\partial \theta}{\partial z}\frac{\partial \psi}{\partial \theta}\right) + 1\right]. \tag{7.69}$$

7.4.1 Hydraulic Properties

The hydraulic conductivity k_i (mm s^{-1}) and the soil matric potential ψ_i (mm) for layer i vary with volumetric soil water θ_i and soil texture ($\%sand_i$ and $\%clay_i$, section 1.2.5) based on the work of Clapp and Hornberger (1978) and Cosby et al. (1984).

The hydraulic conductivity is defined at the interface of two adjacent layers $z_{h,i}$ (Figure 7.2) and is a function of the water content of the two layers and the saturated hydraulic conductivity at the interface

$$k\left[z_{h,i}\right] = \begin{Bmatrix} k_{sat}\left[z_{h,i}\right]\left[\dfrac{0.5\left(\theta_{liq,i} + \theta_{liq,i+1}\right)}{0.5\left(\theta_{sat,i} + \theta_{sat,i+1}\right)}\right]^{2B_i+3} & 1 \le i \le 9 \\ k_{sat}\left[z_{h,i}\right]\left[\dfrac{\theta_{liq,i}}{\theta_{sat,i}}\right]^{2B_i+3} & i = 10 \end{Bmatrix}. \tag{7.70}$$

The saturated hydraulic conductivity $k_{sat}\left[z_{h,i}\right]$ (mm s^{-1}) follows the TOPMODEL concept (Beven and Kirkby 1979) in assuming an exponential decrease with depth as

$$k_{sat}\left[z_{h,i}\right] = 0.0070556 \times 10^{-0.884+0.0153\left(\%sand\right)_i}\left[\exp\left(-\frac{z_{h,i}}{z_*}\right)\right] \tag{7.71}$$

where $z_* = 0.5$ m is the length scale for the decrease in $k_{sat}\left[z_{h,i}\right]$. The water content at saturation (i.e., porosity) is

$$\theta_{sat,i} = 0.489 - 0.00126(\%sand)_i \tag{7.72}$$

and the exponent "B" is

$$B_i = 2.91 + 0.159(\%clay)_i . \tag{7.73}$$

If the effective porosity of either layer ($\theta_{sat,i} - \theta_{ice,i}$ or $\theta_{sat,i+1} - \theta_{ice,i+1}$) is less than the impermeable liquid water content ($\theta_{imp} = 0.05$) or if the volumetric liquid water content of layer i ($\theta_{liq,i}$) is less than 0.001, then $k\left[z_{h,i}\right] = 0$ (no flow).

The soil matric potential (mm) is defined at the node depth z_i of each layer i (Figure 7.2). For unfrozen soils ($T_i > T_f$),

$$\psi_i = \psi_{sat,i}\left(\frac{\theta_{liq,i}}{\theta_{sat,i}}\right)^{-B_i} \ge -1\times 10^8 \qquad 0.01 \le \frac{\theta_{liq,i}}{\theta_{sat,i}} \le 1 \tag{7.74}$$

where the saturated soil matric potential (mm) is

$$\psi_{sat,i} = -10.0\times 10^{1.88-0.0131(\%sand)_i} . \tag{7.75}$$

For frozen or partially frozen soils ($T_i \le T_f$), the soil matric potential is a function of temperature only (Fuchs et al. 1978)

$$\psi_i = 1\times 10^3 \frac{L_f}{g}\frac{T_i - T_f}{T_i} \ge -1\times 10^8 \tag{7.76}$$

where L_f is the latent heat of fusion (J kg^{-1}) (Table 1.4), g is the gravitational acceleration (m s^{-2}) (Table 1.4), T_i is the temperature of the i^{th} layer (K), and T_f is the freezing temperature of water (K) (Table 1.4).

7.4.2 Numerical Solution

With reference to Figure 7.2, the equation for conservation of mass can be integrated over each layer as

$$\int_{-z_{h,i}}^{-z_{h,i-1}} \frac{\partial \theta}{\partial t} dz = -\int_{-z_{h,i}}^{-z_{h,i-1}} \frac{\partial q}{\partial z} dz - \int_{-z_{h,i}}^{-z_{h,i-1}} e\, dz \ . \tag{7.77}$$

Note that the integration limits are negative since z is defined as positive upward from the soil surface. This equation can be written as

$$\Delta z_i \frac{\partial \theta_{liq,i}}{\partial t} = -q_{i-1} + q_i - e_i \tag{7.78}$$

where q_i is the flux of water across interface $z_{h,i}$, q_{i-1} is the flux of water across interface $z_{h,i-1}$, and e_i is a layer-averaged soil moisture sink term (evapotranspiration loss) defined as positive for flow out of the layer (mm s^{-1}). Taking the finite difference with time and evaluating the fluxes implicitly at time $n+1$ yields

$$\frac{\Delta z_i \Delta \theta_{liq,i}}{\Delta t} = -q_{i-1}^{n+1} + q_i^{n+1} - e_i \tag{7.79}$$

where $\Delta \theta_{liq,i} = \theta_{liq,i}^{n+1} - \theta_{liq,i}^{n}$ is the change in volumetric soil liquid water of layer i in time Δt and Δz_i is the thickness of layer i (mm).

The water removed by transpiration in each layer e_i is a function of the total transpiration E_v^t (section 5) and the effective root fraction $r_{e,i}$

$$e_i = r_{e,i} E_v^t \ . \tag{7.80}$$

Figure 7.2. Schematic diagram of numerical scheme used to solve for soil water fluxes. Shown are three soil layers, $i-1$, i, and $i+1$. The soil matric potential ψ and volumetric soil water θ_{liq} are defined at the layer node depth z. The hydraulic conductivity $k\left[z_h\right]$ is defined at the interface of two layers z_h. The layer thickness is Δz. The soil water fluxes q_{i-1} and q_i are defined as positive upwards. The soil moisture sink term e (evapotranspiration loss) is defined as positive for flow out of the layer.

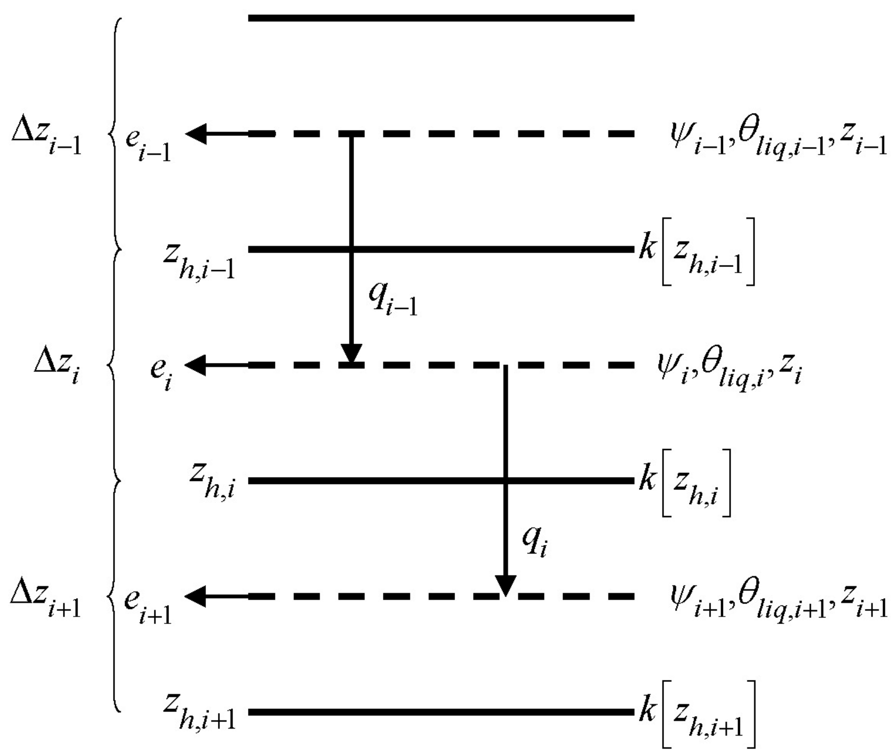

Note that because more than one plant functional type (PFT) may share a soil column, the transpiration E_v^t is a weighted sum of transpiration from all PFTs whose weighting depends on PFT area as

$$E_v^t = \sum_{j=1}^{npft} \left(E_v^t\right)_j \left(wt\right)_j \tag{7.81}$$

where $npft$ is the number of PFTs sharing a soil column, $\left(E_v^t\right)_j$ is the transpiration from the j^{th} PFT on the column, and $\left(wt\right)_j$ is the relative area of the j^{th} PFT with respect to the column. The effective root fraction $r_{e,i}$ is also a column-level quantity that is a weighted sum over all PFTs. The weighting depends on the per unit area transpiration of each PFT and its relative area as

$$r_{e,i} = \frac{\sum_{j=1}^{npft} \left(r_{e,i}\right)_j \left(E_v^t\right)_j \left(wt\right)_j}{\sum_{j=1}^{npft} \left(E_v^t\right)_j \left(wt\right)_j} \tag{7.82}$$

where $\left(r_{e,i}\right)_j$ is the effective root fraction for the j^{th} PFT

$$\left(r_{e,i}\right)_j = \frac{\left(r_i\right)_j w_i}{\left(\beta_t\right)_j} \tag{7.83}$$

and $\left(r_i\right)_j$ is the fraction of roots in layer i for the j^{th} PFT (section 8), w_i is a soil dryness or plant wilting factor for layer i (section 8), and β_t is a wetness factor for the total soil column for the j^{th} PFT (section 8).

The soil water fluxes in equation (7.79), which are a function of $\theta_{liq,i}$ and $\theta_{liq,i+1}$ because of their dependence on hydraulic conductivity and soil matric potential (e.g., equation (7.67)), can be linearized about $\partial \theta$ using a Taylor series expansion as

$$q_i^{n+1} = q_i^n + \frac{\partial q_i}{\partial \theta_{liq,i}} \Delta \theta_{liq,i} + \frac{\partial q_i}{\partial \theta_{liq,i+1}} \Delta \theta_{liq,i+1} \tag{7.84}$$

$$q_{i-1}^{n+1} = q_{i-1}^n + \frac{\partial q_{i-1}}{\partial \theta_{liq,i-1}} \Delta \theta_{liq,i-1} + \frac{\partial q_{i-1}}{\partial \theta_{liq,i}} \Delta \theta_{liq,i} . \tag{7.85}$$

Substitution of these expressions for q_i^{n+1} and q_{i-1}^{n+1} into equation (7.79) results in a tridiagonal equation set of the form

$$r_i = a_i \Delta \theta_{liq,i-1} + b_i \Delta \theta_{liq,i} + c_i \Delta \theta_{liq,i+1} \tag{7.86}$$

where

$$a_i = -\frac{\partial q_{i-1}}{\partial \theta_{liq,i-1}} \tag{7.87}$$

$$b_i = \frac{\partial q_i}{\partial \theta_{liq,i}} - \frac{\partial q_{i-1}}{\partial \theta_{liq,i}} - \frac{\Delta z_i}{\Delta t} \tag{7.88}$$

$$c_i = \frac{\partial q_i}{\partial \theta_{liq,i+1}} \tag{7.89}$$

$$e_i = s_i + q_{i-1}^n - q_i^n . \tag{7.90}$$

For the interior soil layers, $1 < i < 10$, the following relationships required for the solution of the tridiagonal set of equations can be derived from Darcy's law (equation (7.66))

$$q_{i-1}^n = -k\left[z_{h,i-1}\right]\left[\frac{\left(\psi_{i-1} - \psi_i\right) + \left(z_i - z_{i-1}\right)}{z_i - z_{i-1}}\right] \tag{7.91}$$

$$q_i^n = -k\left[z_{h,i}\right]\left[\frac{\left(\psi_i - \psi_{i+1}\right) + \left(z_{i+1} - z_i\right)}{z_{i+1} - z_i}\right] \tag{7.92}$$

$$\frac{\partial q_{i-1}}{\partial \theta_{liq,i-1}} = -\left[\frac{k\left[z_{h,i-1}\right]}{z_i - z_{i-1}} \frac{\partial \psi_{i-1}}{\partial \theta_{liq,i-1}}\right] - \frac{\partial k\left[z_{h,i-1}\right]}{\partial \theta_{liq,i-1}} \left[\frac{\left(\psi_{i-1} - \psi_i\right) + \left(z_i - z_{i-1}\right)}{z_i - z_{i-1}}\right] \tag{7.93}$$

$$\frac{\partial q_{i-1}}{\partial \theta_{liq,i}} = \left[\frac{k\left[z_{h,i-1}\right]}{z_i - z_{i-1}} \frac{\partial \psi_i}{\partial \theta_{liq,i}}\right] - \frac{\partial k\left[z_{h,i-1}\right]}{\partial \theta_{liq,i}} \left[\frac{\left(\psi_{i-1} - \psi_i\right) + \left(z_i - z_{i-1}\right)}{z_i - z_{i-1}}\right] \tag{7.94}$$

$$\frac{\partial q_i}{\partial \theta_{liq,i}} = -\left[\frac{k\left[z_{h,i}\right]}{z_{i+1} - z_i} \frac{\partial \psi_i}{\partial \theta_{liq,i}}\right] - \frac{\partial k\left[z_{h,i}\right]}{\partial \theta_{liq,i}} \left[\frac{\left(\psi_i - \psi_{i+1}\right) + \left(z_{i+1} - z_i\right)}{z_{i+1} - z_i}\right] \tag{7.95}$$

$$\frac{\partial q_i}{\partial \theta_{liq,i+1}} = \left[\frac{k\left[z_{h,i}\right]}{z_{i+1} - z_i} \frac{\partial \psi_{i+1}}{\partial \theta_{liq,i+1}}\right] - \frac{\partial k\left[z_{h,i}\right]}{\partial \theta_{liq,i+1}} \left[\frac{\left(\psi_i - \psi_{i+1}\right) + \left(z_{i+1} - z_i\right)}{z_{i+1} - z_i}\right]. \tag{7.96}$$

The derivatives of the soil matric potential at the node depth are derived from equation (7.74) for unfrozen soil

$$\frac{\partial \psi_{i-1}}{\partial \theta_{liq,i-1}} = -B_{i-1} \frac{\psi_{i-1}}{\theta_{liq,i-1}} \tag{7.97}$$

$$\frac{\partial \psi_i}{\partial \theta_{liq,i}} = -B_i \frac{\psi_i}{\theta_{liq,i}} \tag{7.98}$$

$$\frac{\partial \psi_{i+1}}{\partial \theta_{liq,i+1}} = -B_{i+1} \frac{\psi_{i+1}}{\theta_{liq,i+1}} \tag{7.99}$$

with the constraint $0.01\theta_{sat,i} \le \theta_{liq,i} \le \theta_{sat,i}$, and for frozen soil

$$\frac{\partial \psi_{i-1}}{\partial \theta_{liq,i-1}} = \frac{\partial \psi_i}{\partial \theta_{liq,i}} = \frac{\partial \psi_{i+1}}{\partial \theta_{liq,i+1}} = 0\,. \tag{7.100}$$

The derivatives of the hydraulic conductivity at the layer interface are derived from equation (7.70)

$$\frac{\partial k\left[z_{h,i-1}\right]}{\partial \theta_{liq,i-1}} = \frac{\partial k\left[z_{h,i-1}\right]}{\partial \theta_{liq,i}} = \left(2B_{i-1} + 3\right) k_{sat}\left[z_{h,i-1}\right] \left[\frac{0.5\left(\theta_{liq,i-1} + \theta_{liq,i}\right)}{0.5\left(\theta_{sat,i-1} + \theta_{sat,i}\right)}\right]^{2B_{i-1}+2} \left[\frac{0.5}{\theta_{sat,i-1}}\right] \tag{7.101}$$

$$\frac{\partial k\left[z_{h,i}\right]}{\partial \theta_{liq,i}} = \frac{\partial k\left[z_{h,i}\right]}{\partial \theta_{liq,i+1}} = \left\{ \begin{array}{ll} \left(2B_i + 3\right) k_{sat}\left[z_{h,i}\right] \left[\frac{\left(\theta_{liq,i} + \theta_{liq,i+1}\right)}{\left(\theta_{sat,i} + \theta_{sat,i+1}\right)}\right]^{2B_i+2} \left[\frac{0.5}{\theta_{sat,i}}\right] & 1 \le i \le 9 \\ \left(2B_i + 3\right) k_{sat}\left[z_{h,i}\right] \left[\frac{\theta_{liq,i}}{\theta_{sat,i}}\right]^{2B_i+2} \left[\frac{1}{\theta_{sat,i}}\right] & i = 10 \end{array} \right\}. \tag{7.102}$$

If the effective porosity of either layer is less than θ_{imp} or if the volumetric liquid water content of layer i is less than 0.001, then $\frac{\partial k\left[z_{h,i}\right]}{\partial \theta_{liq,i}} = 0$.

For the bottom soil layer ($i = 10$), the boundary condition is the hydraulic conductivity of the bottom layer, $q_i^{n+1} = -k\left[z_{h,i}\right]^{n+1}$, and the water balance equation is

$$\frac{\Delta z_i \Delta \theta_{liq,i}}{\Delta t} = -q_{i-1}^{n+1} - k\left[z_{h,i}\right]^{n+1} - e_i . \tag{7.103}$$

The hydraulic conductivity can be linearized about $\partial \theta$ as

$$k\left[z_{h,i}\right]^{n+1} = k\left[z_{h,i}\right]^{n} + \frac{\partial k\left[z_{h,i}\right]}{\partial \theta_{liq,i}} \Delta \theta_{liq,i} . \tag{7.104}$$

After grouping like terms, the coefficients of the tridiagonal set of equations for $i = 10$ are

$$a_i = -\frac{\partial q_{i-1}}{\partial \theta_{liq,i-1}} \tag{7.105}$$

$$b_i = -\left[\frac{\partial k\left[z_{h,i}\right]}{\partial \theta_{liq,i}} + \frac{\partial q_{i-1}}{\partial \theta_{liq,i}} + \frac{\Delta z_i}{\Delta t}\right] \tag{7.106}$$

$$c_i = 0 \tag{7.107}$$

$$r_i = e_i + q_{i-1}^{n} + k\left[z_{h,i}\right]^{n} . \tag{7.108}$$

For the top soil layer ($i = 1$), the boundary condition is the infiltration rate (section 7.3), $q_{i-1}^{n+1} = -q_{infl}^{n+1}$, and the water balance equation is

$$\frac{\Delta z_i \Delta \theta_{liq,i}}{\Delta t} = q_{infl}^{n+1} + q_i^{n+1} - e_i \ . \tag{7.109}$$

After grouping like terms, the coefficients of the tridiagonal set of equations for $i = 1$ are

$$a_i = 0 \tag{7.110}$$

$$b_i = \frac{\partial q_i}{\partial \theta_{liq,i}} - \frac{\Delta z_i}{\Delta t} \tag{7.111}$$

$$c_i = \frac{\partial q_i}{\partial \theta_{liq,i+1}} \tag{7.112}$$

$$r_i = e_i - q_{infl}^{n+1} - q_i^n \ . \tag{7.113}$$

Upon solution of the tridiagonal equation set (Press et al. 1992), the liquid water contents are updated as follows

$$w_{liq,i}^{n+1} = w_{liq,i}^n + \Delta \theta_{liq,i} \Delta z_i \ . \tag{7.114}$$

The volumetric water content is

$$\theta_i = \frac{w_{liq,i}}{\Delta z_i \rho_{liq}} + \frac{w_{ice,i}}{\Delta z_i \rho_{ice}} \ . \tag{7.115}$$

7.5 Sub-surface Drainage

Sub-surface drainage is the sum of lateral drainage from soil layers 6-9 and drainage out of the bottom of the soil column plus any adjustments required to keep the liquid water content of each layer between maximum and minimum values. The total sub-surface drainage q_{drai} (mm s^{-1}) is

$$q_{drai} = q_{drai,wet} + q_{drai,dry} + \frac{w_{liq}^{excess}}{\Delta t} - \frac{w_{liq}^{deficit}}{\Delta t} + k\left[z_{h,10}\right] + \frac{\partial k\left[z_{h,10}\right]}{\partial \theta_{liq,10}} \Delta \theta_{liq,10} \quad (7.116)$$

where $q_{drai,wet}$ and $q_{drai,dry}$ are the lateral drainage from the saturated and unsaturated areas (mm s^{-1}), respectively, w_{liq}^{excess} is the amount of liquid water (mm) in excess of saturation in all layers, $w_{liq}^{deficit}$ is the amount of liquid water (mm) required to keep all soil layers above zero liquid water content, $k\left[z_{h,10}\right]$ is the drainage out of the bottom of the soil column (hydraulic conductivity of layer $i = 10$) (mm s^{-1}) (section 7.4.1), and $\frac{\partial k\left[z_{h,10}\right]}{\partial \theta_{liq,10}} \Delta \theta_{liq,10}$ is the change in hydraulic conductivity due to the change in liquid water content of layer $i = 10$ (mm s^{-1}) (section 7.4.2). Explicit drainage q_{drai} is not allowed for glaciers and wetlands.

Drainage from the saturated fraction is

$$q_{drai,wet} = f_{sat}\, l_b \exp\left(-z_w\right) \quad (7.117)$$

where f_{sat} is the saturated fraction (section 7.3), $l_b = 1\times 10^{-5}$ mm s^{-1} is a base flow parameter, and z_w is the mean water table depth (dimensionless) (section 7.3). Drainage from the unsaturated fraction is

$$q_{drai,dry} = \left(1 - f_{sat}\right) k_D \overline{w}_b^{\,2B_1 + 3} \quad (7.118)$$

where $k_D = 0.04$ mm s^{-1} is the saturated soil hydraulic conductivity for the bottom layers contributing to the base flow, and $\overline{w}_b$ is the soil layer thickness and hydraulic conductivity weighted wetness in layers 6-9

$$\bar{w}_b = \frac{\sum_{i=6}^{9} s_i \Delta z_i k\left[z_{h,i}\right]}{\sum_{i=6}^{9} \Delta z_i k\left[z_{h,i}\right]} \tag{7.119}$$

where s_i is the soil wetness for layer i, Δz_i is the soil layer thickness (mm), and $k\left[z_{h,i}\right]$ is the hydraulic conductivity at the layer interface (mm s^{-1}) (section 7.4.1). The soil wetness s_i is defined as

$$s_i = \frac{\theta_{ice,i} + \theta_{liq,i}}{\theta_{sat,i}} \le 1 \tag{7.120}$$

where $\theta_{sat,i}$ is the saturated volumetric water content (section 7.4.1), and $\theta_{ice,i}$ and $\theta_{liq,i}$ are the volumetric ice and liquid water contents

$$\theta_{ice,i} = \frac{w_{ice,i}}{\Delta z_i \rho_{ice}} \le \theta_{sat,i} \tag{7.121}$$

$$\theta_{liq,i} = \frac{w_{liq,i}}{\Delta z_i \rho_{liq}} \le \theta_{sat,i} - \theta_{ice,i} \tag{7.122}$$

and ρ_{liq} and ρ_{ice} are the density of liquid water and ice (kg m^{-3}, Table 1.4). Note that $\theta_{liq,i}$ and $k\left[z_{h,i}\right]$ used here are values prior to the vertical diffusion calculations. Saturated and unsaturated drainage, $q_{drai,wet}$ and $q_{drai,dry}$, is not allowed for soil columns that have ice present ($\sum_{i=1}^{N} w_{ice,i} > 0$).

The liquid water in layers 6-9 is updated for the saturated and unsaturated drainage after accounting for vertical diffusion (section 7.4) as

$$\Delta w_{liq,i} = -\Delta t \left(q_{drai,wet} + q_{drai,dry}\right) \frac{\Delta z_i k\left[z_{h,i}\right]}{\sum_{i=6}^{9} \Delta z_i k\left[z_{h,i}\right]} \qquad 6 \le i \le 9 \tag{7.123}$$

where $\Delta w_{liq,i}$ is the change in liquid water content of layer i. Two adjustments are made to keep $w_{liq,i}$ within physical constraints of $0 \le w_{liq,i} \le \left(\theta_{sat,i} - \theta_{ice,i}\right)\Delta z_i$. First, to help prevent negative $w_{liq,i}$, each layer is successively brought up to $w_{liq,i} = 0$ by taking the required amount of water from the layer below. If the total amount of water in the soil column is insufficient to accomplish this, the water is subtracted from the sub-surface drainage q_{drai} (i.e., the $w_{liq}^{deficit}$ term in equation (7.116)). Second, soil water in excess of the effective porosity is removed and added to sub-surface drainage q_{drai} (i.e., the w_{liq}^{excess} term in equation (7.116)). Liquid water is allowed to pond on the surface soil layer so that the maximum amount of water for this layer is defined as

$$w_{liq}^{pond} + \left(\theta_{sat,1} - \theta_{ice,1}\right)\Delta z_1 \tag{7.124}$$

where $w_{liq}^{pond} = 10$ kg m^{-2}.

The soil surface layer liquid water and ice contents are then updated for dew q_{sdew}, frost q_{frost}, or sublimation q_{subl} (section 5.4) as

$$\Delta w_{liq,1} = q_{sdew}\Delta t \tag{7.125}$$

$$\Delta w_{ice,1} = q_{frost}\Delta t \tag{7.126}$$

$$\Delta w_{ice,1} = -q_{subl}\Delta t\,. \tag{7.127}$$

7.6 Runoff from glaciers, wetlands, and snow-capped surfaces

All surfaces are constrained to have a snow water equivalent $W_{sno} \le 1000$ kg m^{-2}. For snow-capped surfaces other than glaciers and wetlands, all solid and liquid precipitation reaching the ground and dew in solid or liquid form, is explicitly assigned to the runoff term q_{rgwl} as

$$q_{rgwl} = q_{grnd,ice} + q_{grnd,liq} + q_{sdew} + q_{frost} \tag{7.128}$$

and snow pack properties are unchanged. For glaciers and wetlands, the runoff term q_{rgwl} is calculated from the residual of the water balance as

$$q_{rgwl} = q_{grnd,ice} + q_{grnd,liq} - E_g - E_v - \frac{\left(W_b^{n+1} - W_b^n\right)}{\Delta t} \tag{7.129}$$

where W_b^n and W_b^{n+1} are the beginning and ending water balances defined as

$$W_b = W_{can} + W_{sno} + \sum_{i=1}^{N} \left(w_{ice,i} + w_{liq,i}\right). \tag{7.130}$$

Currently, glaciers and wetlands are non-vegetated and $E_v = W_{can} = 0$. The runoff term q_{rgwl} may be negative for glaciers, wetlands, and lakes (section 9.3), which reduces the total amount of runoff available to the River Transport Model (RTM) (section 10).

8. Stomatal Resistance and Photosynthesis

Leaf stomatal resistance, which is needed for the water vapor flux (section 5), is coupled to leaf photosynthesis in a manner similar to Collatz et al. (1991) (see also Sellers et al. 1992)

$$\frac{1}{r_s} = m \frac{A}{c_s} \frac{e_s}{e_i} P_{atm} + b \qquad (8.1)$$

where r_s is leaf stomatal resistance (s m^2 μmol^{-1}), m is a plant functional type dependent empirical parameter (Table 8.2) (Collatz et al. 1991), A is leaf photosynthesis (μmol CO_2 m^{-2} s^{-1}), c_s is the CO_2 concentration at the leaf surface (Pa), e_s is the vapor pressure at the leaf surface (Pa), e_i is the saturation vapor pressure (Pa) inside the leaf at the vegetation temperature T_v, P_{atm} is the atmospheric pressure (Pa), and $b = 2000$ is the minimum stomatal conductance (μmol m^{-2} s^{-1}) when $A = 0$. b was chosen to give a maximum stomatal resistance of 20000 s m^{-1} (the conversion factor is 1 s m^{-1} = $1 \times 10^{-9} R_{gas} \frac{\theta_{atm}}{P_{atm}}$ μmol^{-1} m^2 s). The difference between this equation and that used by Collatz et al. (1991) is that they used net photosynthesis (i.e., photosynthesis minus respiration) instead of photosynthesis. Collatz et al.'s (1991) derivation of this equation is empirical, using net photosynthesis. However, use of net photosynthesis causes stomatal conductance to be less than the minimum conductance b at night or in the winter, when plants do not photosynthesize but still respire. In contrast, using photosynthesis ensures that stomatal conductance equals b when there is no photosynthesis.

Leaf photosynthesis is $A = \min\left(w_c, w_j, w_e\right)$. Photosynthesis in C_3 plants is based on the models of Farquhar et al. (1980) and Collatz et al. (1991). Photosynthesis in C_4 plants is based on the models of Collatz et al. (1992) and Dougherty et al. (1994). The RuBP carboxylase (Rubisco) limited rate of carboxylation w_c (μ mol CO_2 m^{-2} s^{-1}) is

$$w_c = \left\{\begin{array}{ll} \dfrac{\left(c_i - \Gamma_*\right)V_{\max}}{c_i + K_c\left(1 + o_i/K_o\right)} & \text{for } C_3 \text{ plants} \\ V_{\max} & \text{for } C_4 \text{ plants} \end{array}\right\} \quad c_i - \Gamma_* \ge 0. \tag{8.2}$$

The maximum rate of carboxylation allowed by the capacity to regenerate RuBP (i.e., the light-limited rate) w_j (μ mol CO_2 m^{-2} s^{-1}) is

$$w_j = \left\{\begin{array}{ll} \dfrac{\left(c_i - \Gamma_*\right)4.6\phi\alpha}{c_i + 2\Gamma_*} & \text{for } C_3 \text{ plants} \\ 4.6\phi\alpha & \text{for } C_4 \text{ plants} \end{array}\right\} \quad c_i - \Gamma_* \ge 0. \tag{8.3}$$

The export limited rate of carboxylation for C_3 plants and the PEP carboxylase limited rate of carboxylation for C_4 plants w_e (μ mol CO_2 m^{-2} s^{-1}) is

$$w_e = \left\{\begin{array}{ll} 0.5V_{\max} & \text{for } C_3 \text{ plants} \\ 4000V_{\max}\dfrac{c_i}{P_{atm}} & \text{for } C_4 \text{ plants} \end{array}\right\}. \tag{8.4}$$

Collatz et al. (1992) used the term $1800V_{\max}$ (their k) for C_4 w_e. However, when this value was used, photosynthesis saturated at extremely low values of ambient CO_2. The term $4000V_{\max}$ resulted in saturation at about 400 ppm, which is more consistent with observations.

In these equations, c_i is the internal leaf CO_2 concentration (Pa) and $o_i = 0.209P_{atm}$ is the O_2 concentration (Pa). K_c and K_o, the Michaelis-Menten constants (Pa) for CO_2

and O_2, vary with vegetation temperature T_v (ºC) (section 5) according to the Q_{10} function as in Collatz et al. (1991)

$$K_c = K_{c25} \left(a_{kc} \right)^{\frac{T_v - 25}{10}} \tag{8.5}$$

$$K_o = K_{o25} \left(a_{ko} \right)^{\frac{T_v - 25}{10}} \tag{8.6}$$

where $K_{c25} = 30.0$ and $K_{o25} = 30000.0$ are values (Pa) at 25ºC, and $a_{kc} = 2.1$ and $a_{ko} = 1.2$ are the relative changes in K_{c25} and K_{o25}, respectively, for a 10ºC change in temperature (Collatz et al. 1991). The CO_2 compensation point Γ_* (Pa) is

$$\Gamma_* = \frac{1}{2} \frac{K_c}{K_o} 0.21 o_i . \tag{8.7}$$

The term 0.21 represents the ratio of maximum rates of oxygenation to carboxylation, which is virtually constant with temperature (Farquhar and von Caemmerer 1982). α is the quantum efficiency (μmol CO_2 per μmol photons) (Table 8.2) (Landsberg 1986), and ϕ is the absorbed photosynthetically active radiation (W m^{-2}) (section 4.1), which is converted to photosynthetic photon flux assuming 4.6 μmol photons per Joule.

The maximum rate of carboxylation varies with temperature and soil water

$$V_{\max} = V_{\max 25} \left(a_{v\max} \right)^{\frac{T_v - 25}{10}} f\left(T_v \right) \beta_t \tag{8.8}$$

where $V_{\max 25}$ is the value at 25ºC (μmol CO_2 m^{-2} s^{-1}) (Table 8.2), $a_{v\max} = 2.4$ is the Q_{10} parameter (Collatz et al. 1991), and β_t is a soil moisture limitation function. Values of $V_{\max 25}$ for each plant functional type were obtained from published estimates (Wullschleger 1993, Kucharik et al. 2000) and are consistent with the canopy scaling.

$f\left(T_v\right)$ is a function that mimics thermal breakdown of metabolic processes (Farquhar et al. 1980, Collatz et al. 1991)

$$f\left(T_v\right) = \left[1 + \exp\left(\frac{-22000 + 710\left(T_v + T_f\right)}{0.001R_{gas}\left(T_v + T_f\right)}\right)\right]^{-1} \tag{8.9}$$

where T_f is the freezing temperature of water (K) (Table 1.4), and R_{gas} is the universal gas constant (J K^{-1} kmol^{-1}) (Table 1.4). The function β_t ranges from one when the soil is wet to near zero when the soil is dry and depends on the root distribution of the plant functional type and the soil water potential of each soil layer

$$\beta_t = \sum_i w_i r_i \geq 1 \times 10^{-10} \tag{8.10}$$

where w_i is a soil dryness or plant wilting factor for layer i, and r_i is the fraction of roots in layer i.

The plant wilting factor w_i is

$$w_i = \left\{ \begin{array}{ll} \dfrac{\psi_{\max} - \psi_i}{\psi_{\max} + \psi_{sat,i}} & \text{for } T_i > T_f \\ 0 & \text{for } T_i \leq T_f \end{array} \right\} \tag{8.11}$$

where $\psi_{\max}$ is a constant describing the wilting point potential of leaves ($\psi_{\max} = -1.5 \times 10^5$ mm), ψ_i is the soil water matric potential (mm) of layer i, T_i is the temperature (K), and $\psi_{sat,i}$ is the saturated soil matric potential (mm) (section 7.4.1). Here, the soil water matric potential ψ_i is defined somewhat differently than in section 7.4.1

$$\psi_i = \psi_{sat,i} s_i^{-B_i} \geq \psi_{\max} \tag{8.12}$$

where s_i is the soil wetness for layer i with respect to the effective porosity and B_i is the Clapp and Hornberger (1978) parameter (section 7.4.1). The soil wetness s_i is

$$s_i = \frac{\theta_{liq,i}}{\theta_{sat,i} - \theta_{ice,i}} \geq 0.01 \tag{8.13}$$

where $\theta_{ice,i} = w_{ice,i} \big/ \left(\rho_{ice} \Delta z_i\right) \leq \theta_{sat,i}$, and $\theta_{liq,i} = w_{liq,i} \big/ \left(\rho_{liq} \Delta z_i\right) \leq \theta_{sat,i} - \theta_{ice,i}$. $w_{ice,i}$ and $w_{liq,i}$ are the ice and liquid water contents (kg m^{-2}) (section 7), $\theta_{sat,i}$ is the saturated volumetric water content (section 7.4.1), ρ_{ice} and ρ_{liq} are the densities of ice and liquid water (kg m^{-3}) (Table 1.4), and Δz_i is the soil layer thickness (m) (section 6.1).

The root fraction r_i in each soil layer depends on the plant functional type

$$r_i = \begin{Bmatrix} 0.5 \begin{bmatrix} \exp\left(-r_a z_{h,i-1}\right) + \exp\left(-r_b z_{h,i-1}\right) - \\ \exp\left(-r_a z_{h,i}\right) - \exp\left(-r_b z_{h,i}\right) \end{bmatrix} & \text{for } 1 \leq i < 10 \\ 0.5\left[\exp\left(-r_a z_{h,i-1}\right) + \exp\left(-r_b z_{h,i-1}\right)\right] & \text{for } i = 10 \end{Bmatrix} \tag{8.14}$$

where $z_{h,i}$ (m) is the depth from the soil surface to the interface between layers i and $i+1$ ($z_{h,0} = 0$, the soil surface) (section 6.1), and r_a and r_b are plant functional type – dependent root distribution parameters adopted from Zeng (2001) (Table 8.1).

Table 8.1. Plant functional type root distribution parameters.

	Root Distribution	
Plant Functional Type	r_a	r_b
NET Temperate	7.0	2.0
NET Boreal	7.0	2.0
NDT Boreal	7.0	2.0
BET Tropical	7.0	1.0
BET temperate	7.0	1.0
BDT tropical	6.0	2.0
BDT temperate	6.0	2.0
BDT boreal	6.0	2.0
BES temperate	7.0	1.5
BDS temperate	7.0	1.5
BDS boreal	7.0	1.5
C_3 grass arctic	11.0	2.0
C_3 grass	11.0	2.0
C_4 grass	11.0	2.0
Crop1	6.0	3.0
Crop2	6.0	3.0

The CO_2 concentration at the leaf surface c_s (Pa), the internal leaf CO_2 concentration c_i (Pa), and the vapor pressure at the leaf surface e_s (Pa) are calculated assuming there is negligible capacity to store CO_2 and water at the leaf surface so that, with reference to Figure 8.1,

$$A = \frac{c_a - c_i}{\left(1.37 r_b + 1.65 r_s\right) P_{atm}} = \frac{c_a - c_s}{1.37 r_b P_{atm}} = \frac{c_s - c_i}{1.65 r_s P_{atm}} \tag{8.15}$$

and the transpiration fluxes are related as

$$\frac{e'_a - e_i}{\left(r_b + r_s\right)} = \frac{e'_a - e_s}{r_b} = \frac{e_s - e_i}{r_s} \tag{8.16}$$

where r_b is leaf boundary layer resistance (s m^2 μmol^{-1}) (section 5.3), the terms 1.37 and 1.65 are the ratios of diffusivity of CO_2 to H_2O for the leaf boundary layer resistance and stomatal resistance (Landsberg 1986), $c_a = 355 \times 10^{-6} P_{atm}$ is the atmospheric CO_2 concentration (Pa), and the vapor pressure of air (Pa) is $e'_a = \max\left(\min\left(e_a, e_i\right), 0.25 e_i\right)$.

Figure 8.1. Schematic diagram of photosynthesis.

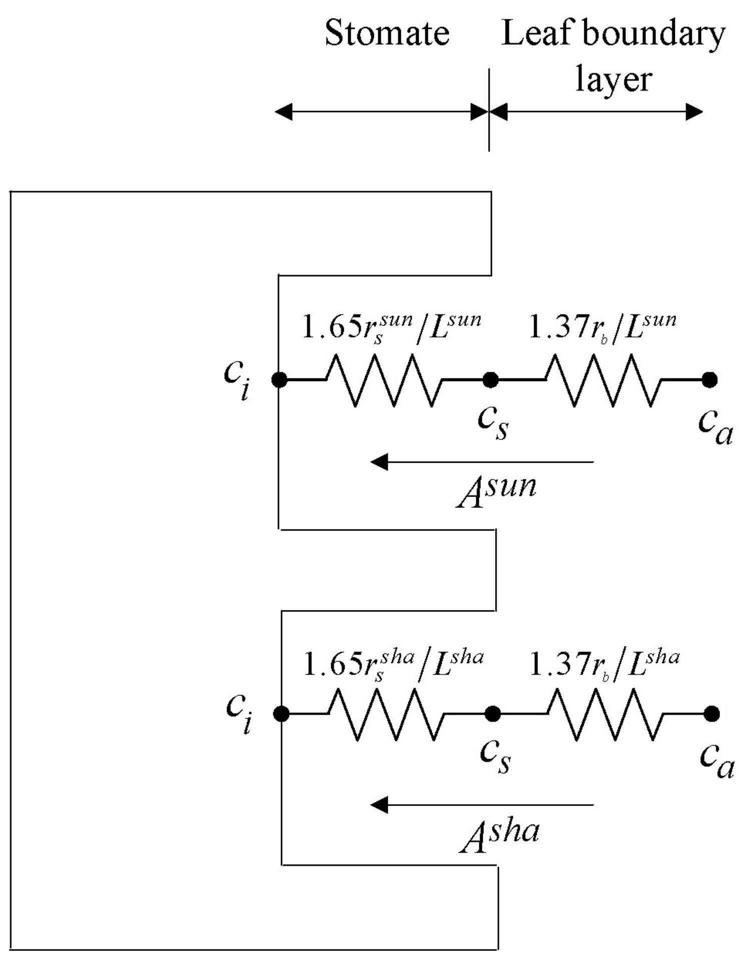

The lower limit $0.25e_i$ is used to prevent numerical instability in the iterative stomatal resistance calculation. For C_4 plants, this lower limit is $0.40e_i$ because C_4 plants are not as sensitive to vapor pressure as C_3 plants. The vapor pressure of air in the plant canopy e_a is determined from

$$e_a = \frac{P_{atm} q_s}{0.622} \tag{8.17}$$

where q_s is the specific humidity of canopy air (kg kg^{-1}) (section 5.3).

Equations (8.15) and (8.16) are solved for c_s and e_s

$$c_s = c_a - 1.37 r_b P_{atm} A \quad \geq 1\times 10^{-6} \tag{8.18}$$

$$e_s = \frac{e'_a r_s + e_i r_b}{r_b + r_s}. \tag{8.19}$$

Substitution of equation (8.19) into equation (8.1) yields a quadratic equation for stomatal resistance

$$\left(\frac{mAP_{atm} e'_a}{c_s e_i} + b\right) r_s^2 + \left(\frac{mAP_{atm} r_b}{c_s} + b r_b - 1\right) r_s - r_b = 0. \tag{8.20}$$

Stomatal resistance r_s is the larger of the two roots that satisfy the quadratic equation. This equation is iterated three times with an initial arbitrary value of $c_i = 0.7 c_a$ for C_3 plants and $c_i = 0.4 c_a$ for C_4 plants used to calculate A. Subsequent values for c_i are given by

$$c_i = c_s - 1.65 r_s P_{atm} A \quad \geq 0. \tag{8.21}$$

These equations are solved for sunlit and shaded leaves using average absorbed photosynthetically active radiation for sunlit and shaded leaves [ϕ^{sun}, ϕ^{sha} (section 4.1)] to give sunlit and shaded stomatal resistance ($r_s^{sun}, r_s^{sha} \le 20000$ s m^{-1}) and photosynthesis (A^{sun}, A^{sha}). Canopy photosynthesis is $A^{sun}L^{sun} + A^{sha}L^{sha}$, where L^{sun} and L^{sha} are the sunlit and shaded leaf area indices (section 4.1). Canopy conductance is $\frac{1}{r_s^{sun}} L^{sun} + \frac{1}{r_s^{sha}} L^{sha}$.

Table 8.2. Plant functional type photosynthetic parameters

Plant functional type	$V_{\max 25}$	α	m
NET Temperate	51	0.06	6
NET Boreal	43	0.06	6
NDT Boreal	43	0.06	6
BET Tropical	75	0.06	9
BET temperate	69	0.06	9
BDT tropical	40	0.06	9
BDT temperate	51	0.06	9
BDT boreal	51	0.06	9
BES temperate	17	0.06	9
BDS temperate	17	0.06	9
BDS boreal	33	0.06	9
C_3 arctic grass	43	0.06	9
C_3 grass	43	0.06	9
C_4 grass	24	0.04	5
Crop1	50	0.06	9
Crop2	50	0.06	9

$V_{\max 25}$, μmol m^{-2} s^{-1}. α, μmol CO_2 per μmol photons

9. Lake Model

The lake model is from Zeng et al. (2002), which utilized concepts from the lake models of Bonan (1996), Henderson-Sellers (1985, 1986), Hostetler and Bartlein (1990) and the coupled lake-atmosphere model of Hostetler et al. (1993, 1994). All lakes are currently "deep" lakes of 50 m depth. Temperatures are simulated for ten layers with layer thicknesses Δz_i of 0.1, 1, 2, 3, 4, 5, 7, 7, 10.45, and 10.45 m, and node depths z_i located at the center of each layer (i.e., 0.05, 0.6, 2.1, 4.6, 8.1, 12.6, 18.6, 25.6, 34.325, 44.775 m). Lake surface fluxes closely follow the formulations for non-vegetated surfaces (section 5.2). The lake surface temperature T_g is solved for simultaneously with the surface fluxes. Snow on lakes is based on a bulk approach, not on the multi-layer model described in section 7.2.

9.1 Surface Fluxes and Surface Temperature

The sensible heat flux (W m^{-2}) is

$$H_g = -\rho_{atm} C_p \frac{\left(\theta_{atm} - T_g\right)}{r_{ah}} \tag{9.1}$$

where ρ_{atm} is the density of moist air (kg m^{-3}) (section 5), C_p is the specific heat capacity of air (J kg^{-1} K^{-1}) (Table 1.4), θ_{atm} is the atmospheric potential temperature (K) (section 5), T_g is the lake surface temperature (K), and r_{ah} is the aerodynamic resistance to sensible heat transfer (s m^{-1}) (section 5.1).

The water vapor flux (kg m^{-2} s^{-1}) is

$$E_g = -\frac{\rho_{atm}\left(q_{atm} - q_{sat}^{T_g}\right)}{r_{aw}} \tag{9.2}$$

where q_{atm} is the atmospheric specific humidity (kg kg^{-1}) (section 1.2.1), $q_{sat}^{T_g}$ is the saturated specific humidity (kg kg^{-1}) (section 5.5) at the lake surface temperature T_g, and r_{aw} is the aerodynamic resistance to water vapor transfer (s m^{-1}) (section 5.1).

The zonal and meridional momentum fluxes are

$$\tau_x = -\rho_{atm} \frac{u_{atm}}{r_{am}} \tag{9.3}$$

$$\tau_y = -\rho_{atm} \frac{v_{atm}}{r_{am}} \tag{9.4}$$

where u_{atm} and v_{atm} are the zonal and meridional atmospheric winds (m s^{-1}) (section 1.2.1), and r_{am} is the aerodynamic resistance for momentum (s m^{-1}) (section 5.1).

The heat flux into the lake surface G (W m^{-2}) (positive into the surface) is

$$G = \frac{\lambda_1}{\Delta z_1}\left(T_g - T_1\right) \tag{9.5}$$

where λ_1 is the thermal conductivity (W m^{-1} K^{-1}), Δz_1 is the thickness (m), and T_1 is the temperature (K) of the top lake layer. If snow is on the frozen lake, the depth of snow z_{sno} (m) (section 9.3) is combined with the thickness of the top lake layer, Δz_1, to create a snow/soil layer of thickness $\Delta z_1 + z_{sno}$. The thermal conductivity is

$$\lambda_1 = \begin{Bmatrix} \lambda_{liq} & T_g > T_f \\ \lambda_{ice} & T_g \le T_f \end{Bmatrix} \tag{9.6}$$

where λ_{liq} and λ_{ice} are the thermal conductivities of water and ice (W m^{-1} K^{-1}) (Table 1.4), and T_f is the freezing temperature of water (K) (Table 1.4).

The absorbed solar radiation $\vec{S}_g$ is

$$\vec{S}_g = \sum_{\Lambda} S_{atm} \downarrow_{\Lambda}^{\mu} \left(1-\alpha_{g,\Lambda}^{\mu}\right) + S_{atm} \downarrow_{\Lambda} \left(1-\alpha_{g,\Lambda}\right) \tag{9.7}$$

where $S_{atm} \downarrow_{\Lambda}^{\mu}$ and $S_{atm} \downarrow_{\Lambda}$ are the incident direct beam and diffuse solar fluxes (W m^{-2}) and Λ denotes the visible ($< 0.7\,\mu\text{m}$) and near-infrared ($\geq 0.7\,\mu\text{m}$) wavebands (section 1.2.1), and $\alpha_{g,\Lambda}^{\mu}$ and $\alpha_{g,\mu}$ are the direct beam and diffuse lake albedos (section 3.2).

The net longwave radiation (positive toward the atmosphere) is

$$\vec{L}_g = L_g \uparrow - L_{atm} \downarrow \tag{9.8}$$

where $L_g \uparrow$ is the upward longwave radiation from the surface, $L_{atm} \downarrow$ is the downward atmospheric longwave radiation (section 1.2.1). The upward longwave radiation from the surface is

$$L \uparrow = \left(1-\varepsilon_g\right) L_{atm} \downarrow + \varepsilon_g \sigma \left(T_g^n\right)^4 + 4\varepsilon_g \sigma \left(T_g^n\right)^3 \left(T_g^{n+1} - T_g^n\right) \tag{9.9}$$

where $\varepsilon_g = 0.97$ is the lake surface emissivity, σ is the Stefan-Boltzmann constant (W m^{-2} K^{-4}) (Table 1.4), and $T_g^{n+1} - T_g^n$ is the difference in lake surface temperature between Newton-Raphson iterations (see below).

The sensible heat H_g, the water vapor flux E_g through its dependence on the saturated specific humidity, the net longwave radiation $\vec{L}_g$, and the ground heat flux G, all depend on the lake surface temperature T_g. Newton-Raphson iteration is applied to solve for T_g and the surface fluxes as

$$\Delta T_g = \frac{\vec{S}_g - \vec{L}_g - H_g - \lambda E_g - G}{\frac{\partial \vec{L}_g}{\partial T_g} + \frac{\partial H_g}{\partial T_g} + \frac{\partial \lambda E_g}{\partial T_g} + \frac{\partial G}{\partial T_g}} \tag{9.10}$$

where $\Delta T_g = T_g^{n+1} - T_g^n$ and the subscript "n" indicates the iteration. Therefore, the surface temperature T_g^{n+1} can be written as

$$T_g^{n+1} = \frac{\vec{S}_g - \vec{L}_g - H_g - \lambda E_g - G + T_g^n \left(\frac{\partial \vec{L}_g}{\partial T_g} + \frac{\partial H_g}{\partial T_g} + \frac{\partial \lambda E_g}{\partial T_g} + \frac{\partial G}{\partial T_g} \right)}{\frac{\partial \vec{L}_g}{\partial T_g} + \frac{\partial H_g}{\partial T_g} + \frac{\partial \lambda E_g}{\partial T_g} + \frac{\partial G}{\partial T_g}} \tag{9.11}$$

where the partial derivatives are

$$\frac{\partial \vec{L}_g}{\partial T_g} = 4\varepsilon_g \sigma \left(T_g^n\right)^3 , \tag{9.12}$$

$$\frac{\partial H_g}{\partial T_g} = \frac{\rho_{atm} C_p}{r_{ah}} , \tag{9.13}$$

$$\frac{\partial \lambda E_g}{\partial T_g} = \frac{\lambda \rho_{atm}}{r_{aw}} \frac{dq_{sat}^{T_g}}{dT_g} , \tag{9.14}$$

$$\frac{\partial G}{\partial T_g} = \frac{\lambda_1}{\Delta z_1} . \tag{9.15}$$

The fluxes of momentum, sensible heat, and water vapor are solved for simultaneously with lake surface temperature as follows. The stability-related equations are the same as for non-vegetated surfaces (section 5.2).

1. An initial guess for the wind speed V_a including the convective velocity U_c is obtained from eq. (5.24) assuming an initial convective velocity $U_c = 0$ m s^{-1} for stable conditions ($\theta_{v,atm} - \theta_{v,s} \geq 0$ as evaluated from eq. (5.50)) and $U_c = 0.5$ for unstable conditions ($\theta_{v,atm} - \theta_{v,s} < 0$).

2. An initial guess for the Monin-Obukhov length L is obtained from the bulk Richardson number using equations (5.46) and (5.48).

3. The following system of equations is iterated three times:

- Thermal conductivity λ_1 (eq. (9.6))
- Friction velocity u_* (eqs. (5.32), (5.33), (5.34), (5.35))
- Potential temperature scale θ_* (eqs. (5.37), (5.38), (5.39), (5.40))
- Humidity scale q_* (eqs. (5.41), (5.42), (5.43), (5.44))
- Aerodynamic resistances r_{am}, r_{ah}, and r_{aw} (eqs. (5.55), (5.56), (5.57))
- Lake surface temperature T_g^{n+1} (eq. (9.11))
- Sensible heat flux H_g is updated for T_g^{n+1} (eq. (9.1))
- Water vapor flux E_g is updated for T_g^{n+1} as

$$E_g = -\frac{\rho_{atm}}{r_{aw}}\left[q_{atm} - q_{sat}^{T_g} - \frac{\partial q_{sat}^{T_g}}{\partial T_g}\left(T_g^{n+1} - T_g^n\right)\right] \tag{9.16}$$

  where the last term on the right side of equation (9.16) is the change in saturated specific humidity due to the change in T_g between iterations.

- Saturated specific humidity $q_{sat}^{T_g}$ and its derivative $\frac{dq_{sat}^{T_g}}{dT_g}$ are updated for T_g^{n+1} (section 5.1).
- Virtual potential temperature scale θ_{v*} (eq. (5.17))
- Wind speed including the convective velocity, V_a (eq. (5.24))
- Monin-Obukhov length L (eq. (5.49)).

Once the final lake surface temperature has been calculated, if there is snow on the lake ($W_{sno} > 0.5$ kg m^{-2}) and $T_g > T_f$, the surface temperature is reset to freezing temperature and the surface fluxes H_g, E_g are re-evaluated with $T_g = T_f$ using equations (9.1) and (9.16). The final ground heat flux G is calculated from the residual of the energy balance

$$G = \vec{S}_g - \left(L_g \uparrow - L_{atm} \downarrow\right) - H_g - \lambda E_g \tag{9.17}$$

where $L_g \uparrow$ is evaluated from equation (9.9). If the ground heat flux $G > 0$ (i.e., there is a flux of heat into the snow), the energy (W m^{-2}) available to melt snow (phase change energy) is

$$E_p = G \le \frac{W_{sno} L_f}{\Delta t} \tag{9.18}$$

where L_f is the latent heat of fusion (J kg^{-1}) (Table 1.4) and Δt is the time step (s). This equation limits snowmelt to be less than or equal to the amount of snow on the lake surface. Any excess energy is used to warm the top lake layer. The rate of snowmelt is $M = E_p / L_f$ (kg m^{-2} s^{-1}).

The roughness lengths used to calculate r_{am}, r_{ah}, and r_{aw} are $z_{0m} = z_{0h} = z_{0w} = z_{0m,g}$. The momentum roughness length $z_{0m,g} = 0.01$ for unfrozen lakes ($T_g \ge T_f$) and $z_{0m,g} = 0.04$ for frozen lakes ($T_g < T_f$) whether snow-covered or not. The displacement height $d = 0$. When converting water vapor flux to an energy flux, the term λ is defined as follows

$$\lambda = \begin{cases} \lambda_{sub} & T_{atm} \le T_f \\ \lambda_{vap} & T_{atm} > T_f \end{cases} \tag{9.19}$$

where λ_{sub} and λ_{vap} are the latent heat of sublimation and vaporization, respectively (J kg^{-1}) (Table 1.4).

9.2 Lake Temperatures

The governing equation for lake temperature, assuming constant cross-sectional area with depth, is (Hostetler and Bartlein 1990)

$$\frac{\partial T}{\partial t} = \frac{\partial}{\partial z}\left[\left(\kappa_m + \kappa_e\right)\frac{\partial T}{\partial z}\right] + \frac{1}{c_{liq}}\frac{d\phi}{dz} \tag{9.20}$$

where T is lake temperature (K), $\kappa_m = \lambda_{liq} / c_{liq}$ and κ_e are the molecular and eddy diffusion coefficients for heat (m^2 s^{-1}), λ_{liq} is the thermal conductivity of water (W m^{-1} K^{-1}) (Table 1.4), $c_{liq} = C_{liq}\rho_{liq}$ is the volumetric heat capacity of water (J m^{-3} K^{-1}) where C_{liq} is the specific heat capacity of water (J kg^{-1} K^{-1}) (Table 1.4) and ρ_{liq} is the density of water (kg m^{-3}) (Table 1.4), ϕ is a subsurface solar radiation heat source term (W m^{-2}), and z is depth from the surface (m). Using a method similar to that for snow/soil (section 6.1), this equation is solved numerically to calculate temperatures for 10-layer lakes with boundary conditions of zero heat flux at the bottom and the net flux of energy at the surface F_0 (W m^{-2})

$$F_0 = \beta \vec{S}_g - \vec{L}_g - H_g - \lambda E_g - E_p \tag{9.21}$$

where $\beta = 0.4$ is the fraction of $\vec{S}_g$ absorbed in the surface layer and E_p is phase change energy (W m^{-2}).

Similar to snow/soil, the heat flux F_i (W m^{-2}) from layer i to $i+1$ is

$$F_i = -c_{liq}\left[\left(T_i - T_{i+1}\right)\left(\frac{\Delta z_i}{2\left(\kappa_m + \kappa_{e,i}\right)} + \frac{\Delta z_{i+1}}{2\left(\kappa_m + \kappa_{e,i+1}\right)}\right)^{-1}\right] \tag{9.22}$$

which is derived assuming the heat flux from i (depth z_i) to the interface between i and $i+1$ (depth $z_i + 0.5\Delta z_i$) equals the heat flux from the interface to $i+1$ (depth z_{i+1}), i.e.,

$$-c_{liq}\left(\kappa_m+\kappa_{e,i}\right)\left(\frac{T_i-T_m}{\frac{1}{2}\Delta z_i}\right)=-c_{liq}\left(\kappa_m+\kappa_{e,i+1}\right)\left(\frac{T_m-T_{i+1}}{\frac{1}{2}\Delta z_{i+1}}\right) \tag{9.23}$$

where T_m is the interface temperature.

The energy balance for the i^{th} layer is

$$\frac{c_{liq}\Delta z_i}{\Delta t}\left(T_i^{n+1}-T_i^n\right)=-F_{i-1}+F_i+\left(\phi_{i-\frac{1}{2}}-\phi_{i+\frac{1}{2}}\right) \tag{9.24}$$

where the superscripts n and $n+1$ indicate values at the beginning and end of the time step, respectively, and Δt is the time step (s). This equation is solved using the Crank-Nicholson method, which combines the explicit method with fluxes evaluated at n (F_{i-1}^n, F_i^n) and the implicit method with fluxes evaluated at $n+1$ (F_{i-1}^{n+1}, F_i^{n+1})

$$\frac{c_{liq}\Delta z_i}{\Delta t}\left(T_i^{n+1}-T_i^n\right)=\alpha\left(-F_{i-1}^n+F_i^n\right)+\left(1-\alpha\right)\left(-F_{i-1}^{n+1}+F_i^{n+1}\right)+\left(\phi_{i-\frac{1}{2}}-\phi_{i+\frac{1}{2}}\right) \tag{9.25}$$

where $\alpha=0.5$, resulting in a tridiagonal system of equations

$$r_i=a_iT_{i-1}^{n+1}+b_iT_i^{n+1}+c_iT_{i+1}^{n+1}. \tag{9.26}$$

For the top lake layer $i=1$, $F_{i-1}=F_0$, and the equations are

$$T_i^{n+1}-T_i^n=\frac{\Delta t}{\Delta z_i}\frac{F_0}{c_{liq}}-\left[\left(\frac{T_i^n-T_{i+1}^n+T_i^{n+1}-T_{i+1}^{n+1}}{\dfrac{\Delta z_i}{\kappa_m+\kappa_{e,i}}+\dfrac{\Delta z_{i+1}}{\kappa_m+\kappa_{e,i+1}}}\right)+\frac{\phi_{i-\frac{1}{2}}-\phi_{i+\frac{1}{2}}}{c_{liq}}\right] \tag{9.27}$$

$$a_i=0 \tag{9.28}$$

$$b_i=1+\frac{\Delta t}{\Delta z_i}\left(\frac{\Delta z_i}{\kappa_m+\kappa_{e,i}}+\frac{\Delta z_{i+1}}{\kappa_m+\kappa_{e,i+1}}\right)^{-1} \tag{9.29}$$

$$c_i=-\frac{\Delta t}{\Delta z_i}\left(\frac{\Delta z_i}{\kappa_m+\kappa_{e,i}}+\frac{\Delta z_{i+1}}{\kappa_m+\kappa_{e,i+1}}\right)^{-1} \tag{9.30}$$

$$r_i = T_i^n + \frac{\Delta t}{\Delta z_i}\left[\frac{F_0}{c_{liq}} - \left(T_i^n - T_{i+1}^n\right)\left(\frac{\Delta z_i}{\kappa_m + \kappa_{e,i}} + \frac{\Delta z_{i+1}}{\kappa_m + \kappa_{e,i+1}}\right)^{-1} + \frac{\phi_{i-\frac{1}{2}} - \phi_{i+\frac{1}{2}}}{c_{liq}}\right]. \tag{9.31}$$

The boundary condition at the bottom of the lake column is zero heat flux, $F_i = 0$, resulting in, for $i = 10$,

$$T_i^{n+1} - T_i^n = \frac{\Delta t}{\Delta z_i}\left[\left(\frac{T_{i-1}^n - T_i^n + T_{i-1}^{n+1} - T_i^{n+1}}{\frac{\Delta z_{i-1}}{\kappa_m + \kappa_{e,i-1}} + \frac{\Delta z_i}{\kappa_m + \kappa_{e,i}}}\right) + \frac{\phi_{i-\frac{1}{2}} - \phi_{i+\frac{1}{2}}}{c_{liq}}\right] \tag{9.32}$$

$$a_i = -\frac{\Delta t}{\Delta z_i}\left(\frac{\Delta z_{i-1}}{\kappa_m + \kappa_{e,i-1}} + \frac{\Delta z_i}{\kappa_m + \kappa_{e,i}}\right)^{-1} \tag{9.33}$$

$$b_i = 1 + \frac{\Delta t}{\Delta z_i}\left(\frac{\Delta z_{i-1}}{\kappa_m + \kappa_{e,i-1}} + \frac{\Delta z_i}{\kappa_m + \kappa_{e,i}}\right)^{-1} \tag{9.34}$$

$$c_i = 0 \tag{9.35}$$

$$r_i = T_i^n + \frac{\Delta t}{\Delta z_i}\left[\left(T_{i-1}^n - T_i^n\right)\left(\frac{\Delta z_{i-1}}{\kappa_m + \kappa_{e,i-1}} + \frac{\Delta z_i}{\kappa_m + \kappa_{e,i}}\right)^{-1} + \frac{\phi_{i-\frac{1}{2}} - \phi_{i+\frac{1}{2}}}{c_{liq}}\right]. \tag{9.36}$$

For the interior lake layers, $1 < i < 10$,

$$\begin{aligned} T_i^{n+1} - T_i^n = {} & \frac{\Delta t}{\Delta z_i}\left(T_{i-1}^n - T_i^n + T_{i-1}^{n+1} - T_i^{n+1}\right)\left(\frac{\Delta z_{i-1}}{\kappa_m + \kappa_{e,i-1}} + \frac{\Delta z_i}{\kappa_m + \kappa_{e,i}}\right)^{-1} \\ & - \frac{\Delta t}{\Delta z_i}\left(T_i^n - T_{i+1}^n + T_i^{n+1} - T_{i+1}^{n+1}\right)\left(\frac{\Delta z_i}{\kappa_m + \kappa_{e,i}} + \frac{\Delta z_{i+1}}{\kappa_m + \kappa_{e,i+1}}\right)^{-1} \\ & + \frac{\Delta t}{\Delta z_i}\left(\frac{\phi_{i-\frac{1}{2}} - \phi_{i+\frac{1}{2}}}{c_{liq}}\right) \end{aligned} \tag{9.37}$$

$$a_i = -\frac{\Delta t}{\Delta z_i}\left(\frac{\Delta z_{i-1}}{\kappa_m + \kappa_{e,i-1}} + \frac{\Delta z_i}{\kappa_m + \kappa_{e,i}}\right)^{-1} \tag{9.38}$$

$$b_i = 1 + \frac{\Delta t}{\Delta z_i}\left(\frac{\Delta z_{i-1}}{\kappa_m + \kappa_{e,i-1}} + \frac{\Delta z_i}{\kappa_m + \kappa_{e,i}}\right)^{-1} + \frac{\Delta t}{\Delta z_i}\left(\frac{\Delta z_i}{\kappa_m + \kappa_{e,i}} + \frac{\Delta z_{i+1}}{\kappa_m + \kappa_{e,i+1}}\right)^{-1} \tag{9.39}$$

$$c_i = -\frac{\Delta t}{\Delta z_i}\left(\frac{\Delta z_i}{\kappa_m + \kappa_{e,i}} + \frac{\Delta z_{i+1}}{\kappa_m + \kappa_{e,i+1}}\right)^{-1} \tag{9.40}$$

$$\begin{aligned} r_i = T_i^n &+ \frac{\Delta t}{\Delta z_i}\left(T_{i-1}^n - T_i^n\right)\left(\frac{\Delta z_{i-1}}{\kappa_m + \kappa_{e,i-1}} + \frac{\Delta z_i}{\kappa_m + \kappa_{e,i}}\right)^{-1} \\ &- \frac{\Delta t}{\Delta z_i}\left(T_i^n - T_{i+1}^n\right)\left(\frac{\Delta z_i}{\kappa_m + \kappa_{e,i}} + \frac{\Delta z_{i+1}}{\kappa_m + \kappa_{e,i+1}}\right)^{-1} \\ &+ \frac{\Delta t}{\Delta z_i}\frac{\phi_{i-\frac{1}{2}} - \phi_{i+\frac{1}{2}}}{c_{liq}} \end{aligned} \tag{9.41}$$

The eddy diffusion coefficient $\kappa_{e,i}$ (m^2 s^{-1}) for layers $1 \le i < 10$ is

$$\kappa_{e,i} = \left\{ \begin{array}{ll} \dfrac{kw^* z_i}{P_0\left(1 + 37Ri^2\right)}\exp\left(-k^* z_i\right) & T_g > T_f \\ 0 & T_g \le T_f \end{array} \right\} \tag{9.42}$$

where k is the von Karman constant (Table 1.4), $P_0 = 1$ is the neutral value of the turbulent Prandtl number, z_i is the node depth (m), the surface friction velocity (m s^{-1}) is $w^* = 0.0012u_2$, and k^* varies with latitude ϕ as $k^* = 6.6u_2^{-1.84}\sqrt{\left|\sin\phi\right|}$. For the bottom layer, $\kappa_{e,10} = \kappa_{e,9}$. As in Hostetler and Bartlein (1990), the 2-m wind speed u_2 (m s^{-1}) is used to evaluate w^* and k^* rather than the 10-m wind used by Henderson-Sellers (1985). The 2-m wind speed is

$$u_2 = \frac{u_*}{k}\ln\left(\frac{2}{z_{0m}}\right) \ge 1. \tag{9.43}$$

The Richardson number is

$$Ri = \frac{-1 + \sqrt{1 + \frac{40N^2 k^2 z_i^2}{w^{*^2} \exp\left(-2k^* z_i\right)}}}{20} \tag{9.44}$$

where

$$N^2 = -\frac{g}{\rho_i} \frac{\partial \rho}{\partial z} \tag{9.45}$$

and g is the acceleration due to gravity (m s^{-2}) (Table 1.4), ρ_i is the density of water (kg m^{-3}), and $\frac{\partial \rho}{\partial z}$ is approximated as $\frac{\rho_{i+1} - \rho_i}{z_{i+1} - z_i}$. The density of water is (Hostetler and Bartlein 1990)

$$\rho_i = 1000\left(1 - 1.9549 \times 10^{-5} \left|T_i - 277\right|^{1.68}\right). \tag{9.46}$$

The term $\phi_{i-\frac{1}{2}}$ is the solar radiation flux into the top of the i^{th} layer (depth $z = z_i - \frac{1}{2}\Delta z_i$) and $\phi_{i+\frac{1}{2}}$ is the solar radiation flux out of the bottom of the i^{th} layer (depth $z = z_i + \frac{1}{2}\Delta z_i$). For $z > z_a$, where $z_a = 0.6$ m is the base of the surface absorption layer, the solar radiation at depth z is (Henderson-Sellers 1986)

$$\phi = \left(1 - \beta\right) \vec{S}_g \exp\left[-\eta\left(z - z_a\right)\right] \tag{9.47}$$

where $\eta = 0.1$ is the light extinction coefficient for water. The net solar radiation flux absorbed by layers $1 \le i < 10$, $\phi_{i-\frac{1}{2}} - \phi_{i+\frac{1}{2}}$, for an unfrozen lake ($T_g > T_f$), is then

$$\phi_{i-\frac{1}{2}} - \phi_{i+\frac{1}{2}} = \left(1 - \beta\right) \vec{S}_g \left\{\exp\left[-\eta\left(z_i - \frac{1}{2}\Delta z_i - z_a\right)\right] - \exp\left[-\eta\left(z_i + \frac{1}{2}\Delta z_i - z_a\right)\right]\right\}. \tag{9.48}$$

For the bottom layer $i = 10$, $\phi_{i+\frac{1}{2}} = 0$, and

$$\phi_{i-\frac{1}{2}} - \phi_{i+\frac{1}{2}} = \left(1 - \beta\right) \vec{S}_g \left\{\exp\left[-\eta\left(z_i - \frac{1}{2}\Delta z_i - z_a\right)\right]\right\}. \tag{9.49}$$

For frozen lakes, the solar radiation is absorbed in the surface layer only so that

$$\phi_{i-\frac{1}{2}} - \phi_{i+\frac{1}{2}} = \begin{Bmatrix} (1-\beta)\vec{S}_g & i = 1 \\ 0 & 1 < i \le 10 \end{Bmatrix}. \tag{9.50}$$

Convective mixing occurs using the same scheme as in Hostetler et al.'s (1993, 1994) coupled lake-atmosphere model. Unfrozen lakes overturn when $\rho_i > \rho_{i+1}$, in which case the layer thickness weighted average temperature for layers 1 to $i+1$ is applied to layers 1 to $i+1$ and the densities are updated. This scheme is applied iteratively to layers $1 \le i < 10$.

The solution for lake temperature conserves energy as

$$\sum_{i=1}^{10} \frac{c_{liq} \Delta z_i}{\Delta t} \left(T_i^{n+1} - T_i^n \right) = F_0 + \sum_{i=1}^{10} \left(\phi_{i-\frac{1}{2}} - \phi_{i+\frac{1}{2}} \right). \tag{9.51}$$

9.3 Lake Hydrology

The volume of water in lakes is assumed to be constant, i.e., lake levels and area do not change. The runoff term q_{rgwl} (section 7.6) accounts for the excess or deficit of water required to keep the lake volume constant as

$$q_{rgwl} = q_{rain} + q_{sno} - E_g - \frac{W_{sno}^{n+1} - W_{sno}^n}{\Delta t} \tag{9.52}$$

where q_{rain} and q_{sno} are atmospheric inputs of rain and snow (kg m^{-2} s^{-1}) (section 1.2.1), E_g is the water vapor flux (kg m^{-2} s^{-1}) (section 9.1), and $W_{sno}^{n+1} - W_{sno}^n$ is the change in snow mass (kg m^{-2}) in time step Δt (s).

The snow mass is updated for melt and sublimation or frost as

$$W_{sno}^{n+1} = \begin{cases} W_{sno}^{n} + \left(q_{sno} - M - q_{subl} + q_{frost}\right)\Delta t \ge 0 & W_{sno} \le 1000 \\ W_{sno}^{n} - \left(M + q_{subl}\right)\Delta t \ge 0 & W_{sno} > 1000 \\ 0 & T_g > T_f \end{cases} \tag{9.53}$$

where M is snowmelt (kg m^{-2} s^{-1}) (section 9.1), q_{subl} is the sublimation from snow (kg m^{-2} s^{-1}), and q_{frost} is frost on snow (kg m^{-2} s^{-1}). As with snow on ground, W_{sno} is capped to not exceed 1000 kg m^{-2}. The depth of snow z_{sno} (m) is $z_{sno} = W_{sno} / \rho_{sno}$ assuming a constant density of snow $\rho_{sno} = 250$ kg m^{-3}. The water vapor flux E_g (section 9.1) is partitioned into q_{subl} or q_{frost} as

$$q_{subl} = \min\left(E_g, \frac{W_{sno}}{\Delta t} - M\right) \qquad E_g \ge 0 \tag{9.54}$$

$$q_{frost} = \left|E_g\right| \qquad E_g < 0 \text{ and } T_g < T_f + 0.1. \tag{9.55}$$

10. River Transport Model (RTM)

The RTM was developed to route total runoff from the land surface model to either the active ocean or marginal seas which enables the hydrologic cycle to be closed (Branstetter 2001, Branstetter and Famiglietti 1999). This is needed to model ocean convection and circulation, which is affected by freshwater input. It also provides another method of diagnosing the performance of the land model because the river flow can be directly compared to gauging station data (e.g., Dai and Trenberth 2002).

The RTM uses a linear transport scheme at 0.5º resolution to route water from each grid cell to its downstream neighboring grid cell. The change in storage S of river water within a RTM grid cell (m^3 s^{-1}) is

$$\frac{dS}{dt} = \sum F_{in} - F_{out} + R \tag{10.1}$$

where $\sum F_{in}$ is the sum of inflows of water from neighboring upstream grid cells (m^3 s^{-1}), F_{out} is the flux of water leaving the grid cell in the downstream direction (m^3 s^{-1}), and R is the total runoff generated by the land model (m^3 s^{-1}). Downstream water flow direction in each grid cell is determined as one of eight compass points (north, northeast, east, southeast, south, southwest, west, and northwest) based on the steepest downhill slope as determined from a digital elevation model (Graham et al. 1999). The flux of water leaving the grid cell F_{out} is

$$F_{out} = \frac{v}{d} S \tag{10.2}$$

where v is the effective water flow velocity (m s^{-1}), d is the distance between centers of neighboring grid cells (m), and S is the volume of river water stored within the grid cell (m^3). The effective water flow velocity is a global constant and is chosen to be $v = 0.35$ m s^{-1} following Miller et al. (1994). The distance d between two grid cell centers depends on river direction, latitude, and longitude as

$$d = \sqrt{\Delta x^2 + \Delta y^2} . \tag{10.3}$$

The distance in the zonal direction Δx (m) is

$$\Delta x = \left(1 \times 10^3 \left|\theta_{i,j} - \theta_{i*,j*}\right| R_e\right)\left[0.5\left(\cos\phi_{i,j} + \cos\phi_{i*,j*}\right)\right] \tag{10.4}$$

where $\theta_{i,j}$ and $\theta_{i*,j*}$ are the latitudes (radians) of the upstream and downstream grid cells, $\phi_{i,j}$ and $\phi_{i*,j*}$ are the longitudes (radians) of the upstream and downstream grid cells, R_e is the radius of the earth (km) (Table 1.4), and i and j are grid cell indices. The distance in the meridional direction Δy (m) is

$$\Delta y = \left(1 \times 10^3 \left|\theta_{i,j} - \theta_{i*,j*}\right| R_e\right). \tag{10.5}$$

The RTM is generally run at a time step greater than that of the CLM because of computational constraints (Vertenstein et al., 2004). The total runoff from the land model at each time step is accumulated until the RTM is invoked. The total runoff at the land model resolution (kg m^{-2} s^{-1}) is

$$R = q_{over} + q_{drai} + q_{rgwl} \tag{10.6}$$

where q_{over} is surface runoff (section 7.3), q_{drai} is sub-surface drainage (section 7.5), and q_{rgwl} is runoff from glaciers, wetlands, and lakes (all in kg m^{-2} s^{-1}) (sections 7.6 and 9.3). The runoff at the land model resolution is interpolated to the resolution of RTM and converted to units of m^3 s^{-1} for use in equation (10.1) by multiplying by $1 \times 10^{-3} A$ where A is the area (m^2) of the RTM grid cell.

The RTM grid cells that are at river mouths, hence providing freshwater flux to the ocean, are identified by examining each RTM ocean grid cell and determining if a RTM land grid cell flows to that ocean grid cell. River mouth grid cells are also assigned if any overlapping grid cells at the land model resolution contain land. When used as part of the Community Climate System Model, the ocean freshwater fluxes at the RTM resolution are passed to the flux coupler which distributes the fluxes to the appropriate ocean grid cells. When used with the Community Atmosphere Model or when run offline, RTM serves only as a diagnostic tool. The river-routing scheme conserves water globally as

$$\sum_{i,j}\left(\frac{dS}{dt}\right)_{i,j} = \sum_{i,j} R_{i,j} \, . \tag{10.7}$$

11. Volatile Organic Compounds

Terrestrial biogenic volatile organic compound (BVOC) emissions from vegetation are simulated following the algorithm of Guenther et al. (1995) as described in Levis et al. (2003). Emissions from soils, which are lower than vegetation emissions by at least one order of magnitude, are not simulated. Five types of BVOC fluxes are estimated: isoprene, monoterpenes, other VOC (OVOC), other reactive VOC (ORVOC), and carbon monoxide (CO). The BVOC fluxes are

$$F_i = \varepsilon_i D \gamma_i \tag{11.1}$$

where F_i is the BVOC flux (μg C m^{-2} ground area h^{-1}) for emission type i, ε_i is the plant functional type dependent emission capacity for emission type i (μg C g^{-1} dry foliar mass h^{-1}) normalized to an incident photosynthetically active radiation (PAR) flux of 1000 μmol m^{-2} s^{-1} and a leaf temperature T_v of 303.15 K, D is the foliar density (g dry foliar mass m^{-2} ground area), and γ_i is a dimensionless empirical activity adjustment factor for emission type i that modulates emissions in response to incident PAR (isoprene only) and leaf temperature (Guenther et al. 1993). Emission capacities ε_i (Table 11.1) are taken from Guenther et al. (2000), Guenther et al. (1994), and Guenther et al. (1995) as described in Levis et al. (2003). The foliar density is calculated from

$$D = \frac{L}{0.5 SLA} \tag{11.2}$$

where L is the exposed leaf area index (m^2 leaf area m^{-2} ground area) (section 2.3), and SLA is the specific leaf area (m^2 leaf area g^{-1} C) for each plant functional type (Table 11.1) (Kucharik et al. 2000). The factor 0.5 converts SLA from g^{-1} C to g^{-1} dry foliar mass.

The activity adjustment factor is

$$\gamma_i = \left(C_{L,sun} + C_{L,sha}\right)_i C_{T,i} \tag{11.3}$$

where $C_{L,sun}$ and $C_{L,sha}$ are light dependence factors for sunlit and shaded leaves and C_T is a temperature dependence factor. The light dependence factor is

$$\left(C_{L,sun} + C_{L,sha}\right)_i = \begin{Bmatrix} \dfrac{\alpha C_{L1} Q_{sun}}{\sqrt{1+\alpha^2 Q_{sun}^2}} + \dfrac{\alpha C_{L1} Q_{sha}}{\sqrt{1+\alpha^2 Q_{sha}^2}} & i=1 \\ 1 & i=2,\ldots,5 \end{Bmatrix} \tag{11.4}$$

where $\alpha = 0.0027$ and $C_{L1} = 1.066$ are empirical coefficients, and Q_{sun} and Q_{sha} are the flux of PAR on sunlit and shaded leaves (μ mol photons m^{-2} s^{-1}) calculated from

$$Q_{sun} = 4.6\left(S_{atm}\downarrow_{vis}^{\mu} + f_{sun} S_{atm}\downarrow_{vis}\right) \tag{11.5}$$

$$Q_{sha} = 4.6\left[\left(1-f_{sun}\right) S_{atm}\downarrow_{vis}\right] \tag{11.6}$$

where $S_{atm}\downarrow_{vis}^{\mu}$ and $S_{atm}\downarrow_{vis}$ are the incident visible direct beam and diffuse solar fluxes (W m^{-2}) (section 1.2.1), f_{sun} is the sunlit fraction of the canopy (section 4.1), and the factor 4.6 is in μ mol photons J^{-1}. The temperature dependence factor is

$$C_{T,i} = \begin{Bmatrix} \dfrac{\exp\left[\dfrac{C_{T1}\left(T_v - T_s\right)}{0.001 R_{gas} T_v T_s}\right]}{C_{T3} + \exp\left[\dfrac{C_{T2}\left(T_v - T_m\right)}{0.001 R_{gas} T_v T_s}\right]} & i=1 \\ \exp\left[\beta\left(T_v - T_s\right)\right] & i=2,\ldots,5 \end{Bmatrix} \tag{11.7}$$

where $C_{T1} = 9.5\times 10^4$ J mol^{-1}, $C_{T2} = 2.3\times 10^5$ J mol^{-1}, $C_{T3} = 0.961$, $T_m = 314$ K, and $\beta = 0.09$ K^{-1} are empirical constants, T_v is vegetation temperature (K) (section 5), T_s is leaf temperature at a standard condition ($T_s = 303$ K), and R_{gas} is the universal gas constant (J K^{-1} $kmol^{-1}$) (Table 1.4).

Table 11.1. Plant functional type VOC emission capacities and specific leaf area.

Plant functional type	ε_1 (isoprene)	ε_2 (monoterpenes)	ε_3 (OVOC)	ε_4 (ORVOC)	ε_5 (CO)	SLA
NET Temperate	2.0	2.0	1.0	1.0	0.3	0.0125
NET Boreal	4.0	2.0	1.0	1.0	0.3	0.0125
NDT Boreal	0.0	1.6	1.0	1.0	0.3	0.0125
BET Tropical	24	0.4	1.0	1.0	0.3	0.0250
BET temperate	24	0.8	1.0	1.0	0.3	0.0250
BDT tropical	24	0.8	1.0	1.0	0.3	0.0250
BDT temperate	24	0.8	1.0	1.0	0.3	0.0250
BDT boreal	24	0.8	1.0	1.0	0.3	0.0250
BES temperate	24	0.8	1.0	1.0	0.3	0.0250
BDS temperate	24	0.8	1.0	1.0	0.3	0.0250
BDS boreal	24	0.8	1.0	1.0	0.3	0.0250
C_3 arctic grass	0.0	0.1	1.0	1.0	0.3	0.0200
C_3 grass	0.0	0.1	1.0	1.0	0.3	0.0200
C_4 grass	0.0	0.1	1.0	1.0	0.3	0.0200
Crop1	0.0	0.1	1.0	1.0	0.3	0.0200
Crop2	0.0	0.1	1.0	1.0	0.3	0.0200

ε_i (µg C g^{-1} dry foliar mass h^{-1}). SLA (m^2 leaf area g^{-1} C)

12. Offline CLM

In offline mode (uncoupled to an atmospheric model), the atmospheric forcing required by CLM is supplied by a dataset. The forcing requirements are the same as in Table 1.1, however, the inputs may be provided by alternative sources as follows.

The reference heights for temperature, wind, and specific humidity ($z_{atm,h}$, $z_{atm,m}$, $z_{atm,w}$) (m) are set to 30 m if not supplied by the user.

Only the magnitude of the wind (m s^{-1}) is required and the individual components, u_{atm} and v_{atm}, are set equal to each other.

The potential temperature $\overline{\theta_{atm}}$ (K) is derived from the atmospheric temperature T_{atm} as

$$\overline{\theta_{atm}} = T_{atm} \left(\frac{P_{srf}}{P_{atm}} \right)^{R_{da}/C_p} \tag{12.1}$$

where P_{srf} is the surface pressure (Pa), P_{atm} is the pressure at height z_{atm} (Pa), C_p is the specific heat capacity of air (J kg^{-1} K^{-1}) (Table 1.4), and R_{da} is the gas constant for dry air (J kg^{-1} K^{-1}) (Table 1.4). The surface pressure $P_{srf} = 101325$ Pa if not provided by the user.

The specific humidity q_{atm} (kg kg^{-1}) can be derived from a user-supplied relative humidity RH (%) as

$$q_{atm} = \frac{0.622 e_{atm}}{P_{atm} - 0.378 e_{atm}} \tag{12.2}$$

where the atmospheric vapor pressure e_{atm} (Pa) is derived from the water ($T_{atm} > T_f$) or ice ($T_{atm} \le T_f$) saturation vapor pressure $e_{sat}^{T_{atm}}$ as $e_{atm} = \frac{RH}{100} e_{sat}^{T_{atm}}$ where T_f is the freezing temperature of water (K) (Table 1.4). The specific humidity can also be derived from a user-supplied dewpoint temperature T_{dew} (K) as

$$q_{atm} = \frac{0.622 e_{sat}^{T_{dew}}}{P_{atm} - 0.378 e_{sat}^{T_{dew}}}. \tag{12.3}$$

Here, e_{sat}^{T}, the saturation vapor pressure as a function of temperature, is derived from Lowe's (1977) polynomials.

The atmospheric pressure P_{atm} (Pa) is set equal to the surface pressure P_{srf} if provided by the user or to the standard atmospheric pressure $P_{std} = 101325$ Pa.

The atmospheric longwave radiation $L_{atm} \downarrow$ (W m^{-2}) can also be derived from the atmospheric vapor pressure e_{atm} and temperature T_{atm} as

$$L_{atm} \downarrow = 0.70 + 5.95 \times 10^{-5} \times 0.01 e_{atm} \exp\left(\frac{1500}{T_{atm}}\right) \sigma T_{atm}^{4} \tag{12.4}$$

where σ is the Stefan-Boltzmann constant (W m^{-2} K^{-4}) (Table 1.4).

Convective and large-scale precipitation may be provided separately (in which case they will be added) or as total precipitation P (mm s^{-1}). All precipitation falls as rain, $q_{rain} = P$, if $T_{atm} > T_f + T_c$ where T_{atm} is the atmospheric temperature (K), T_f is freezing temperature of water (K) (Table 1.4), and $T_c = 2.5$ is the critical threshold temperature (K). In the case of snow ($T_{atm} \le T_f + T_c$), all precipitation is assigned to snow $q_{sno} = P$

and the land model determines the fraction of precipitation that is in liquid phase based on atmospheric temperature

$$f_{P,liq} = \begin{Bmatrix} 0 & T_{atm} \le T_f \\ -54.632 + 0.2T_{atm} & T_f < T_{atm} \le T_f + 2 \\ 0.4 & T_f + 2 < T_{atm} \le T_f + T_c \\ 1 & T_{atm} > T_f + T_c \end{Bmatrix}. \tag{12.5}$$

The term $f_{P,liq}$ is used to determine the total rate of liquid and solid precipitation reaching the ground, $q_{grnd,liq}$ and $q_{grnd,ice}$ (kg m^{-2} s^{-1}) as

$$q_{grnd,liq} = \begin{Bmatrix} q_{thru,liq} + q_{drip,liq} & T_{atm} > T_f + T_c \\ f_{P,liq}\left(q_{thru,ice} + q_{drip,ice}\right) & T_{atm} \le T_f + T_c \end{Bmatrix} \tag{12.6}$$

$$q_{grnd,ice} = \begin{Bmatrix} 0 & T_{atm} > T_f + T_c \\ \left(1 - f_{P,liq}\right)\left(q_{thru,ice} + q_{drip,ice}\right) & T_{atm} \le T_f + T_c \end{Bmatrix}. \tag{12.7}$$

where $q_{thru,liq}$ and $q_{thru,ice}$ are liquid and solid throughfall, and $q_{drip,liq}$ and $q_{drip,ice}$ are liquid and solid canopy drip (kg m^{-2} s^{-1}). Equations (12.6) and (12.7) replace equations (7.10) and (7.11) in section 7.1.

Total incident solar radiation S_{atm} (W m^{-2}) may be provided by the user, in which case the individual components are $S_{atm} \downarrow_{vis}^{\mu} = 0.7\left(0.5S_{atm}\right)$, $S_{atm} \downarrow_{nir}^{\mu} = 0.7\left(0.5S_{atm}\right)$, $S_{atm} \downarrow_{vis} = 0.3\left(0.5S_{atm}\right)$, $S_{atm} \downarrow_{nir} = 0.3\left(0.5S_{atm}\right)$. The user may also provide the total direct and diffuse solar radiation, $S_{atm} \downarrow^{\mu}$ and $S_{atm} \downarrow$, which are each equally apportioned into the visible and near-infrared wavebands (e.g., $S_{atm} \downarrow_{vis}^{\mu} = 0.5S_{atm} \downarrow^{\mu}$, $S_{atm} \downarrow_{nir}^{\mu} = 0.5S_{atm} \downarrow^{\mu}$).

In addition to the surface data described in section 1.2.3, the northern (E_N), eastern (E_E), southern (E_S), and western (E_W) edges of the grid (degrees) are also required. For global grids, $E_N = 90^\circ$, $E_S = -90^\circ$, $E_E = 180^\circ$, and $E_E = -180^\circ$. For partial grids, $-90^\circ \le E_S < 90^\circ$, $E_S < E_N \le 90^\circ$, $-180^\circ \le E_W < 180^\circ$, and $E_W < E_E \le 180^\circ$.

13. References

Anderson, E.A. 1976. A point energy and mass balance model of a snow cover. NOAA Technical Report NWS 19, Office of Hydrology, National Weather Service, Silver Spring, MD.

André, J.-C., Goutorbe, J.-P., and Perrier, A. 1986. HAPEX-MOBILHY: A hydrologic atmosphere experiment for the study of water budget and evaporation flux at the climatic scale. Bull. Meteor. Soc. 67:138-144.

Arya, S.P. 2001. Introduction to Meteorology. Academic Press, San Diego, CA.

Berger, A.L. 1978a. Long-term variations of daily insolation and quaternary climatic changes. J. Atmos. Sci. 35:2362-2367.

Berger, A.L. 1978b. A simple algorithm to compute long-term variations of daily or monthly insolation. Contribution de l'Institut d'Astronomie et de Géophysique, Université Catholique de Louvain, Louvain-la-Neuve, No. 18.

Berger, A., Loutre, M.-F., and Tricot, C. 1993. Insolation and Earth's orbital periods. J. Geophys. Res. 98:10341-10362.

Beven, K.J., and Kirkby, M.J. 1979. A physically based variable contributing area model of basin hydrology. Hydrol. Sci. Bull. 24: 43-69.

Bonan, G.B. 1996. A land surface model (LSM version 1.0) for ecological, hydrological, and atmospheric studies: Technical description and user's guide. NCAR Technical Note NCAR/TN-417+STR, National Center for Atmospheric Research, Boulder, CO.

Bonan, G.B. 1998. The land surface climatology of the NCAR Land Surface Model coupled to the NCAR Community Climate Model. J. Climate 11:1307-1326.

Bonan, G.B. 2002. Ecological Climatology: Concepts and Applications. Cambridge University Press.

Bonan, G.B., Oleson, K.W., Vertenstein, M., Levis, S., Zeng, X., Dai, Y., Dickinson, R.E., and Yang, Z.-L. 2002a. The land surface climatology of the Community Land Model coupled to the NCAR Community Climate Model. J. Climate 15: 3123-3149.

Bonan, G.B., Levis, S., Kergoat, L., and Oleson, K.W. 2002b. Landscapes as patches of plant functional types: An integrating concept for climate and ecosystem models. Global Biogeochem. Cycles 16: 5.1-5.23.

Branstetter, M.L., and Famiglietti, J.S. 1999. Testing the sensitivity of GCM-simulated runoff to climate model resolution using a parallel river transport algorithm. Preprints, 14^{th} Conference on Hydrology, Dallas, TX, Amer. Meteor. Soc., 391-392.

Branstetter, M.L. 2001. Development of a parallel river transport algorithm and applications to climate studies. Ph.D. dissertation, University of Texas at Austin.

Clapp, R.B., and Hornberger, G.M. 1978. Empirical equations for some soil hydraulic properties. Water Resour. Res. 14:601-604.

Cogley, J.G. 1991. GGHYDRO – Global Hydrographic Data Release 2.0. Trent Climate Note 91-1, Dept. Geography, Trent University, Peterborough, Ontario.

Collatz, G.J., Ball, J.T., Grivet, C., and Berry, J.A. 1991. Physiological and environmental regulation of stomatal conductance, photosynthesis, and transpiration: A model that includes a laminar boundary layer. Agric. For. Meteorol. 54:107-136.

Collatz, G.J., Ribas-Carbo, M., and Berry, J.A. 1992. Coupled photosynthesis-stomatal conductance model for leaves of C_4 plants. Aust. J. Plant Physiol. 19:519-538.

Cosby, B.J., Hornberger, G.M., Clapp, R.B., and Ginn, T.R. 1984. A statistical exploration of the relationships of soil moisture characteristics to the physical properties of soils. Water Resour. Res. 20:682-690.

Dai, Y., and Zeng, Q. 1997. A land surface model (IAP94) for climate studies. Part I: formulation and validation in off-line experiments. Adv. Atmos. Sci. 14:433-460.

Dai, Y., and Coauthors 2001. Common Land Model: Technical documentation and user's guide [Available online at http://climate.eas.gatech.edu/dai/clmdoc.pdf].

Dai Y., Zeng, X., Dickinson, R.E., Baker, I., Bonan, G.B., Bosilovich, M.G., Denning, A. S., Dirmeyer, P.A., Houser, P.R., Niu, G., Oleson, K.W., Schlosser, C.A., and Yang, Z.-L. 2003. The Common Land Model. Bull. Amer. Meteor. Soc. 84:1013-1023.

Dai, A., and Trenberth, K.E. 2002. Estimates of freshwater discharge from continents: Latitudinal and seasonal variations. J. Hydrometeor. 3:660-687.

DeFries, R.S., Hansen, M.C., Townshend, J.R.G., Janetos, A.C., and Loveland, T.R. 2000. A new global 1-km dataset of percentage tree cover derived from remote sensing. Global Change Biol. 6:247-254.

de Vries, D.A. 1963. Thermal Properties of Soils. In: W.R. van Wijk (editor) Physics of the Plant Environment. North-Holland, Amsterdam.

Dickinson, R.E., 1983. Land surface processes and climate-surface albedos and energy balance. Adv. Geophys. 25:305-353.

Dickinson, R.E., Henderson-Sellers, A., Kennedy, P.J. 1993. Biosphere-Atmosphere Transfer Scheme (BATS) version 1e as coupled to the NCAR Community Climate Model. NCAR Technical Note NCAR/TN-387+STR. National Center for Atmospheric Research, Boulder, CO.

Dirmeyer, P.A., Dolman, A.J., and Sato, N. 1999. The pilot phase of the Global Soil Wetness Project. Bull. Amer. Meteor. Soc. 80:851-878.

Dorman, J.L., and Sellers, P.J. 1989. A global climatology of albedo, roughness length and stomatal resistance for atmospheric general circulation models as represented by the simple biosphere model (SiB). J. Appl. Meteor. 28:833-855.

Dougherty, R.L., Bradford, J.A., Coyne, P.I., and Sims, P.L. 1994. Applying an empirical model of stomatal conductance to three C-4 grasses. Agric. For. Meteor. 67:269-290.

Eidenshink, J.C., and Faundeen, J.L. 1994. The 1km AVHRR global land data set: First stages in implementation. Int. J. Remote Sens. 15:3443-3462.

Farouki, O.T. 1981. The thermal properties of soils in cold regions. Cold Regions Sci. and Tech., 5:67-75.

Farquhar, G.D., von Caemmerer, S., and Berry, J.A. 1980. A biochemical model of photosynthetic CO_2 assimilation in leaves of C_3 species. Planta 149:78-90.

Farquhar, G.D., and von Caemmerer, S. 1982. Modeling of photosynthetic response to environmental conditions. pp. 549-587. In: O.L. Lange, P.S. Nobel, C.B. Osmond, and H. Zeigler (editors) Encyclopedia of Plant Physiology. Vol. 12B. Physiological Plant Ecology. II. Water Relations and Carbon Assimilation. Springer-Verlag, New York.

Flatau, P.J., Walko, R.L., and Cotton, W.R. 1992. Polynomial fits to saturation vapor pressure. J. Appl. Meteor. 31:1507-1513.

Fuchs, M., Campbell, G.S., and Papendick, R.I. 1978. An analysis of sensible and latent heat flow in a partially frozen unsaturated soil. Soil Sci. Soc. Amer. 42:379-385.

Gash, J.H.C., Nobre, C.A., Roberts, J.M., and Victoria, R.L. 1996. An overview of ABRACOS. pp. 1-14. In: J.H.C. Gash, C.A. Nobre, J.M. Roberts, and R.L. Victoria (eds) Amazonian Deforestation and Climate. John Wiley and Sons, Chichester, England.

Global Soil Data Task 2000. Global soil data products CD-ROM (IGBP-DIS). International Geosphere-Biosphere Programme-Data and Information Available Services [Available online at http://www.daac.ornl.gov].

Graham, S.T., Famiglietti, J.S., Maidment, D.R. 1999. Five-minute, 1/2º, and 1º data sets of continental watersheds and river networks for use in regional and global hydrologic and climate system modeling studies. Water Resour. Res. 35:583-587.

Guenther, A., Zimmerman, P.R., Harley, P.C., Monson, R.K., and Fall, R. 1993. Isoprene and monoterpene emission rate variability: Model evaluations and sensitivity analyses. J. Geophys. Res. 98:12609-12617.

Guenther, A., Zimmerman, P., and Wildermuth, M. 1994. Natural volatile organic compound emission rate estimates for U.S. woodland landscapes. Atmos. Environ. 28:1197-1210.

Guenther, A., Hewitt, C.N., Erickson, D., Fall, R., Geron, C., Graedel, T., Harley, P., Klinger, L., Lerdau, M., McKay, W.A., Pierce, T., Scholes, B., Steinbrecher, R., Tallamraju, R., Taylor, J., and Zimmerman, P. 1995. A global model of natural volatile organic compound emissions. J. Geophys. Res. 100:8873-8892.

Guenther, A., Geron, C., Pierce, T., Lamb, B., Harley, P., and Fall, R. 2000. Natural emissions of non-methane volatile organic compounds, carbon monoxide, and oxides of nitrogen from North America. Atmos. Environ. 34:2205-2230.

Henderson-Sellers, B. 1985. New formulation of eddy diffusion thermocline models. Appl. Math. Modelling 9:441-446.

Henderson-Sellers, B. 1986. Calculating the surface energy balance for lake and reservoir modeling: A review. Rev. Geophys 24:625-649.

Henderson-Sellers, A., Yang, Z.-L., and Dickinson, R.E. 1993. The project for intercomparison of land-surface parameterization schemes. Bull. Amer. Meteor. Soc. 74: 1335-1349.

Hoffman, F., Vertenstein, M., Levis, S., Thornton, P., and Oleson, K. 2004. Community Land Model Version 3.0 (CLM3.0) Developer's Guide [Available online at http://www.cgd.ucar.edu/tss].

Hostetler, S.W., and Bartlein, P.J. 1990. Simulation of lake evaporation with application to modeling lake level variations of Harney-Malheur Lake, Oregon. Wat. Resour. Res. 26:2603-2612.

Hostetler, S.W., Bates, G.T., and Giorgi, F. 1993. Interactive coupling of a lake thermal model with a regional climate model. J. Geophys. Res. 98:5045-5057.

Hostetler, S.W., Giorgi, F., Bates, G.T., and Bartlein, P.J. 1994. Lake-atmosphere feedbacks associated with paleolakes Bonneville and Lahontan. Science 263:665-668.

Jordan, R. 1991. A One-dimensional Temperature Model for a Snow Cover: Technical Documentation for SNTHERM.89. U.S. Army Cold Regions Research and Engineering Laboratory, Special Report 91-16.

Kucharik, C.J., Foley, J.A., Delire, C., Fisher, V.A., Coe, M.T., Lenters, J.D., Young-Molling, C., Ramankutty, N., Norman, J.M., and Gower, S.T. 2000. Testing the performance of a dynamic global ecosystem model: Water balance, carbon balance, and vegetation structure. Global Biogeochem. Cycles 14:795-825.

Landsberg, J.J. 1986. Physiological Ecology of Forest Production. Academic Press, London.

Levis, S., Wiedinmyer, C., Bonan, G.B., Guenther, A. 2003. Simulating biogenic volatile organic compound emissions in the Community Climate System Model. J. Geophy. Res. 108, 4659, doi:10.1029/2002JD003203.

Levis, S., Bonan, G.B., Vertenstein, M., and Oleson, K.W. 2004. The Community Land Model's Dynamic Global Vegetation Model (CLM-DGVM): Technical description and user's guide. NCAR Technical Note NCAR/TN-459+IA. National Center for Atmospheric Research, Boulder, CO.

Loveland, T.R., Reed, B.C., Brown, J.F., Ohlen, D.O., Zhu, Z., Yang, L., and Merchant, J.W. 2000. Development of a global land cover characteristics database and IGBP DISCover from 1 km AVHRR data. Int. J. Remote Sens. 21:1303-1330.

Lowe, P.R. 1977. An approximating polynomial for the computation of saturation vapor pressure. J. Appl. Meteor. 16:100-103.

Miller, J.R., Russell, G.L., and Caliri, G. 1994. Continental-scale river flow in climate models. J. Climate 7:914-928.

Oleson, K.W., and Bonan, G.B. 2000. The effects of remotely-sensed plant functional type and leaf area index on simulations of boreal forest surface fluxes by the NCAR land surface model. J. Hydrometeor. 1:431-446.

Panofsky, H.A., and Dutton, J.A. 1984. Atmospheric Turbulence: Models and Methods for Engineering Applications. John Wiley and Sons, New York.

Philip, J.R. 1957. Evaporation, and moisture and heat fields in the soil. J. Meteor. 14:354-366.

Press, W.H., Teukolsky, S.A., Vetterling, W.T., and Flannery, B.P. 1992. Numerical Recipes in FORTRAN: The Art of Scientific Computing. Cambridge University Press, New York.

Sellers, P.J. 1985. Canopy reflectance, photosynthesis and transpiration. Int. J. Remote Sens. 6:1335-1372.

Sellers, P.J., Mintz, Y., Sud, Y.C., and Dalcher, A. 1986. A simple biosphere model (SiB) for use within general circulation models. J. Atmos. Sci. 43:505-531.

Sellers, P.J., Hall, F.G., Asrar, G., Strebel, D.E., and Murphy, R.E. 1988. The First ISLSCP Field Experiment (FIFE). Bull. Amer. Meteor. Soc. 69:22-27.

Sellers, P.J., Berry, J.A., Collatz, G.J., Field, C.B., and Hall, F.G. 1992. Canopy reflectance, photosynthesis, and transpiration. III. A reanalysis using improved leaf models and a new canopy integration scheme. Remote Sens. Environ. 42:187-216.

Sellers, P.J., and Coauthors 1995. The Boreal Ecosystem-Atmosphere Study (BOREAS): An overview and early results from the 1994 field year. Bull. Amer. Meteor. Soc. 76:1549-1577.

Stull, R.B. 1988. An Introduction to Boundary Layer Meteorology. Kluwer Academic Publishers, Dordrecht.

Unland, H.E., Houser, P.R., Shuttleworth, W.J., and Yang, Z.-L. 1996. Surface flux measurement and modeling at a semi-arid Sonoran Desert site. Agric. For. Meteorol. 82:119-153.

Vertenstein, M., Hoffman, F., Oleson, K., and Levis, S. 2004. Community Land Model Version 3.0 (CLM3.0) User's Guide [Available online at http://www.cgd.ucar.edu/tss].

Wiscombe, W.J., and Warren, S.G. 1980. A model for the spectral albedo of snow. I. Pure snow. J. Atmos. Sci. 37:2712-2733.

Wullschleger, S.D. 1993. Biochemical limitations to carbon assimilation in C_3 plants – A retrospective analysis of the A/C_i curves from 109 species. J. Exp. Bot. 44:907-920.

Yang, Z.-L. 1998. Technical note of a 10-layer soil moisture and temperature model. Unpublished manuscript.

Zeng, X., and Dickinson, R.E. 1998. Effect of surface sublayer on surface skin temperature and fluxes. J.Climate 11:537-550.

Zeng, X., Zhao, M., and Dickinson R.E. 1998. Intercomparison of bulk aerodynamic algorithms for the computation of sea surface fluxes using the TOGA COARE and TAO data. J. Climate 11:2628-2644.

Zeng, X. 2001. Global vegetation root distribution for land modeling. J. Hydrometeor. 2:525-530.

Zeng, X., Shaikh, M., Dai, Y., Dickinson, R.E., and Myneni, R. 2002. Coupling of the Common Land Model to the NCAR Community Climate Model. J. Climate 15:1832-1854.

Zeng, X., Dickinson, R.E., Barlage, M., Dai, Y., Wang, G., and Oleson, K. 2004. Treatment of under-canopy turbulence in land models. J. Climate, submitted.

Zilitinkevich, S.S. 1970. Dynamics of the Atmospheric Boundary Layer. Leningrad Gidrometeor.